**CNWRA** *A center of excellence in earth sciences and engineering*

A Division of Southwest Research Institute™
6220 Culebra Road • San Antonio, Texas, U.S.A. 78228-5166
(210) 522-5160 • Fax (210) 522-5155

October 31, 2001
Contract No. NRC-02-97-009
Account No. 20.01402.571

U.S. Nuclear Regulatory Commission
ATTN: Tae Ahn
Two White Flint North
11545 Rockville Pike
Mail Stop T7 C6
Washington, DC 20555

Subject: Submittal of report "Effect of In-Package Chemistry on the Degradation of Vitrified High-Level Radioactive Waste and Spent Nuclear Fuel Cladding" (CNWRA 2002-01), Intermediate Milestone 01402.571.180

Reference: Letter from T. Ahn to V. Jain dated September 28, 2001—Acceptance of Intermediate Milestone 01402.571.180, "Effect of In-Package Chemistry on the Degradation of Vitrified High-Level Waste and Spent Nuclear Fuel Cladding"

Dear Dr. Ahn:

Enclosed is the subject report that was revised based on NRC staff comments. This report documents the effects of in-package environment on the degradation of high-level waste glass and Zircaloy cladding and changes to solution chemistry through interactions with waste package internal structural components. In addition, the report provides a review and assessment of the DOE model abstractions for high-level waste glass, Zircaloy cladding, and in-package chemistry used for the Total System Performance Assessment–Site Recommendation. Also enclosed with the report is CNWRA staff responses to the NRC comments.

If you have any questions regarding this report, please feel free to contact Yi-Ming Pan at (210) 522-6640 or Gustavo Cragnolino at (210) 522-5539.

Sincerely yours,

Vijay Jain
Element Manager
Corrosion Science & Process Engineering

VJ:YMP:jg
Enclosure

cc:

| | | | | | |
|---|---|---|---|---|---|
| J. Linehan | K. Stablein | D. Brooks | T. Essig | Y.-M. Pan | T. Nagy (contracts) |
| B. Meehan | B. Leslie | T. McCartin | A. Henry | C. Brossia | |
| E. Whitt | T. Ahn | T. Bloomer | W. Patrick | G. Cragnolino | |
| J. Greeves | C. Greene | J. Andersen | CNWRA Dirs. | O. Pensado | |
| J. Piccone | S. Wastler | J. Thomas | CNWRA EMs | P. Maldonado | |

Washington Office • Twinbrook Metro Plaza #210
12300 Twinbrook Parkway • Rockville, Maryland 20852-1606

## RESPONSES TO NRC COMMENTS ON IM 01402.571.180

## "EFFECT OF IN-PACKAGE CHEMISTRY ON THE DEGRADATION OF VITRIFIED HIGH-LEVEL RADIOACTIVE WASTE AND SPENT NUCLEAR FUEL CLADDING"

**Reviewer 1**

1. **Add the relevant agreements of TSPAI and Range of Operating Temperature Technical Exchanges for all chapters. Examples include TSPAI 3.08 and TSPAI 3.14 for in-package chemistry.**

   Accept. TSPAI agreements 3.08 and 3.14 are relevant to the subissue related to in-package chemistry. Agreements added.

2. **In the second paragraph of p. 6, the stage 3 leach excursion was bounded by using the stage one leach rate in TSPA.**

   ANL studies conducted in saturated conditions using PCT test showed that the Stage III corrosion rate is bounded by Stage I corrosion rate. However, the excursion referenced in this paragraph is a result of drip-test conditions which is not considered in the model abstraction. Text added to clarify this point.

3. **Confirm that the last sentence in p. 11 is a correct statement.**

   The TSPA-SR contains a sensitivity analysis of waste type, both CSNF waste and a combined case of HLW glass and DSNF waste. The sentence deleted.

4. **The conclusion is recommended to make it clear that the potential effects of iron were tested and the results showed the significance of the pH effects.**

   Accept. Additional text added.

5. **In the first two sentences of p. 28, the boron release may not be conservative (rather realistic) for the assessment of Tc release because Tc may not be incorporated in the secondary phases.**

   Boron provides a conservative upper bound because boron is released at a rate similar to alkali ions and is not incorporated into secondary phases similar to Tc. Text modified to indicate this change.

6. **In the last sentence of p. 33, add hydride embrittlement.**

   In the sentence only the failure modes considered by the DOE in the referenced document are listed. Hydride embrittlement is not included by the DOE and therefore no change is needed in the sentence. However, a paragraph has been added in Section 3.1.2 to indicate that in the CLST IRSR Revision 3 the possibility of hydride embrittlement is addressed and requires further evaluation by the DOE, as covered by agreement CLST 3.08.

7. **Clarify the last sentence in p. 35 starting "This analysis, however, contradict—".**

In at least two FEPs DOE accepts the existence of acidic conditions as a result of radiolysis and microbial activity indicating that acidic conditions may promote localized corrosion of Zircaloy cladding, a statement which is not correct. However, when discussing pitting in the document referenced in the same paragraph as the sentence noted above, DOE claimed that the pH is not sufficiently low to have $Fe^{3+}$ ions in solution, in clear contradiction with the statement in the FEPs document. Text modified to clarify this point.

8. **In 3.2.2, address in a sentence on the discussion going on with Westinghouse. Full clarification can be made later in other places. Putting aside this clarification, it is still unclear why the oxide formation would promotes pitting from the discussion of results themselves (especially the second paragraph in p. 45 and the second paragraph in p. 51).**

The discussion on p. 45 reports the observation that the breakdown potential increased with hydrothermal oxidation but the repassivation potential did not. With respect to p. 51, it was observed that the open circuit potential was above the repassivation potential for the oxidized samples, especially when other oxidants were added (e.g., hydrogen peroxide, ferric chloride). Because the measured open circuit potential for the oxidized samples is greater than the repassivation potential, there is sufficient driving force as given by the overpotential (difference between the open circuit potential and the repassivation potential) to promote pitting corrosion, even though an extremely long time interval may be needed to initiate it. This is in contrast to the as-polished cases where the open circuit potential for these specimens is well below the repassivation potential and thus pitting is not possible without polarization or the addition of other oxidizing species. Thus, as discussed on p. 51 one plausible reason why pitting was not observed at open circuit on the oxidized samples stems from a limitation in the cathodic kinetics resulting from the insulating nature of the oxide. This has been clarified.

9. **Correct the uniform corrosion rate in the second sentence of the second paragraph in p. 53.**

Accept, correction made.

<u>Reviewer 2</u>

1. **Focus was diluted by glass and Zircaloy corrosion. Need to concentrate on in-package chemistry, and how glass and Zircaloy affect in-package chemistry.**

The main purpose of this IM is to evaluate the effect of environmental variables that could exist inside waste packages on the degradation of high-level waste glass and Zircaloy cladding and their performance in the proposed repository. Preliminary results on the evolution of in-package chemistry are also presented. Nevertheless, additional experimental efforts and simulations are planned to justify the range of environmental conditions expected inside breached waste packages, including the effects of waste package components. Statements have been made in the report.

2. **Gadolinium-stainless steel has not been developed, has it? Is this the same as stainless steel with GdPO4? There was a cracking problem when Gd-ss was**

**rolled. (p. 55)**

This is unknown. However, $GdPO_4$ is known to be a neutron absorber that is required for criticality control within the canister for some DOE spent nuclear fuels. No significant effect is expected on the in-package chemistry modeling. No change made.

3. **KTI agreements for degradation of vitrified high-level waste, for example, CLST 4.02 and 4.03, are the same as 3.02 and 3.03, as is CLST 4.01 and 3.01. Are the correct KTI agreements listed? If they are both used interchangeably (3.0x and 4.0x), why not drop the redundant agreements? (p.75)**

   The cited agreements checked. Corrections made.

4. **I found the sans serif font hard to read.**

   Corrections made using the arial font according to the NRC guidance of adopting IRSR/NUREG format style for all reports.

5. **How is the in-package chemistry changed by juvenile failures?**

   Juvenile failures are not addressed in this IM. In addition, the DOE in-package chemistry model simulates the conditions after the initial breach of the waste packages. However, the inclusion of juvenile failures has been addressed in the CLST technical exchange. Agreement CLST 3.01 that covers the path forward for resolving this concern has been mentioned in the report.

6. **Although alluded to, transient effects of initial water entering the waste package are not addressed per se. (p. 76) CLST 3.02**

   The transient effects have not been evaluated in the experimental investigations conducted by the CNWRA. These effects could be important to the pH evolution of the in-package solution. DOE agreed to address the transient effects according to agreement CLST 3.02, which has been mentioned in the report.

<u>Reviewer 3</u>

1. **Page xviii; Middle of paragraph 2. "This model will be acceptable if the DOE can demonstrate....." Is the paper making a Regulatory acceptance statement?**

   The reference statement is made from the point of view of sufficiency review to provide comments on sufficiency of the DOE approach in evaluating cladding degradation. It is not intended to make a regulatory acceptance statement, but "will be" was replaced by "could be" in the text.

2. **Page xviii; Bottom of paragraph 2. "The corrosion potential can reach the repassivation potential...." The corrosion potential is a fixed item for specific conditions. Is this sentence saying in the FeCl3 environment that the corrosion potential equals the repassivation potential?**

   This statement is not entirely correct. The corrosion potential, in general, is not fixed and

can vary significantly in a given environment. With respect to the question raised, additions of ferric chloride were observed to increase the corrosion potential above the repassivation potential. This was clarified.

3. **Page xix: 4th line. "The approach taken by the DOE in determining...is appropriate." Is the paper making a Regulatory acceptance statement?**

The text was modified according to CLST IRSR and reviews of the in-package chemistry AMRs to clarify that the DOE treatment may not be appropriate. Updated revision will be provided by DOE according to CLST agreements.

4. **Page 2, 2nd paragraph. "Through the process of...three subissued are considered closed, pending additional....." Is the item closed-pending or closed?**

Accept. All the referenced subissues are considered closed-pending. Change made.

5. **Page 5, 3rd paragraph, middle. "In addition, the reaction products in the altered surface layer reach the saturation concentration...." What is the saturation concentration? When do the products reach their thermodynamic limit?**

The saturation concentration refers to the solubility limits of the reaction products in the altered surface layer, which is likely to occur in Stage III of the long-term glass corrosion process. Formation of secondary phases results. Text modified.

6. **Page 6, 2nd paragraph. How is the surface area calculated for obtaining the calculated dissolution rate values? Should anything be added that expresses caution with using these numbers?**

In the TSPA-SR a constant value of $5.63 \times 10^{-5}$ $m^2/g$ for the specific surface area is used to calculate the glass degradation rate. This value can be obtained in two steps. First, an initial surface area of 94.6 $m^2$ is calculated by multiplying the geometric surface area of each glass log by a cracking factor of 20. Then the specific surface area is computed by dividing the initial surface area by the initial weight of the glass log (1682 Kg). DOE claims that the constant value of $5.63 \times 10^{-5}$ $m^2/g$ provides a conservative bound for the specific surface area. The technical basis for estimating the specific surface area for high-level waste glasses should be provided by the DOE. Text modified to address this point.

7. **Page 8, Equation 2-2. Equation 2-2 is Eq 2-1 rearranged. How is Eq 2-2 simpler?**

In Eq. 2-2 the affinity term $(1-Q/K)$ is combined with the intrinsic dissolution rate $k_0$ to give the term $k_{eff}$ that, in turn, reduces the number of the model parameters and variables. Therefore Eq. 2-2 is a simpler approach compared with Eq. 2-1. This has been clarified.

8. **Page 9, 1st paragraph and Table 2-1. "The MCC-1 test results indicate that neither...dissolution rate..is sensitive..." NR(B) has a standard deviation close to 50% of the value. How is it not sensitive?**

Accept. Even though the standard deviation of the normalized boron dissolution rates

NR(B) is about 50% of the sample, the NR(B) values are in the same order of magnitude. Therefore the dissolution rate is not substantially affected by the amount of aluminum in the waste glasses. Text modified.

9. **Page 9, Last paragraph. The technical explanation for 6.9+-0.5 is not written in the text. Please add a sentence explaining 6.9 = mean + 1 s.d.**

Accept. Additional sentence added.

10. **Page 17, first line. "Especially int the high...". Int should be just 'in'.**

Accept. Text corrected.

11. **Page 18, 2nd paragraph. "The substantially lower NLRb values...." What is this in comparison to? DI water or the lower FeClx concentrations?**

The paragraph describes the observation that low $NLR_B$ values were measured for WVDP Ref. 6 glass in 0.25 M $FeCl_3$ solution after 10 days of leaching. The rates are even lower than those in other solutions. Text modified to clarify this point.

12. **Page 18, 3rd paragraph. "In all cases, except the leachates..." In figure 2-7, it appears (this is a copy and I don't have the data set) that the final pH levels are lower than the initial pH levels.**

From the glass leaching tests, the final pH values of the solutions are generally higher than the initial pH except the high concentration iron chloride solution tests.
Text modified.

13. **Page 23, 3rd paragraph. "This theory is supported by....in Figure 2-5." Could not find the inductively coupled plasma atomic emission spectrometry analyses results in the figures.**

The boron leach rates plotted in Figure 2-5 are from the inductively coupled plasma atomic emission spectrometry analyses. No change made.

14. **Page 23, 3rd paragraph. "In the case of glass dissolution...(Figures 2-5 and 2-7)." Is the paper referring to Figure 2-6 instead of 2-5?**

Accept. Text corrected.

CNWRA 2002-01

# EFFECT OF IN-PACKAGE CHEMISTRY ON THE DEGRADATION OF VITRIFIED HIGH-LEVEL RADIOACTIVE WASTE AND SPENT NUCLEAR FUEL CLADDING

*Prepared for*

**U.S. Nuclear Regulatory Commission**
**Contract NRC–02–97–009**

*Prepared by*

**Center for Nuclear Waste Regulatory Analyses**
**San Antonio, Texas**

**October 2001**

CNWRA 2002-01

# EFFECT OF IN-PACKAGE CHEMISTRY ON THE DEGRADATION OF VITRIFIED HIGH-LEVEL RADIOACTIVE WASTE AND SPENT NUCLEAR FUEL CLADDING

*Prepared for*

**U.S. Nuclear Regulatory Commission**
**Contract NRC–02–97–009**

*Prepared by*

**Y.-M. Pan**
**C.S. Brossia**
**G.A. Cragnolino**
**V. Jain**
**O. Pensado**
**N. Sridhar**

**Center for Nuclear Waste Regulatory Analyses**
**San Antonio, Texas**

**October 2001**

# PREVIOUS REPORTS IN SERIES

| Number | Name | Date Issued |
|---|---|---|
| CNWRA 91-004 | A Review of Localized Corrosion of High-Level Nuclear Waste Container Materials—I | April 1991 |
| CNWRA 91-008 | Hydrogen Embrittlement of Candidate Container Materials | June 1991 |
| CNWRA 92-021 | A Review of Stress Corrosion Cracking of High-Level Nuclear Waste Container Materials—I | August 1992 |
| CNWRA 93-003 | Long-Term Stability of High-Level Nuclear Waste Container Materials: I—Thermal Stability of Alloy 825 | February 1993 |
| CNWRA 93-004 | Experimental Investigations of Localized Corrosion of High-Level Nuclear Waste Container Materials | February 1993 |
| CNWRA 93-014 | A Review of the Potential for Microbially Influenced Corrosion of High-Level Nuclear Waste Containers | June 1993 |
| CNWRA 94-010 | A Review of Degradation Modes of Alternate Container Designs and Materials | April 1994 |
| CNWRA 94-028 | Environmental Effects on Stress Corrosion Cracking of Type 316L Stainless Steel and Alloy 825 as High-Level Nuclear Waste Container Materials | October 1994 |
| CNWRA 95-010 | Experimental Investigations of Failure Processes of High-Level Radioactive Waste Container Materials | May 1995 |
| CNWRA 95-020 | Expert-Panel Review of the Integrated Waste Package Experiments Research Project | September 1995 |
| CNWRA 96-004 | Thermal Stability and Mechanical Properties of High-Level Radioactive Waste Container Materials: Assessment of Carbon and Low-Alloy Steels | May 1996 |
| CNWRA 97-010 | An Analysis of Galvanic Coupling Effects on the Performance of High-Level Nuclear Waste Container Materials | August 1997 |
| CNWRA 98-004 | Effect of Galvanic Coupling Between Overpack Materials of High-Level Nuclear Waste Containers—Experimental and Modeling Results | March 1998 |

## PREVIOUS REPORTS IN SERIES (continued)

| Number | Name | Date Issued |
|---|---|---|
| CNWRA 98-008 | Effects of Environmental Factors on Container Life | July 1998 |
| CNWRA 99-003 | Assessment of Performance Issues Related to Alternate Engineered Barrier System Materials and Design Options | September 1999 |
| CNWRA 99-004 | Effects of Environmental Factors on the Aqueous Corrosion of High-Level Radioactive Waste Containers—Experimental Results and Models | September 1999 |
| CNWRA 2000-06 | Assessment of Methodologies to Confirm Container Performance Model Predictions | January 2001 |
| CNWRA 2001-003 | Effect of Environment on the Corrosion of Waste Package and Drip Shield Materials | September 2001 |

# ABSTRACT

The U.S. Department of Energy (DOE) identified limited release of radionuclides from the engineering barriers as one of five system attributes that contribute significantly to performance of the proposed high-level nuclear waste repository at Yucca Mountain, Nevada. The chemistry of the aqueous environment inside the breached waste packages and the performance of spent nuclear fuel cladding and waste forms are critical to the release of radionuclides from the waste packages. These topics were addressed by the U.S. Nuclear Regulatory Commission (NRC) in a number of key technical issues. Through the process of prelicensing consultation for issue resolution between the NRC and DOE, issues related to in-package environment and degradation of high-level waste glass and spent nuclear fuel cladding are considered closed-pending. To assist the NRC in the resolution of these issues and assessing their significance for postclosure performance of the proposed repository, the Center for Nuclear Waste Regulatory Analyses (CNWRA) performed studies to evaluate the effect of environment variables on the degradation of high-level waste glass and Zircaloy cladding and changes to solution chemistry through interactions with waste packages. The experimental results are used to evaluate the performance of glass waste form and Zircaloy cladding in the proposed repository. The purpose of this report is to present the CNWRA results and provide a review of the DOE model abstractions of high-level waste glass degradation, cladding degradation, and in-package chemistry that support the Total System Performance Assessment–Site Recommendation. In this context, a number of deficiencies are identified in the DOE approach and technical bases for use in performance assessment calculations. These deficiencies include the ranges of solution chemistry that could exist inside the waste packages and the consequences of the evolved in-package chemistry environments, the effect of waste package corrosion products that could influence corrosion mechanisms and dissolution rates of high-level waste glass, and the effect of environmental variables on localized corrosion and stress corrosion cracking of Zircaloy cladding. Existing agreements between the NRC and the DOE cover the path forward for resolving all of these deficiencies.

# CONTENTS


| Section | | | Page |
|---|---|---|---|
| PREVIOUS REPORTS IN SERIES | | | iii |
| ABSTRACT | | | v |
| FIGURES | | | ix |
| TABLES | | | xiii |
| ACKNOWLEDGMENTS | | | xv |
| EXECUTIVE SUMMARY | | | xvii |
| 1 | INTRODUCTION | | 1 |
| 2 | DEGRADATION OF THE VITRIFIED HIGH-LEVEL WASTE | | 5 |
| | 2.1 | DOE INVESTIGATIONS | 5 |
| | | 2.1.1 High-Level Waste Glass Degradation | 5 |
| | | 2.1.2 DOE Model Abstraction | 7 |
| | | 2.1.3 Assessment of the DOE Approach | 13 |
| | 2.2 | CNWRA INVESTIGATIONS | 14 |
| | | 2.2.1 Effect of Corrosion Products on Glass Leaching | 15 |
| | | 2.2.2 Dissolution Kinetics and Model Abstraction | 25 |
| | | 2.2.3 CNWRA Approach to Performance Estimation | 30 |
| 3 | DEGRADATION OF COMMERCIAL SPENT NUCLEAR FUEL CLADDING | | 33 |
| | 3.1 | DOE INVESTIGATIONS | 33 |
| | | 3.1.1 DOE Model Abstraction | 34 |
| | | 3.1.2 Assessment of the DOE Approach | 35 |
| | 3.2 | CNWRA INVESTIGATIONS | 37 |
| | | 3.2.1 As-Polished Zircaloy-4 | 37 |
| | | 3.2.2 Hydrothermally Oxidized Zircaloy-4 | 45 |
| | | 3.2.3 CNWRA Model Abstraction and Performance Estimation | 52 |
| 4 | IN-PACKAGE CHEMISTRY | | 55 |
| | 4.1 | DOE INVESTIGATIONS | 55 |
| | | 4.1.1 DOE Model Abstraction | 55 |
| | | 4.1.2 Assessment of the DOE Approach | 59 |
| | 4.2 | CNWRA INVESTIGATIONS | 62 |
| | | 4.2.1 Evolution of Solution Chemistry in Pits and Crevices | 63 |
| | | 4.2.2 Effect of Waste Package Internal Geometry on Solution Chemistry | 64 |
| 5 | FUTURE WORK | | 73 |
| 6 | SUMMARY AND CONCLUSIONS | | 75 |
| | 6.1 | DEGRADATION OF THE VITRIFIED HIGH-LEVEL WASTE | 75 |
| | 6.2 | DEGRADATION OF COMMERCIAL SPENT NUCLEAR FUEL CLADDING | 76 |
| | 6.3 | IN-PACKAGE CHEMISTRY | 76 |
| 7 REFERENCES | | | 79 |

# FIGURES


| Figure | | Page |
|---|---|---|
| 2-1 | Plots of Dissolution Rates Using Eqs. (2-3) and (2-4) Versus pH at Four Different Temperatures | 9 |
| 2-2 | Glass Dissolution Rate Calculated Using Eq. (2-3) Versus Measured Stage III Reaction Rates | 12 |
| 2-3 | Range of Glass Degradation Rate Verses Time Since the Waste Package First Perforated | 12 |
| 2-4 | Cumulative Normalized Leach Concentration for Boron Versus Time for WVDP Ref. 6 and DWPF Blend 1 Glasses in Various Solutions at 90 °C | 19 |
| 2-5 | Normalized Leach Rate for Boron Versus Time for WVDP Ref. 6 and DWPF Blend 1 Glasses in Various Solutions at 90 °C | 20 |
| 2-6 | Normalized Leach Rates for Various Elements as a Function of Time for WVDP Ref. 6 Glass in 0.25 M $FeCl_3$ Solution at 90 °C | 21 |
| 2-7 | Leachate pH Versus Time for WVDP Ref. 6 Glass in Various Solutions at 90 °C | 21 |
| 2-8 | Linear Regression Plot of Normalized Leach Rate for Boron Versus Leachate pH after First Solution Replacement for WVDP Ref. 6 and DWPF Blend 1 Glasses in Various Solutions at 90 °C | 22 |
| 2-9 | Scanning Electron Micrographs of WVDP Ref. 6 Glass (a) Before Leaching and After Leaching in (b) Deionized Water and (c) 0.25 M $FeCl_3$ Solution at 90 °C | 24 |
| 2-10 | Normalized Leach Rate for Various Elements Versus Leachate pH after First Solution Replacement for (a) WVDP Ref. 6 and (b) DWPF Blend 1 Glasses at Various Temperatures | 26 |
| 2-11 | Linear Regression of Normalized Leach Rate for Boron Versus Leachate pH after First Solution Replacement for (a) WVDP Ref. 6 and (b) DWPF Blend 1 Glasses at Various Temperatures | 27 |
| 2-12 | Comparison of Calculated Glass Dissolution Rates Using Different Rate Expressions | 29 |
| 2-13 | Calculated Mean Dose Rates for Three Cases from 200 Realizations | 31 |
| 2-14 | Calculated Release Rates for Various Radionuclides for the Nominal Case from 200 Realizations | 32 |
| 2-15 | Calculated Release Rates for Various Radionuclides for Case A from 200 Realizations | 32 |
| 3-1 | Potentiodynamic Polarization Curve for Zircaloy-4 in Deaerated, Simulated J–13 Well Water (pH 8.4) Containing 0.1 M NaCl at 95 °C | 38 |
| 3-2 | Scanning Electron Microscopy Micrograph Showing Typical Pitting Morphology Observed after Polarization of Zircaloy-4 | 39 |
| 3-3 | Breakdown Potentials as a Function of Chloride Concentration for Zircaloy-4 in Simulated J–13 Well Water; $E_b(V_{SHE}) = 0.079–0.131 \log [Cl^-]$ | 39 |
| 3-4 | Repassivation Potentials as a Function of Chloride Concentration for Zircaloy-4 in Simulated J–13 Well Water; $E_{rp}(V_{SHE}) = 0.038–0.083 \log [Cl^-]$ | 40 |

# FIGURES (continued)


| Figure | | Page |
|---|---|---|
| 3-5 | Effect of pH on the Critical Potentials Measured for Zircaloy-4 in Simulated J–13 Well Water Containing 0.1 M NaCl at 95 °C | 42 |
| 3-6 | Breakdown and Repassivation Potentials Measured in Solutions with and without J–13 Well Water Anions as Well as Higher Concentrations of Inhibiting Anions | 42 |
| 3-7 | Effect of $H_2O_2$ and $FeCl_3$ Additions on the Open Circuit Potential of a Polished Zircaloy-4 Specimen in Simulated J–13 Well Water Containing 1 M NaCl at 25 and 95 °C | 44 |
| 3-8 | Cyclic Potentiodynamic Polarization Curves for Mechanically Polished and Hydrothermal Oxide Covered Specimens of Zircaloy-4 in Deaerated 0.1 M NaCl Solution at 95 °C Using a Scan Rate of 0.167 mV/s | 45 |
| 3-9 | Breakdown Potentials as a Function of Chloride Concentration for Mechanically Polished Specimens of Zircaloy-4 in Simulated J–13 Well Water Compared to Values Obtained for Specimens Covered with a Hydrothermally Grown Oxide | 46 |
| 3-10 | Anodic Current Density as a Function of Time for Mechanically Polished and Oxide Covered Specimens of Zircaloy-4 with Various Film Thicknesses in 0.1 M NaCl Solution at 95 °C under an Applied Potential of 0.125 $V_{SHE}$ | 47 |
| 3-11 | Low Magnification Photograph Showing the Typical Morphology of the Localized Corrosion Observed after Anodic Potentiostatic Polarization of Zircaloy-4 Specimen Covered with a Hydrothermally Grown Oxide Film in Chloride Containing Solutions at Potentials above $E_{rp}$ | 48 |
| 3-12 | Scanning Electron Microscopy Micrograph Showing a Cross-Sectional View of the Localized Corrosion Observed after Anodic Potentiostatic Polarization of Zircaloy-4 Specimen Covered with a Hydrothermally Grown Oxide Film in Chloride Containing Solutions at Potentials above $E_{rp}$ | 49 |
| 3-13 | Scanning Electron Microscopy Micrograph Showing a More Detailed View of the Localized Corrosion and the Appearance of the Corrosion Products Observed after Anodic Potentiostatic Polarization of Zircaloy-4 Specimen Covered with a Hydrothermally Grown Oxide Film in Chloride Containing Solutions at Potentials above $E_{rp}$ | 49 |
| 3-14 | X-Ray Diffraction Pattern of the Corrosion Products Found in a Pit of Zircaloy-4 Showing, in Addition to the Zircaloy Peaks, the Assignment of the High Intensity Peak to $ZrH_{0.25}$ | 50 |
| 3-15 | Effect of $H_2O_2$ and $FeCl_3$ Additions on the Open Circuit Potential of Zircaloy-4 Specimens, Covered with Hydrothermally Grown Oxide Films of Different Thickness, in Air Saturated 0.1M NaCl Solution at 95 °C | 51 |
| 3-16 | Calculated Failure Times for Zircaloy Cladding Failure Simulated Using the Total-system Performance Assessment Code | 52 |
| 4-1 | A Typical pH Response Surface for the Commercial Spent Nuclear Fuel Waste Packages for 0–2,000 Years Post Breach | 57 |

# FIGURES (continued)


| Figure | | Page |
|---|---|---|
| 4-2 | The pH-Time History for the Commercial Spent Nuclear Fuel Waste Packages | 57 |
| 4-3 | The pH-Time History for the Codisposal Waste Packages | 58 |
| 4-4 | Sensitivity Analysis Showing pH-Time Trajectories for the Commercial Spent Nuclear Fuel Waste Packages Using Zero A516 Steel Dissolution Rate | 60 |
| 4-5 | Sensitivity Analysis Showing pH-Time Trajectories for the Codisposal Waste Packages Using Zero Glass Dissolution Rate | 60 |
| 4-6 | Schematic of the Test Cell That Simulates Internal Waste Package Geometry for In-Package Chemistry Study | 65 |
| 4-7 | Anodic Current Transients Measured on Type 316L Stainless Steel under Potentiostatic Conditions in 0.028 M $Cl^-$ Solution at 20 °C | 67 |
| 4-8 | Anodic Current Transients Measured on Type 316L Stainless Steel under Potentiostatic Conditions in 0.028 M $Cl^-$ Solution at 60 °C | 67 |
| 4-9 | Anodic Current Transients Measured on Type 316L Stainless Steel under Potentiostatic Conditions in 0.028 M $Cl^-$ Solution at 90 °C | 68 |
| 4-10 | Anodic Current Density Measured on Type 316L Stainless Steel under Potentiostatic Conditions in 0.028 M $Cl^-$ Solution for Various Temperatures | 69 |
| 4-11 | Total Charge Measured on Type 316L Stainless Steel under Potentiostatic Conditions in 0.028 M $Cl^-$ Solution for Various Temperatures | 69 |
| 4-12 | Anodic Current Density and Total Charge as a Function of Time Measured on Type 316L Stainless Steel at 200 $mV_{SHE}$ in 0.028 M $Cl^-$ Solution at 20 °C | 71 |

# TABLES


| Table | | Page |
|---|---|---|
| 2-1 | Normalized Boron Dissolution Rate (NR), Al Content, and pH from MCC–1 Tests and Intrinsic Rate Constant for Selected High-Level Waste Glasses | 10 |
| 2-2 | Rate and pH from PCT-A Tests and Calculated $\log_{10} K_{eff}$ Values for Selected High-Level Waste Glasses | 11 |
| 2-3 | Chemical Compositions of Test Glasses (in Weight Percent) | 16 |
| 2-4 | Glass Leaching Solution Test Matrix | 17 |
| 2-5 | Chemical Compositions of Precipitates from Leaching of WVDP Ref. 6 Glass in Various Solutions (in Weight Percent) | 18 |
| 2-6 | Chemical Compositions from Surface Regions of WVDP Ref. 6 Glass before and after leaching (in Weight Percent) | 23 |
| 2-7 | Glass Dissolution Model Parameters Summary | 28 |
| 2-8 | Comparison of Glass Dissolution Model Parameters | 29 |
| 3-1 | Composition of Zircaloy-4 Utilized in Current Study (in Weight Percent) | 37 |
| 3-2 | Weight Gain and Resulting Oxide Thickness During Hydrothermal Oxidation of Zircaloy-4 | 47 |
| 4-1 | Criteria Used to Define the pH Ranges for Commercial Spent Nuclear Fuel Package for Each Abstracted Time Period | 58 |
| 4-2 | Criteria Used to Define the pH Ranges for Codisposal Fuel Package for Each Abstracted Time Period | 59 |
| 4-3 | Total Charge Measured on Type 316L Stainless Steel in 0.028 M $Cl^-$ at Various Applied Potentials and Temperatures for Each In-Package Chemistry Test | 66 |
| 4-4 | Cation Concentrations from Anodic Dissolution and Selectivity Coefficient (Z) for Type 316L Stainless Steel Tested at 200 $mV_{SHE}$ in 0.028 M $Cl^-$ Solution at 20 °C | 70 |
| 4-5 | Solution pH Measured by Micro-Reference Electrode for Type 316L Stainless Steel Tested at Various Applied Potentials in 0.028 M $Cl^-$ at 20 °C | 72 |

# ACKNOWLEDGMENTS

This report was prepared to document work performed by the Center for Nuclear Waste Regulatory Analyses (CNWRA) for the U.S. Nuclear Regulatory Commission (NRC) under Contract No. NRC–02–97–009. The activities reported here were performed on behalf of the NRC Office of Nuclear Material Safety and Safeguards, Division of Waste Management. The report is an independent product of the CNWRA and does not necessarily reflect the views or regulatory position of the NRC.

The authors gratefully acknowledge L. Yang for technical review, the programmatic review of B. Sagar, and the editorial reviews of C. Cudd and A. Woods. Appreciation is due J. Gonzalez for assistance in preparing this report.

**QUALITY OF DATA**: Sources of data are referenced in each chapter. CNWRA-generated laboratory data contained in this report meet quality assurance requirements described in the CNWRA quality assurance manual. Data from other sources, however, are freely used. The respective sources of non-CNWRA data should be consulted for determining levels of quality assurance.

**ANALYSES AND CODES**: The NRC/CNWRA Total-system Performance Assessment (TPA) Code Version 4.1 was used for the performance analyses presented in this report. This code is controlled under the requirements of the CNWRA Technical Operating Procedure (TOP)–018.

# EXECUTIVE SUMMARY

The U.S. Department of Energy (DOE) identified limited release of radionuclides from the engineering barriers as one of five system attributes that contribute significantly to performance of the proposed high-level waste repository at Yucca Mountain, Nevada. Among the factors identified by the DOE in controlling the radionuclide concentration limits in water for postclosure safety are commercial spent nuclear fuel cladding performance and waste form performance. The chemistry of the aqueous environment inside the breached waste packages and the performance of spent nuclear fuel cladding and waste forms are critical to the release of radionuclides from the waste packages. While the DOE included the effect of in-package chemistry on the degradation of waste package internal components, the lack of consideration of the uncertainties associated with the evolution of the in-package environment on waste form dissolution and corrosion of spent nuclear fuel cladding may result in nonconservative estimates of some radionuclide release rates. Two of the 14 integrated subissues the U.S. Nuclear Regulatory Commission (NRC) identified to be abstracted into a performance assessment are the quantity and chemistry of water contacting waste packages and waste forms and radionuclide release rates and solubility limits. These two integrated subissues have been addressed in detail within the framework of the Container Life and Source Term Key Technical Issue Subissues 3 and 4 and the Evolution of the Near-Field Environment Key Technical Issue Subissue 3. Through the process of prelicensing consultation for issue resolution between the DOE and NRC, the statuses of these three subissues are considered closed-pending according to DOE and NRC agreements, which means that the DOE approach and supporting information are appropriate, but additional information is needed for the NRC staff to have the degree of confidence required for regulatory decision making.

To assist the NRC in resolving these subissues and assessing their significance for postclosure performance of the proposed repository, the Center for Nuclear Waste Regulatory Analyses (CNWRA) performed studies to evaluate the effects of the in-package environment on the degradation behavior and predicted performance of high-level waste glass and Zircaloy cladding. The effect of the internal waste package geometry on the evolution of the in-package solution chemistry was also examined. This report presents the results of the work conducted by the CNWRA and a review of the DOE model abstractions in the areas of high-level waste glass, Zircaloy cladding, and in-package chemistry.

In spite of the small radionuclide inventory of high-level waste glass, its contribution to performance assessment could be significant if the radionuclide release rate from high-level waste glass is higher than that from spent nuclear fuel. The high-level waste glass degradation process involves contact of reactants (i.e., groundwater or water vapor) to the glass surface, chemical reaction between the reactants and glass surface, and transport of reaction products away from the reaction zone. The dissolution rate is controlled by the combination of these processes and depends on factors such as chemical composition of the glass and solubilities of the reaction products, exposed surface area, temperature, pH, relative humidity, and chemical compositions of the aqueous environment. A review of the DOE abstraction of radionuclide release rates from glass waste forms in the Total System Performance Assessment–Site Recommendation indicated that DOE has not reasonably accounted for the range of environmental conditions expected inside breached waste packages. In addition, the DOE model abstraction ignores the presence of corrosion products from the dissolution of waste package internal components that could influence glass degradation. The CNWRA has conducted leaching experiments of simulated high-level waste glasses in aqueous solutions of

$FeCl_2$ and $FeCl_3$ resembling the internal waste package environments. The presence of corrosion products such as iron cations, as well as the resultant solution pH, significantly enhances the dissolution of high-level waste glass. Model abstraction and performance assessment analyses using rate expressions that take into account the effect of corrosion products showed that the presence of corrosion products enhances glass dissolution and the subsequent release of radionuclides to the environment. DOE should demonstrate that its abstraction of high-level waste glass degradation captures the range of chemical compositions of water, including the effect of nitric acid formation caused by radiolysis and the effect of interactions with waste package corrosion products, such as FeOOH, $FeCl_2$, and $FeCl_3$, in the anticipated pH range. DOE agreed to provide additional information on high-level waste glass degradation in agreements CLST 3.02, CLST 3.03, and CLST 4.01.

The DOE considered the most likely forms of degradation that may affect the integrity of the commercial spent nuclear fuel cladding during disposal conditions in the proposed repository. DOE developed a model to evaluate Zircaloy cladding degradation as part of the waste form degradation model to determine the rate at which the commercial spent nuclear fuel matrix is exposed to the in-package aqueous environment. The degradation of the commercial spent nuclear fuel cladding is assumed to occur in two stages. The first stage of degradation corresponds to rod failure as a result of perforation of the cladding. The second stage is caused by the progressive exposure of the spent nuclear fuel matrix as a result of splitting (wet unzipping) of the cladding caused by oxidation of the irradiated $UO_2$ pellets by an aqueous environment. The technical bases provided to support the modeling of cladding degradation as a result of both the corrosion by fluoride and the internal stress corrosion cracking by iodine are limited, and no alternative models have been considered for localized corrosion and external stress corrosion cracking. This model could be acceptable if the DOE can demonstrate in the analysis and model report that the environmental conditions are not conducive to localized corrosion or stress corrosion cracking induced by chloride because (i) the chloride concentration is too low, (ii) the corrosion potential is lower than the pitting potential, or (iii) anionic species such as nitrate are present at a sufficiently high concentration ratio with respect to chloride that can act as efficient localized corrosion inhibitors. The hoop stress calculations used to evaluate creep are applicable to the assessment of chloride-induced stress corrosion cracking. The CNWRA evaluated the corrosion behavior of Zircaloy-4 under a wide range of conditions. Based on this work, it was found that Zircaloy-4, either mechanically polished or covered with a hydrothermally grown oxide layer, is susceptible to pitting corrosion in chloride-containing solutions at concentrations above 0.001 M and potentials higher than a repassivation potential. The presence of the hydrothermally grown oxide was not observed to influence the repassivation potential but did increase the breakdown potential and the corrosion potential. The corrosion potential can reach and even exceed the repassivation potential in $FeCl_3$-containing solutions, and, therefore, pitting corrosion of Zircaloy cladding may occur after a long time interval under natural corroding conditions inside a breached container. Additional studies on the kinetics of the cathodic reactions on oxide covered surfaces are needed to evaluate the long-term performance of cladding as an additional metallic barrier to radionuclide release in the disposal of spent nuclear fuel. DOE agreed to provide additional information on cladding degradation in agreements CLST 3.06, CLST 3.07, and CLST 3.09. Hydride embrittlement covered under agreement CLST 3.08 is not discussed in this report because hydrogen entry only occurs under reactor operating conditions. No hydrogen entry is expected under disposal conditions in the oxidizing in-package environment.

The composition of the groundwater entering the waste package can be influenced and modified by natural processes such as evaporation, reactions with host rock, and components of the engineered barriers such as drip shield and waste package materials. Variables, such as pH, carbonate concentration, and redox potential, are influenced by interactions of groundwater with engineered barriers in the repository and have a substantial effect on waste package and waste form corrosion. To study the sensitivity of incoming fluid composition inside the waste package on the outgoing fluid composition, DOE analyzed the interactions between waste form and several variations of groundwater compositions using EQ 3/6. The approach taken by the DOE in determining the range of in-package chemistry may not be appropriate. The DOE in-package chemistry model and abstraction lump various corrosion processes together. This approach could mask effects of waste package corrosion on the groundwater chemistry, and hence, underestimate shifts in pH and redox potential. Additionally, the possible formation of locally aggressive environments in crevices and tight spaces inside the waste package that could enhance the degradation of waste forms and the solubility of radionuclides has been neglected. The CNWRA performed experimental investigations of changes in the solution chemistry through interactions with waste package internal structural components using a test cell that simulates the internal geometry of the waste package. Preliminary results indicated that interactions of waste package internal structural components with the incoming water may have significant influence on the evolution of water chemistry and the subsequent corrosion of waste forms such as spent nuclear fuel. The range of environmental conditions to be expected inside breached waste packages needs to be experimentally determined by the DOE to validate the predictions from the in-package chemistry model. DOE agreed to provide additional information on in-package chemistry in agreements CLST 3.01, CLST 3.02, CLST 3.03, CLST 3.04, CLST 3.05, ENFE 3.03, ENFE 3.04, TSPAI 3.08 and TSPAI 3.14.

This report identifies a number of deficiencies in the DOE approach and technical bases provided for high-level waste glass degradation, cladding degradation, and in-package chemistry that support the Total System Performance Assessment–Site Recommendation. These deficiencies include the ranges of solution chemistry that could exist inside the waste packages and the consequence of the evolved environmental conditions, the effect of waste package corrosion products that could influence corrosion mechanisms and degradation rates of high-level waste glass, and the effect of in-package aqueous environments on localized corrosion and stress corrosion cracking of Zircaloy cladding. As part of the issue resolution process, DOE has agreed to provide additional analyses and documentation to address these deficiencies to produce an adequate basis for NRC to conduct its licensing review. Additional efforts are planned to further evaluate the DOE analyses and documentation that will be provided according to the DOE and NRC agreements. These efforts include analyzing the effects of incoming water composition, localized corrosion, and corrosion products on the evolution of the in-package solution chemistry; measuring the dissolution rates of waste forms under the evolved chemical environments; and examining localized corrosion of Zircaloy cladding in the presence of chemical species generated by corroding waste packages.

# 1 INTRODUCTION

The U.S. Department of Energy (DOE) identified limited release of radionuclides from the engineering barriers as one of five system attributes that contribute significantly to performance of the proposed high-level waste repository at Yucca Mountain, Nevada [Civilian Radioactive Waste Management System Management and Operating Contractor (CRWMS M&O, 2000a)]. Among the factors identified by the DOE in controlling the radionuclide concentration limits in water for postclosure safety are commercial spent nuclear fuel cladding performance and waste form performance. Cladding performance pertains to the role of cladding in limiting wetting of the spent nuclear fuel waste form. Waste form performance relates to the rate of mobilization of radionuclides caused by degradation of the waste form itself such as the uranium oxide ceramic matrix or high-level waste glass waste form. Radionuclide release from the engineered barrier subsystem involves several processes, contact of liquid water with the waste form, the dissolution of the waste form, the solubility limit of radionuclides, transport in liquid water, and interaction with engineered barrier materials. The quantity and chemistry of the water inside the breached waste packages and its contact with the cladding and waste forms are critical to the release of radionuclides from the waste package. As noted by the Advisory Committee on Nuclear Waste,[1,2] chemical mechanisms and processes play a dominant role in the performance of both engineered and natural barriers. It is important to understand the technical bases and performance impacts of chemical processes affecting the engineered barrier system and natural system to determine that the repository will meet the regulatory requirements. Additionally, the U.S. Nuclear Waste Technical Review Board (Nuclear Waste Technical Review Board, 1998) and others (Budnitz, et al., 1999) suggested that additional efforts are needed to predict the ranges of local environmental conditions that could exist inside waste packages and the probabilities of their occurrence.

In the DOE Total System Performance Assessment–Site Recommendation analysis (CRWMS M&O, 2000b), the waste form degradation model contains an in-package chemistry component to predict ranges of chemical conditions inside the waste package to better characterize the uncertainty in the degradation of the cladding and waste form. However, consideration of the uncertainties associated with the evolution of the in-package environment on waste form dissolution and corrosion of Zircaloy cladding is inadequate and may result in nonconservative estimates of some radionuclide release rates. DOE agreed to provide additional information according to agreements CLST 3.01, CLST 3.02, CLST 3.03, CLST 3.04, CLST 3.05, CLST 3.06, CLST 3.07, CLST 3.09, CLST 4.01, ENFE 3.03, ENFE 3.04, TSPAI 3.08 and TSPAI 3.14.

In-package chemistry and degradation of high-level waste glass and cladding are considered under two integrated subissues identified by the U.S. Nuclear Regulatory Commission (NRC) (NRC, 2001a):

ENG 3—Quantity and chemistry of water contacting waste packages and waste forms

---

[1]Garrick, B.J. "Comments on the Importance of Chemistry in the Near Field to DOE's Yucca Mountain Repository License Application." Letter (January 11) to R.A. Meserve, NRC. Washington, DC: NRC. 2000.

[2]Hornberger, G.M. "Review of Chemistry Issues and Related NRC Staff Capability for the Proposed High-Level Waste Repository at Yucca Mountain." Letter (August 13) to R.A. Meserve, NRC. Washington, DC: NRC. 2001.

ENG 4—Radionuclide release rates and solubility limits

These two integrated subissues, which are abstracted into a performance assessment, have been addressed in detail within the framework of two Container Life and Source Term Key Technical Issue Subissues (NRC, 2001b) and one Evolution of the Near-Field Environment Key Technical Issue Subissue (NRC, 2000):

- Container Life and Source Term: Subissue 3—The rate at which radionuclides in spent nuclear fuel are released from the engineered barrier subsystem through the oxidation and dissolution of spent nuclear fuel

- Container Life and Source Term: Subissue 4—The rate at which radionuclides in high-level waste glass are released from the engineered barrier subsystem

- Evolution of the Near-Field Environment: Subissue 3—Effects of coupled thermal-hydrological-chemical processes on the chemical environment for radionuclide release

Through the process of prelicensing issue resolutions between the NRC and DOE, the statuses of these three subissues are considered closed-pending according to DOE and NRC agreements.[3,4]

In support of the NRC high-level waste program on issues that are critical to the postclosure performance of the proposed repository, the Center for Nuclear Waste Regulatory Analyses (CNWRA) performed studies to evaluate the effects of in-package environment on the degradation behavior and predicted performance of the high-level waste glass and Zircaloy cladding. The effect of the internal waste package geometry on the evolution of the in-package solution chemistry is also examined. This report presents the results from the work conducted by the CNWRA and provides a review of the DOE model abstractions in the areas of high-level waste glass, Zircaloy cladding, and in-package chemistry. The experimental results presented in this report will be used for performance assessment calculations to predict the performance of high-level waste glass waste form and Zircaloy cladding in the proposed repository.

Chapter 2 presents issues related to the degradation of the vitrified high-level waste. A review of high-level waste glass degradation processes, the abstraction of the DOE high-level waste glass degradation model used in performance assessment calculations, and an assessment of the model abstraction are provided followed by a summary of the glass leaching work at the CNWRA to evaluate the effect of waste package corrosion products on degradation of high-level waste glass. The performance of high-level waste glass expected under repository conditions is analyzed, using the model parameters derived from these leaching experiments, and compared with the other high-level waste glass case, using the model parameters from the DOE, and a nominal case for spent nuclear fuel.

---

[3]Schlueter, J.R. "NRC/DOE Technical Exchange and Management Meeting on Container Life and Source Term (September 12–13, 2000)." Letter (October 4) to S. Brocoum, DOE. Washington, DC: NRC. 2000.

[4]Reamer, C.W. "NRC/DOE Technical Exchange and Management Meeting on Evolution of the Near-Field Environment (January 9–12, 2001)." Letter (January 26) to S. Brocoum, DOE. Washington, DC: NRC. 2001.

A review of the DOE investigations on degradation of commercial spent nuclear fuel cladding is presented in Chapter 3. The technical bases provided to support the model abstractions for localized corrosion and stress corrosion cracking of Zircaloy cladding, particularly the range of chemical conditions that may prevail in the in-package aqueous environment, are reviewed. The effect of environmental variables on the corrosion behavior of Zircaloy-4, based on work conducted at the CNWRA, and sensitivity analyses to evaluate the performance of Zircaloy cladding are also reported.

The chemistry of water dripping into the waste packages for high-level waste disposal is important to the performance of engineered barriers and the subsequent release of radionuclides to the environment. Chapter 4 offers an overview of the DOE evaluation of the in-package chemistry and assessment of the abstractions for the Total System Performance Assessment–Site Recommendation. Experimental investigations conducted at the CNWRA to evaluate changes to the solution chemistry through interactions with waste package internal structural components are then discussed. This discussion is followed by a summary of conclusions and recommendations for future work to provide support to resolution of the related subissues prior to the license application.

# 2 DEGRADATION OF THE VITRIFIED HIGH-LEVEL WASTE

## 2.1 DOE INVESTIGATIONS

Radionuclide release from the engineered barrier subsystem will depend on several processes: the contact of liquid water with the waste form, the dissolution of the waste form, the solubility limit of radionuclides, transport in liquid water, and interaction with engineered barrier materials. The waste form will begin to decompose once it comes into contact with air, water vapor, and liquid water. In spite of a small radionuclide inventory of high-level waste glass, its contribution to repository performance could be significant if the radionuclide release rate from high-level waste glass is higher than that from spent nuclear fuel (e.g., radionuclide release in colloidal form or pulse release of radionuclides from the hydrated surface layer) (NRC, 2001b). A review of the DOE abstraction of radionuclide release rates from glass waste form presented in the Total System Performance Assessment–Site Recommendation (CRWMS M&O, 2000b) is provided in this chapter.

### 2.1.1 High-Level Waste Glass Degradation

The high-level waste glass corrosion process involves (i) transport and contact of a reactant (i.e., groundwater or water vapor) to the glass surface, (ii) a chemical reaction between the reactant and glass surface, and (iii) transport of reaction products away from the reaction zone.

The high-level waste glass corrosion rate is controlled by the combination of these three processes and depends on factors such as chemical composition of the glass and solubilities of the reaction products in the surrounding fluids, exposed surface area, temperature, pH, relative humidity, and chemical composition of the aqueous environment. The long-term corrosion behavior can be divided into three distinct stages. In Stage I, referred to as the short-term stage, the chemical potential gradient between the glass components and local environment is the steepest. The glass components are released into the local environment at a comparatively high rate. The soluble components, such as boron and alkalis, are released at a higher rate compared with other components, such as silica and aluminum oxide. This higher release rate results in the formation of a layer on the glass surface depleted of soluble components. This layer is often called the altered surface layer. In Stage II, the intermediate stage, the corrosion rate decreases as the concentration of reaction products, particularly hydrated forms of silica, increases in the solution in close contact with the glass. In Stage III, the long-term stage, the glass corrosion rate is further affected because of the reprecipitation of secondary phases that exceed their solubility limits in the altered zone, such as zeolites and clays. Physical processes, such as crystallization, cracking, or exfoliation of the altered surface layers, that occur in Stage III, could influence the glass corrosion rate, as well as the release and transport of colloids and their associated radionuclides. Changes in dissolution rate also depend on the identity, distribution, and surface area of the secondary phases. The transition from one stage to another depends on the glass composition and the local environment. It may take months or years for a highly durable glass to reach Stage II, whereas a nondurable glass may reach Stage II within hours or days.

Several long-term high-level waste glass corrosion studies have been conducted in the past 20 years, and research is currently being conducted at Argonne National Laboratory on simulated high-level waste glasses, simulated glasses doped with relevant radionuclides, and

fully radioactive glasses relevant to the proposed Yucca Mountain repository. Drip tests, designed to simulate slow flow through the breached canisters, have been used by Fortner and Bates (1996) and Fortner, et al. (1997) to study the long-term performance of actinide-doped high-level waste glasses produced by the West Valley Demonstration Project and the Defense Waste Processing Facility. The long-term product consistency test, PCT-B, designed to simulate fully immersed conditions, has been used by Ebert and Tam (1997) to study long-term performance of the defense waste processing facility glasses. In addition, vapor hydration tests, designed to replicate a natural alteration process, are used by Luo, et al. (1997) to compare the dissolution behavior of the Defense Waste Processing Facility glasses with that of naturally occurring basalt glasses. It is evident from the continuing studies at the Argonne National Laboratory that the test conditions (i.e., immersion versus dripping, flow rate, environment composition) strongly influence glass corrosion rates, and it is prudent to develop different tests to characterize various conditions that may exist in the repository. The abstracted model used in performance assessment should appropriately incorporate the insight obtained from these studies. The effect of evolving environments in contact with waste packages has been discussed elsewhere (Brossia, et al., 2001), whereas several aspects of the internal waste package environment are discussed in Chapter 4.

The dissolution rate of the high-level waste glass decreases as the aqueous environment in close contact with the waste packages becomes saturated with glass matrix components, such as silica. Even though the glass corrosion studies referred to previously confirmed that net dissolution rate decreases as the surrounding aqueous environment becomes rich in high-level waste glass matrix components and is bounded by the Stage I corrosion rates, the drip test studies show a steep increase in the radionuclide release rate for plutonium and americium after 400 weeks (Fortner and Bates, 1996). The steep increase in radionuclide release rate was attributed to the spalling of radionuclide-containing colloids from the exposed high-level waste glass surface. If the drip tests conditions are expected to occur, the high-level waste glass abstraction models should account for such spikes in corrosion behavior because these spikes may have a significant effect on radionuclide release.

The dissolution kinetics of the primary phase, as commonly represented by the kinetics of boron release, determines the release rate of high-solubility radionuclides, such as Tc-99. The rate is dependent on the specific surface area of high-level waste glass. The higher the exposed surface area, the higher the radionuclide release. In the Total System Performance Assessment–Site Recommendation analysis (CRWMS M&O, 2000b), a constant value of $5.63 \times 10^{-5}$ $m^2/g$ for the specific surface area is used to calculate the glass dissolution rate. DOE claims that this constant value provides a conservative bound for the specific surface area. The technical basis for estimating the specific surface area for high-level waste glasses should be developed incorporating the effect of surface area on the dissolution rate.

Long-term corrosion studies indicate formation of secondary phases on the exposed surface of the high-level waste glasses. This process depends on the external environment. Long-term product consistency tests using simulated J–13 Well water show the formation of clay, calcium-phosphate, and (Ca, Tu, U) $TiO_3$ as secondary phases, whereas the vapor hydration tests show the accumulation of clay, zeolites, calcium-silicates, weeksite, and potassium-feldspar as secondary phases (Bates, 1998). The formation of different phases under such diverse test conditions is attributed to varying solution chemistries. These test conditions represent two environments that may exist at different times at the proposed repository. The formation of secondary phases may also be influenced by the corrosion

products resulting from corrosion of internal components of the waste packages. Secondary minerals play an important role in radionuclide release because they can incorporate low-solubility radionuclides, such as plutonium and americium, and control their solubility limits. They may also act to block the reactive surface area of the primary phase.

Natural analog studies, coupled with experimental data and geochemical modeling, provide another method of gaining confidence in analyzing long-term corrosion behavior of glasses. Natural analog studies are useful in evaluating the merits of extrapolating short-term experiments to longer time frames. Several natural glasses, especially basalt, have compositions comparable to the high-level waste glasses and have been subjected to conditions similar to those expected in the proposed repository (Ewing, et al., 1998; McKenzie, 1990). The characterization of secondary phases formed on these natural glasses can provide insights into the long-term dissolution behavior of high-level waste glasses.

In a recent study, Luo, et al. (1997) compared formation of secondary phases in the naturally occurring Hawaiian basaltic glasses with the results of vapor hydration tests conducted for 7 years on simulated basaltic and high-level waste borosilicate glasses. Luo, et al. (1997) concluded that secondary phases formed on both simulated natural glasses and high-level waste borosilicate glasses were similar to secondary phases observed in naturally occurring basaltic glasses, and vapor hydration tests could be used to simulate naturally occurring conditions.

Field data on naturally occurring glasses, combined with experimental data and models on the dissolution of high-level waste glasses, could be useful to demonstrate that long-term dissolution behavior under repository conditions can be represented by extrapolating results from short-term laboratory tests. Such data can be important to supplement and support the validity of the existing glass-dissolution data, generally obtained by short-term experiments.

### 2.1.2 DOE Model Abstraction

The basic form of the rate expression adopted by DOE (CRWMS M&O, 2000d) to describe the dissolution of waste glass immersed in water is given by a form of the transition state rate law as

$$\text{Rate}\ (\text{g/day}) = S\left[k_0 \bullet 10^{\eta \bullet \text{pH}} \bullet \exp\left(\frac{-E_a}{RT}\right) \bullet \left(1 - \frac{Q}{K}\right)\right] \qquad (2\text{-}1)$$

where

| | | |
|---|---|---|
| $S$ | — | surface area of glass immersed in water, in units of $m^2$ |
| $k_0$ | — | intrinsic dissolution rate, which depends only on glass composition, in units of $g/(m^2 \bullet day)$ |
| $\eta$ | — | pH dependence coefficient (dimensionless) |
| $E_a$ | — | effective activation energy, in units of kJ/mol |
| $R$ | — | gas constant, which is 8.314 J/(mol • K) |
| $T$ | — | absolute temperature in K |
| $Q$ | — | concentration of dissolved silica in the solution, in units of $g/m^3$ |

$K$ — a quasi-thermodynamic fitting parameter for glass equal to the apparent silica saturation value for the glass, in units of $g/m^3$

Equation (2-1) contains two main factors. The first factor is the forward rate, $k_0 \bullet 10^{\eta \cdot pH}$ exp $(-E_a/RT)$, which represents the dissolution rate in the absence of concentration effects of dissolved silica (and other aqueous species involved in the backward reaction), and the other factor is the reaction affinity term $(1 - Q/K)$, which quantifies the effects of dissolved silica. Because of the complexity in defining parameters and associated uncertainties, a simpler bounding approach was adopted by the DOE (CRWMS M&O, 2000d) that combined $(1 - Q/K)$ with $k_0$. Equation (2-2) was adopted as an abstraction for aqueous degradation of high-level waste glass in the Total System Performance Assessment–Site Recommendation analysis:

$$\frac{\text{Rate}}{S}\left(g/m^2 \bullet \text{day}\right) = k_{\text{eff}} \bullet 10^{\eta \bullet pH} \bullet \exp\left(\frac{-E_a}{RT}\right) \tag{2-2}$$

where

$$k_{\text{eff}} = k_0\left(1 - \frac{Q}{K}\right)$$

In Eq. (2-2) constant values for $k_{\text{eff}}$ are given to bound the range of the function $k_0$ $(1 - Q/K)$. This approach reduces the abstracted model to an equation involving four parameters ($\eta$, $E_a$, $S$, and $k_{\text{eff}}$) and two variables (pH and T).

The pH and the temperature dependences of the glass dissolution rate were determined using a single-pass flow-through test on a five-component glass (Knauss, et al., 1990). Tests were conducted at 20, 50, and 70 °C in pH-buffered solutions ranging from a pH of 1 to 13. The dissolution rate, based on the boron release rate, showed a V-shaped pH dependence, with the minimum occurring at the near-neutral pH of 7.1. Because of the discontinuity in the pH dependence of the log rate at intermediate pHs, separate rate expressions for the model abstraction were obtained for the acid range and the alkaline range.

For the low pH range ($pH < pH_m$)

$$\frac{\text{Rate}}{S}\left(g/m^2 \bullet \text{day}\right) = 10^{(14 \pm 0.5)} \bullet 10^{(-0.6 \pm 0.1) \bullet pH} \bullet \exp\left(\frac{-80 \pm 10}{RT}\right) \tag{2-3}$$

For the high pH range ($pH \geq pH_m$)

$$\frac{\text{Rate}}{S}\left(g/m^2 \bullet \text{day}\right) = 10^{(6.9 \pm 0.5)} \bullet 10^{(0.4 \pm 0.1) \bullet pH} \bullet \exp\left(\frac{-80 \pm 10}{RT}\right) \tag{2-4}$$

where $pH_m$, equal to 7.1, is the pH at which minimum dissolution rate occurs. The rates calculated with the mean values of the parameter ranges using Eqs. (2-3) and (2-4) are plotted in Figure 2-1 (CRWMS M&O, 2000c).

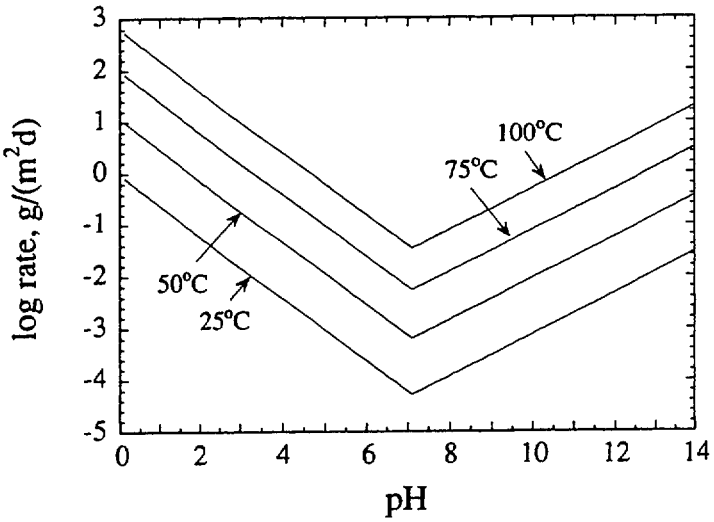


**Figure 2-1. Plots of Dissolution Rates Using Eqs. (2-3) and (2-4) Versus pH at Four Different Temperatures (Ebert, et al., 2001)**

The sensitivity of the intrinsic dissolution rate, $k_0$, to the aluminum content in the glass composition was measured experimentally by conducting short-term Materials Characterization Center tests (MCC–1), using the American Society for Testing and Materials Standard Test Method C1220 (American Society for Testing and Materials, 1999a) under conditions in which the affinity term was maintained close to one because of the absence of concentration effects from the products of the glass dissolution. The selected high-level waste glass compositions represented a likely range of compositions expected for disposal. Table 2-1 shows the normalized boron dissolution rates and the calculated $\log_{10} k_0$ values for nine glasses using the MCC–1 test method. The $k_0$ values were obtained using $\eta = 0.4$, $E_a = 80$ kJ/mol, and $1 - Q/K = 1$ in Eq. (2-1). Note that the pH at 90 °C was estimated by subtracting 0.8 from the pH measured at room temperature. The MCC–1 test results indicate that neither the forward dissolution rate nor the intrinsic dissolution rate is substantially affected by the amount of aluminum present in the waste glass compositions.

The effective rate constant that considers the effect of $(1 - Q/K)$ was experimentally determined using PCT-A following the American Society for Testing and Materials Standard Test Method C1285 (American Society for Testing and Materials, 1999b). The differences between dissolution rates measured using PCT-A and MCC–1 test methods reflect the effect of $(1 - Q/K)$. In PCT-A the value of $(1 - Q/K)$ decreases as a function of time, whereas in the MCC–1 tests, it is constant and equal to 1 as noted above. The $k_{eff}$ values were determined from the PCT-A rates using Eq. (2-2) with $\eta = 0.4$ and $E_a = 80$ kJ/mol. Table 2-2 shows the calculated values of $\log_{10} k_{eff}$ and the results from the PCT-A tests conducted, in addition to three other glasses, with the same nine glasses used for the MCC–1 tests.

**Table 2-1. Normalized Boron Dissolution Rate (NR), Al Content, and pH from MCC–1 Tests and Intrinsic Rate Constant for Selected High-Level Waste Glasses***

| Glass | Al (mass %) | pH† | NR (B) (g/m²•day) | log $k_0$‡ |
|---|---|---|---|---|
| LD6–5412 | 6.8 | 9.3 | 0.47 | 7.78 |
| Hanford-L | 6.3 | 9.5 | 0.97 | 8.02 |
| Hanford-D | 5.4 | 10.5 | 1.8 | 7.89 |
| WVDP Ref.6 | 3.2 | 9.5 | 0.69 | 7.87 |
| SRL 51S | 2.8 | 9.9 | 0.66 | 7.69 |
| SRL 165U | 2.2 | 9.6 | 1.0 | 7.99 |
| SRL 202U | 2.0 | 9.8 | 0.69 | 7.75 |
| SRL 131U | 1.7 | 9.8 | 1.2 | 7.99 |
| PNL 7668 | 0 | 9.2 | 1.1 | 8.19 |
| Mean± Std. Dev. | — | — | 0.95±0.40 | 7.91±0.16 |

*Ebert, W.L., J.C. Cunnane, and T.A. Thornton. "An HLW Glass Degradation Model for TSPA–SR." Proceedings of the 9th International High-Level Radioactive Waste Management Conference, Las Vegas, Nevada, April 29–May 3, 2001. LaGrange Park, Illinois: American Nuclear Society. 2001.
†pH measured at room temperature.
‡For $k_0$ in g/m² • day.

Based on this evaluation, data from the PCT-A tests were used to obtain bounding values for $k_{eff}$. The range of values for $\log_{10} k_{eff}$ used in the total system performance assessment calculations for dissolution in the alkaline range is expressed as 6.9 ± 0.5 (CRWMS M&O, 2000c). Note that the value of 6.9 is the mean plus one standard deviation, as given in Table 2-2. The low end of this range, which is 6.4, represents an average of the values in Table 2-2 for all glasses except SRL EA glass. The high-end of the range, which is 7.4, is the mean plus two standard deviations and bounds the values of all glasses that were evaluated in Table 2-2. Furthermore, the dissolution rate calculated using Eq. (2-2) with the mean parameter values was compared with the long-term dissolution rate (Stage III) for several of the glasses listed in Table 2-2, as shown in Figure 2-2. These results indicate that the rate calculated using Eq. (2-2) provides an upper bound to the measured Stage III rates. In the acidic range, similar analysis was not conducted because of the lack of available data. It was conservatively assumed that Knauss, et al. (1990) data, collected in absence of any feedback effects, can be used for predicting the dissolution behavior of glass in the acidic range. Acidic conditions are anticipated to occur through radiolysis of moist air, microbial effects, and corrosion of internal stainless steel components of the waste packages. The range of values of the intrinsic rate constant, which is 14.0 ± 0.5 determined based on Knauss, et al. (1990) data, is used as bounding values for $\log_{10} k_{eff}$ for dissolution in the acidic range.

| Table 2-2. Rate and pH from PCT-A Tests and Calculated $\log_{10} K_{eff}$ Values for Selected High-Level Waste Glasses* | | | |
|---|---|---|---|
| **Glass** | **pH †** | **PCT-A Rate ($g/m^2 \cdot day$)** | **$\log_{10} k_{eff}$ ‡** |
| LD6-5412 | 11.2 | 0.044 | 5.42 |
| Hanford-L | 10.96 | 0.095 | 6.28 |
| Hanford-D | 10.67 | 0.052 | 6.27 |
| WVDP Ref. 6 | 9.98 | 0.039 | 6.42 |
| SRL 51S | 10.66 | 0.038 | 6.15 |
| SRL 165U | 10.31 | 0.044 | 6.35 |
| SRL 202U | 10.42 | 0.043 | 6.29 |
| SRL 131U | 11.63 | 0.69 | 7.02 |
| PNL 7668 | 9.43 | 0.18 | 7.30 |
| SAN 60 | 9.8 | 0.055 | 6.65 |
| SRL 200S | 10.65 | 0.10 | 6.57 |
| SRL EA | 11.85 | 1.2 | 7.15 |
| Mean ± Std. Dev | — | 0.12 ± 0.19 (without SRL EA) | 6.43 ± 0.48 (without SRL EA) |

*Ebert, W.L., J.C. Cunnane, and T.A. Thornton. "An HLW Glass Degradation Model for TSPA–SR." Proceedings of the 9th International High-Level Radioactive Waste Management Conference, Las Vegas, Nevada, April 29–May 3, 2001. LaGrange Park, Illinois: American Nuclear Society. 2001.
†pH measured at room temperature.
‡ For $k_{eff}$ in $g/m^2 \cdot day$.

In the Total System Performance Assessment–Site Recommendation model (CRWMS M&O, 2000b), a value from each of the parameter distributions in Eqs. (2-3) and (2-4) is sampled and then the glass dissolution rates for both high pH and low pH cases are calculated. The larger of the two rates multiplied by the specific surface area, which is assumed to be $5.63 \times 10^{-5}$ $m^2/g$, gives the glass degradation rate. Results of the total system performance assessment calculations are shown in Figure 2-3. These calculations showed that the glass degradation rate can vary between $10^{-3}$/yr and $5 \times 10^{-8}$/yr. This extremely large uncertainty is associated with uncertainties in the glass modeling parameters in Eqs. (2-3) and (2-4). Note that the results shown in Figure 2-3 were obtained using a glass degradation model based on silicon release rate. While the uncertainty is expected to remain the same, the absolute values could change. Even with the large uncertainty, none of the modeling parameters show significant influence on dose because the contribution of dose from the codisposal package is an order of

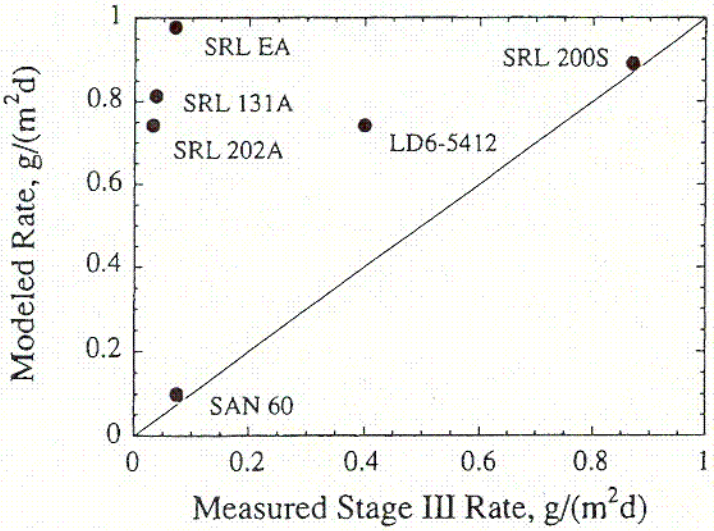


**Figure 2-2. Glass Dissolution Rate Calculated Using Eq. (2-3) Versus Measured Stage III Reaction Rates (Ebert, et al., 2001)**

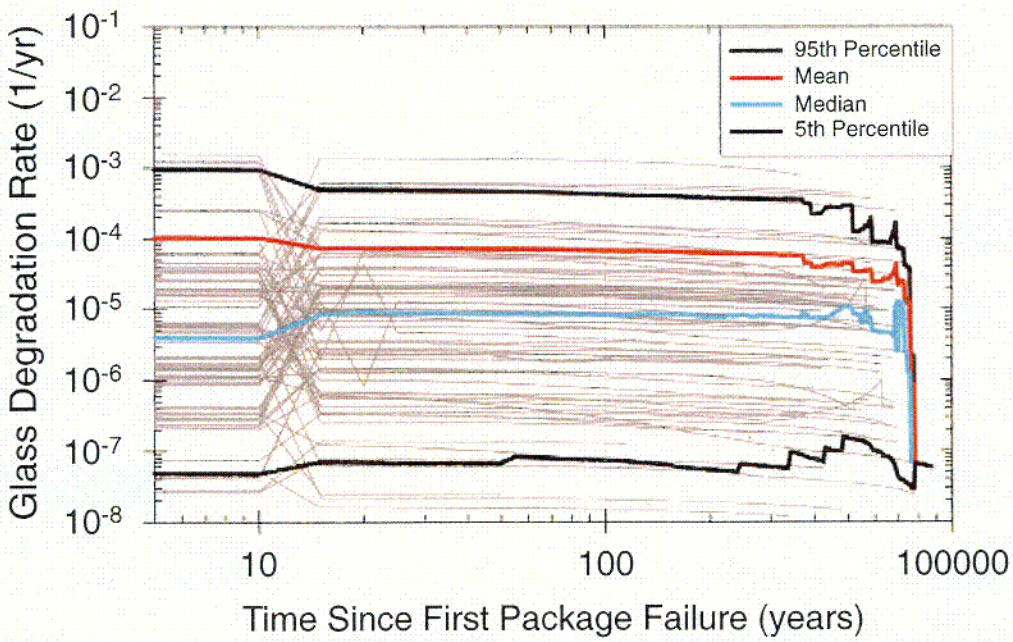


**Figure 2-3. Range of Glass Degradation Rate Verses Time Since the Waste Package First Perforated (CRWMS M&O, 2000b)**



C01

magnitude lower than that from the commercial spent nuclear fuel packages because of lower radionuclide inventory.

In the Supplemental Science and Performance Analyses (CRWMS M&O, 2001a), a sensitivity assessment was performed by assuming an uncertainty multiplier ranging from zero to one in the glass degradation model. The zero corresponds to the formation of an alteration layer that completely halts glass dissolution. For Total System Performance Assessment, a triangular distribution with a peak at $10^{-4}$ was used to evaluate the expected range of dissolution. This implies that the peak value is more likely than the bounds.

### 2.1.3 Assessment of the DOE Approach

The review of the proposed DOE abstraction for the Total System Performance Assessment indicates that this abstraction does not address the following aspects of the degradation process.

- DOE has not reasonably accounted for the range of environmental conditions expected inside breached waste packages in its abstraction of high-level waste glass degradation. Many studies and reviews have been reported on the effects of γ- and α-radiation on the dissolution or alteration of glass waste in moist-air systems (Burns, et al., 1982; Wronkiewicz, et al., 1994, 1997). Wronkiewicz, et al. (1997) reported that, although both γ- and α-radiation have no adverse effect on the dissolution of nuclear glass waste form immersed in water in contact with air, the radiation exposure of the glass waste form to humid air has resulted in a four to tenfold increase of alteration layer thickness relative to samples reacted without radiation exposure. Wronkiewicz, et al. (1997) suggested that the increases for the irradiated humid-air experiments appear to result from condensation of radiolytic-generated acids into the thin film of water contacting the glass surface. The radiolytic acids increased the rate of ion exchange between the glass and the thin film of condensate, resulting in accelerated corrosion rates for the glass. This finding should be considered by the DOE in its evaluation of the dissolution of glass waste form because, after the failure of the waste packages, the glass waste form may be exposed to a thin film of water under dripping conditions, and the radiation dose rate from the long-lasting α-emitters in the glass waste form still may be high enough to produce a significant effect. On the other hand, the radiolysis-induced nitric acid is a stable product under the repository conditions and, therefore, it may accumulate on the surface of the glass waste form and produce an acidic film of water even if the radiation field is low after failure of the waste package. DOE agreed to provide additional information in agreement CLST 3.03.

- DOE conducted limited experiments to determine the possible effect on glass dissolution of corrosion products that could result from dissolution of waste package internal components. These corrosion products, such as FeOOH, $FeCl_2$, and $FeCl_3$, could influence the mechanisms and rates of glass corrosion (Pan, et al., 2001). DOE stated that glass dissolution rates are strongly enhanced under some conditions by dissolved iron (CRWMS M&O, 1998a). The potential effect of iron is particularly important because corrosion of carbon steel and stainless steel inner waste package components could provide significant quantities of dissolved iron. DOE agreed to provide additional information in agreement CLST 3.02.

- The coefficients for the effect of pH as a variable were obtained using a dissolution rate based on silica released from single-pass flow-through tests in buffer solutions ranging from pH 1 to 13 (Knauss, et al., 1990). It is not evident from the Defense High-Level Waste Glass Degradation analysis and model report (CRWMS M&O, 2000c) whether the release rate data used in the calculations represent release rates after initial exposure or after 7, 14, or 28 days of exposure time. This difference is critical to ensure that coefficients for all parameters used in the abstracted equation are determined on the same basis. A parameter such as $k_{eff}$ is based on 7-day release rate data. DOE agreed to provide additional information in agreement CLST 4.01.

- The work of Advocat, et al. (1991), cited in the Defense High-Level Waste Glass Degradation Analysis and Model Report (CRWMS M&O, 2000c) for the effect of pH on release rate, indicates the presence of potassium ions on the surface of the corroded glass. Because the glass had no potassium, the presence of potassium ions is attributed to the ion exchange from KOH or $KH_2PO_4$ used for adjusting the pH of the solutions. The potassium ion, by virtue of its larger size, could lower the release rate from glass by retarding the migration of hydrogen ions in the glass matrix. Such comparisons could lead to erroneous conclusions. DOE agreed to provide additional information in agreement CLST 4.01.

- DOE assumed that the release rate is independent of glass composition. At best, one can state that the intrinsic dissolution rate, $k_0$, can be represented as an expected value of a distribution based on the anticipated variation in glass compositions using a risk-informed performance-based evaluation. In addition, the coefficients for pH and $E_a$ are assumed to be independent of glass composition. Again, the pH dependent coefficient and $E_a$ values should bound the variability expected from glass compositions. This analysis is acceptable as long as it captures the anticipated variability in glass composition. The long-term rates of glass dissolution are covered in agreement CLST 4.01.

To address the deficiencies identified by NRC staff in its review of the DOE abstraction of radionuclide release and solubility limits, DOE agreed at the DOE and NRC Technical Exchange on Container Life and Source Term[5] to provide additional documentation. This information will be provided as part of the issue resolution process, and if provided by DOE by the time of any license application, should furnish sufficient information for NRC to conduct its licensing review.

## 2.2 CNWRA INVESTIGATIONS

The DOE model abstraction for high-level waste glass degradation (CRWMS M&O, 2000d) ignores the presence of corrosion products from the dissolution of waste package internal components, such as FeOOH, $FeCl_2$, and $FeCl_3$, that could influence glass degradation. To evaluate the effects of the internal waste package environment on degradation of high-level waste, the leaching of simulated high-level waste glasses in the presence of corrosion products was investigated. From the glass leaching results, model parameters, including the intrinsic

[5]Schlueter, J.R. "NRC/DOE Technical Exchange and Management Meeting on Container Life and Source Term (September 12–13, 2000)." Letter (October 4) to S. Brocoum, DOE. Washington, DC: NRC. 2000.

dissolution rate, pH dependence coefficient, and activation energy, were determined. An empirical rate expression accounting for the effect of corrosion products on the glass dissolution behavior was used for performance assessment calculations to evaluate the effect of glass waste forms on radionuclide release for the proposed repository.

### 2.2.1 Effect of Corrosion Products on Glass Leaching

Two simulated high-level waste glasses, WVDP Ref. 6 and DWPF Blend 1, produced by the West Valley Demonstration Project and the Defense Waste Processing Facility, were used for dissolution studies. The environmental assessment standard reference glass, SRL EA, was tested as a baseline. The compositions of these three glasses are listed in Table 2-3. To simulate an internal waste package environment, deionized water containing either ferrous or ferric chlorides at concentrations of 0.0025 M and 0.25 M was used. While these test environments do not contain the ionic species present in J–13 Well water, the literature shows that dissolution of glass in deionized water is faster than that in J–13 Well water (McVay and Buckwalter, 1983). The relatively high leach rates observed in deionized water are attributed to solution composition effects because, as elemental concentrations increase in the leachate, elemental release rates decrease. The behavior in deionized water, therefore, bounds the effects of the species present in J–13 Well water.

The test matrix is shown in Table 2-4. All tests were conducted using a modified product consistency test method in accordance with American Society for Testing and Materials Standard Test Method C1285 (American Society for Testing and Materials, 1999b) except that the solutions were replaced at regular intervals. In these tests, 60-$cm^3$ perfluoroalkoxy TFE-fluorocarbon vessels were used. Approximately 3 g of crushed glass with a particle size distribution between -100 to +200 mesh was placed in each vessel. A 30-$cm^3$ test solution was added to each vessel, giving a glass surface area to solution volume ratio of 2,000 $m^{-1}$, as calculated in C1285. The vessels were placed in ovens held at a temperature of 90 °C. The test solution was replaced entirely with an identical volume of fresh solution twice every week, at an interval of alternate 3- and 4-day cycles, during the first 12 weeks. The frequency of solution replacement was later changed to once a week for the second 12-week period, followed by replacement once every 2 weeks for the remaining test time. All experiments were continued for 1 year. At the end of each test period, the vessels were removed from the oven and allowed to cool. A small portion of the leachate was used to measure pH. The leachate was then filtered with a 0.45-$\mu$m syringe filter for cation analysis using the inductively coupled plasma atomic emission spectrometry technique.

The normalized concentration for element $i$, $NC_i$, and the normalized leach rate for element $i$, $NLR_i$, at the $n^{th}$ solution replacement can be calculated by the following equations:

$$NC_i = \frac{C_i}{F_i} \tag{2-5}$$

$$NLR_i = \frac{(NC_i)_n - (NC_i)_{n-1}}{\left(\frac{S}{V}\right)(t_n - t_{n-1})} \tag{2-6}$$

| Table 2-3. Chemical Compositions of Test Glasses (in Weight Percent) | | | |
|---|---|---|---|
| Oxide Compound | SRL EA Glass* | WVDP Ref. 6 Glass† | DWPF Blend 1 Glass‡ |
| $Al_2O_3$ | 3.60 | 6.67 | 4.16 |
| $B_2O_3$ | 11.16 | 11.48 | 8.05 |
| BaO | — | — | 0.18 |
| CaO | 1.23 | 0.66 | 1.03 |
| $Cr_2O_3$ | — | — | 0.13 |
| $Cs_2O$ | — | — | 0.08 |
| CuO | — | — | 0.44 |
| FeO | 1.59 | — | — |
| $Fe_2O_3$ | 7.58 | 11.95 | 10.91 |
| $K_2O$ | 0.04 | 5.15 | 3.68 |
| $La_2O_3$ | 0.28 | — | — |
| $Li_2O$ | 4.21 | 4.84 | 4.44 |
| MgO | 1.79 | 0.18 | 1.41 |
| MnO | 1.36 | 0.51 | — |
| $MnO_2$ | — | — | 2.05 |
| $MoO_3$ | — | — | 0.15 |
| $Na_2O$ | 16.88 | 11.94 | 9.13 |
| $Nd_2O_3$ | — | — | 0.22 |
| NiO | 0.53 | — | 0.89 |
| $P_2O_5$ | — | 2.01 | — |
| $RuO_2$ | — | — | 0.03 |
| $SO_3$ | — | 0.25 | — |
| $SiO_2$ | 48.76 | 42.28 | 51.9 |
| $TiO_2$ | 0.65 | 1.04 | 0.89 |
| ZnO | 0.26 | — | — |
| $ZrO_2$ | 0.48 | 1.28 | 0.14 |
| Total | 100.40 | 100.24 | 99.91 |

*C.M. Jantzen, N.E. Bibler, D.C. Crawford, and M.A. Pickett. "Characterization of the Defense Waste Processing Facility (DWPF) Environmental Assessment (EA) Glass Standard Reference Material (U)." WSRC–TR–92–346. Aiken, South Carolina: Westinghouse Savannah River Company. 1993.
†Composition provided by West Valley Nuclear Services Company, Inc.
‡Composition provided by Westinghouse Savannah River Company.

| Table 2-4. Glass Leaching Solution Test Matrix | | |
|---|---|---|
| **Test Solution** | **Glass Type** | **Initial pH** |
| Deionized Water | — | 5.78 |
| Deionized Water | SRL EA | 5.78 |
| Deionized Water | WVDP Ref. 6 | 5.78 |
| 0.0025 M $FeCl_2$ | WVDP Ref. 6 | 3.95 |
| 0.0025 M $FeCl_3$ | WVDP Ref. 6 | 2.22 |
| 0.25 M $FeCl_2$ | WVDP Ref. 6 | 2.47 |
| 0.25 M $FeCl_3$ | WVDP Ref. 6 | 1.34 |
| 0.25 M HCl | WVDP Ref. 6 | 0.69 |
| Deionized Water | DWPF Blend 1 | 5.78 |
| 0.0025 M $FeCl_2$ | DWPF Blend 1 | 3.95 |
| 0.0025 M $FeCl_3$ | DWPF Blend 1 | 2.22 |
| 0.25 M $FeCl_2$ | DWPF Blend 1 | 2.47 |
| 0.25 M $FeCl_3$ | DWPF Blend 1 | 1.34 |

where

$NC_i$ — in units of $g/m^3$
$C_i$ — concentration of element $i$ in solution, in units of $g/m^3$
$F_i$ — mass fraction of element $i$ in glass (dimensionless)
$NLR_i$ — in units of $g/m^2 \cdot day$
$t_n - t_{n-1}$ — time in days between the $n^{-1th}$ and $n^{th}$ solution replacements
$S/V$ — surface-to-volume ratio, in units of $m^{-1}$

Leaching in the presence of iron chloride causes precipitates to form, especially in the high concentration solutions. Solid precipitates contained in the leachates were air-dried, and precipitate samples were then mounted on glass slides for x-ray diffraction analysis. X-ray diffraction patterns of the solid precipitates suggest the dominant occurrence of akaganeite (β-FeOOH) in all cases. Elemental chemical compositions of the precipitates were analyzed in scanning electron microscopy by energy-dispersive x-ray spectroscopy, and are shown in Table 2-5. Elemental oxygen was not included in the semiquantitative analysis. Contrary to the formation of iron silicate precipitates reported by McVay and Buckwalter (1983) in both deionized water and J–13 groundwater in the presence of ductile iron, a very low silicon content was measured in the precipitates formed in the 0.25 M $FeCl_3$ solution. A substantially higher silicon content, however, was detected in the 0.0025 M $FeCl_3$ precipitates.

Results from the 1-year leaching program, which covered 51 solution replacements, are shown in Figures 2-4 through 2-7. The cumulative $NC_B$ results of the modified product consistency tests in various solutions are shown in Figure 2-4 for WVDP Ref. 6 and the DWPF Blend 1 glasses, respectively. From Figure 2-4, it is apparent that for both glasses the $NC_B$ values in iron chloride solutions were consistently higher than those in deionized water, and leaching in

| Table 2-5. Chemical Compositions of Precipitates from Leaching of WVDP Ref. 6 Glass in Various Solutions (in Weight Percent) | | | | | | | | | | |
|---|---|---|---|---|---|---|---|---|---|---|
| **Test Solution** | **Al** | **Fe** | **K** | **Na** | **P** | **Si** | **Ti** | **S** | **Cl** | **Mn** |
| 0.0025 M $FeCl_3$ | 6.2 | 48.9 | 4.9 | 4.7 | 2.1 | 28.1 | 0.9 | 0.3 | 1.7 | 0.9 |
| 0.25 M $FeCl_2$ | 0.7 | 77.9 | 0.3 | 1.6 | 0.3 | 1.7 | — | — | 17.4 | — |
| 0.25 M $FeCl_3$ | 0.4 | 76.7 | — | — | 0.6 | 0.6 | — | 1.1 | 20.6 | — |

0.25 M $FeCl_3$ solutions exhibited the highest boron release. The $NC_B$ values of the leachates from the first solution replacement of the 0.25 M $FeCl_3$ solution tests were observed to increase by factors of approximately 50 and 70 times for these two glasses in comparison with those in deionized water. In addition, the cumulative $NC_B$ is slightly higher in $FeCl_3$ than in $FeCl_2$ solutions and it is reached the constant value earlier, probably because of the lower pH of the $FeCl_3$ solution. In an attempt to evaluate the effect of the solution pH, additional tests were performed for WVDP Ref. 6 glass in 0.25 M HCl solutions. As shown in Table 2-4, the initial pH of the 0.25 M $FeCl_3$ solution is higher than that of 0.25 M HCl. The leaching results in 0.25 M HCl are also included in Figure 2-4. Although a factor of 30 times the increase in $NC_B$ was measured from the first solution replacement, compared to the deionized water result, the total $NC_B$ in 0.25 M HCl was only approximately half that in 0.25 M $FeCl_3$.

The $NLR_B$ results were also calculated using Eq. (2-6) and are shown in Figure 2-5 for WVDP Ref. 6 and DWPF Blend 1 glasses, respectively. It is apparent that the initial $NLR_B$ values were much higher in the high concentration iron chloride solution tests. In all cases, $NLR_B$ decreased with time, but this tendency is much greater in 0.25 M $FeCl_3$ solutions. Also, the $NLR_B$ was generally higher in the presence of iron chloride in comparison with that in deionized water except in high concentration chloride solutions after prolonged leaching. The substantially low $NLR_B$ values observed for WVDP Ref. 6 glass in 0.25 M $FeCl_3$ solution after only 10 days of leaching are in agreement with the evidence of leveling off of the $NC_B$ after the same leaching period, as shown in Figure 2-4. For the $NLR_{Si}$ results for WVDP Ref. 6 glass in various solutions in all cases, $NLR_{Si}$ remained almost constant throughout the leaching duration. The $NLR_{Si}$ levels depend on the test solution. Higher silicon release rates were measured in the high concentration iron chloride solution tests. The normalized release rates for various elements are shown in Figure 2-6 for WVDP Ref. 6 glass in 0.25 M $FeCl_3$ solution. Figure 2-6 indicates that all elements undergo congruent dissolution during the initial period of 24 days with the exception of silicon and aluminum after 17 days of leaching. DWPF Blend 1 glass also showed a similar trend.

The initial and final pH values of various leachates from WVDP Ref. 6 glass are shown in Figure 2-7. In all cases, except the leachates from the high concentration iron chloride solution tests at each solution replacement, the final pH values were generally higher than the initial. Variations in solution pH showed that, while the pH of the leachates from high concentration iron chloride solutions changed slightly and remained acidic throughout the leaching duration, it substantially increased in all the deionized water and low concentration iron chloride tests. It would be interesting to comment that after the initial period of 80 days, the final pH in the dilute iron chloride solutions reached almost a constant value. Similar changes in leachate pH were also observed for DWPF Blend 1 glass. In addition, leaching in deionized water showed high

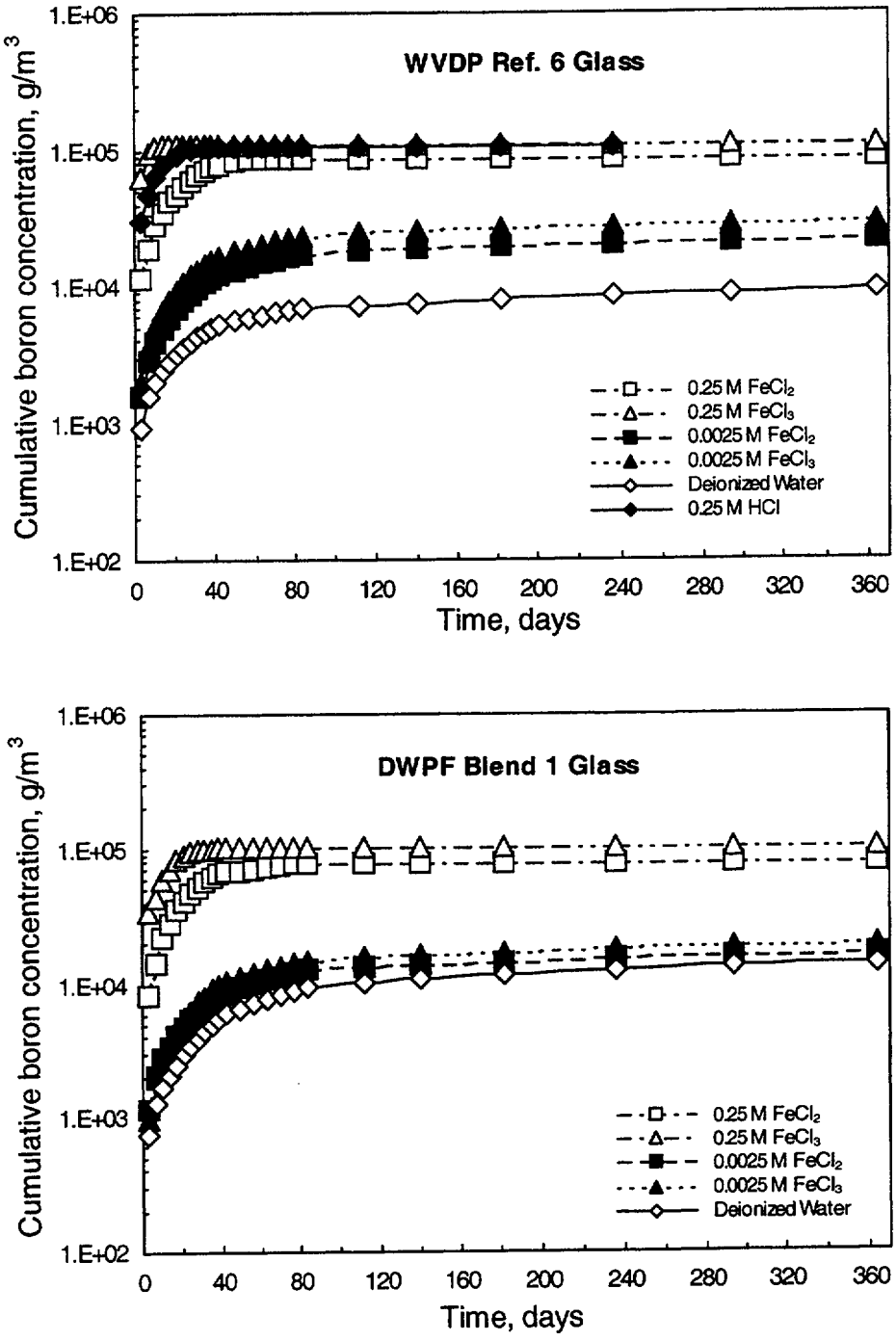


**Figure 2-4. Cumulative Normalized Leach Concentration for Boron Versus Time for WVDP Ref. 6 and DWPF Blend 1 Glasses in Various Solutions at 90 °C**

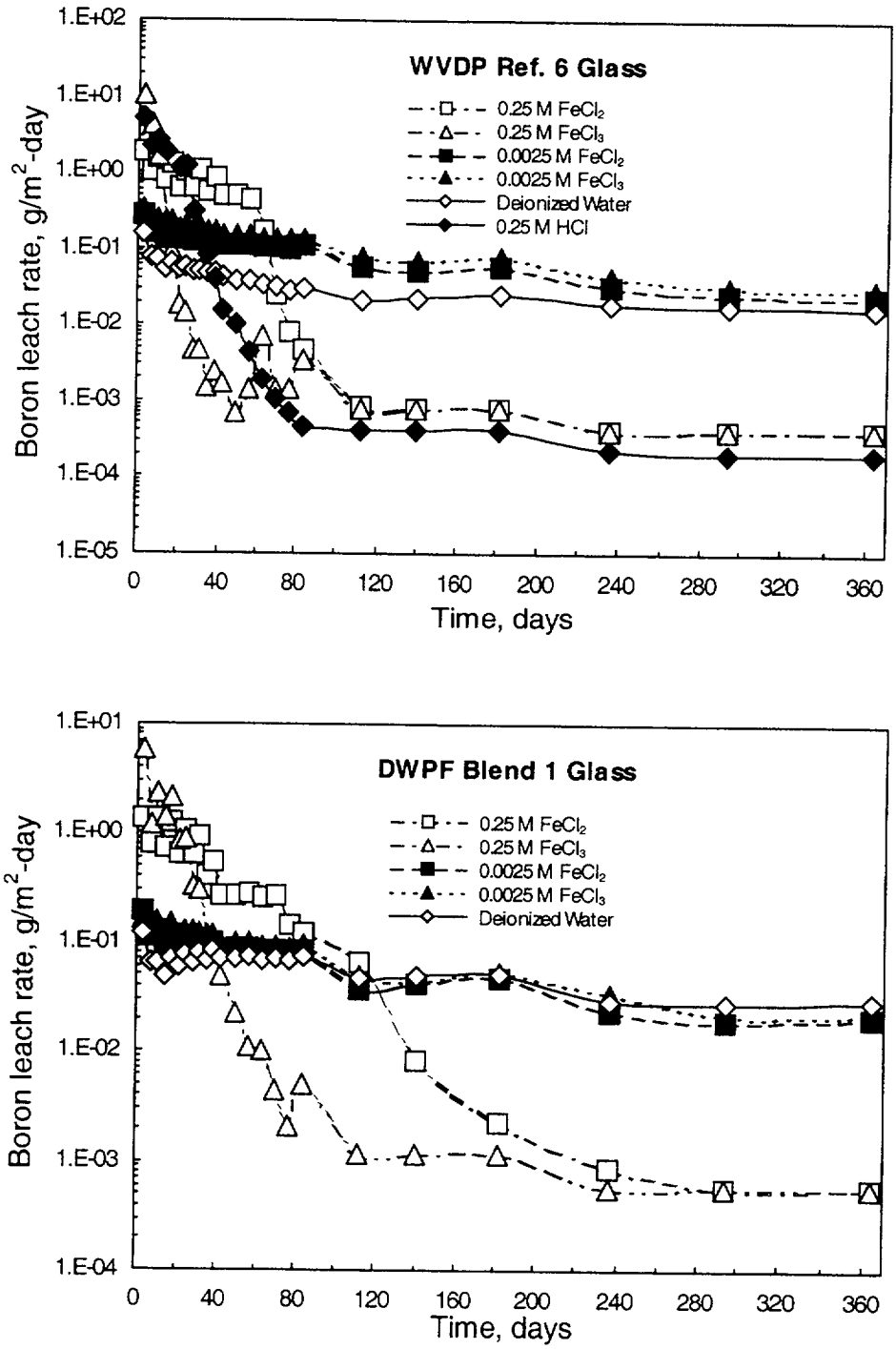


**Figure 2-5. Normalized Leach Rate for Boron Versus Time for WVDP Ref. 6 and DWPF Blend 1 Glasses in Various Solutions at 90 °C**

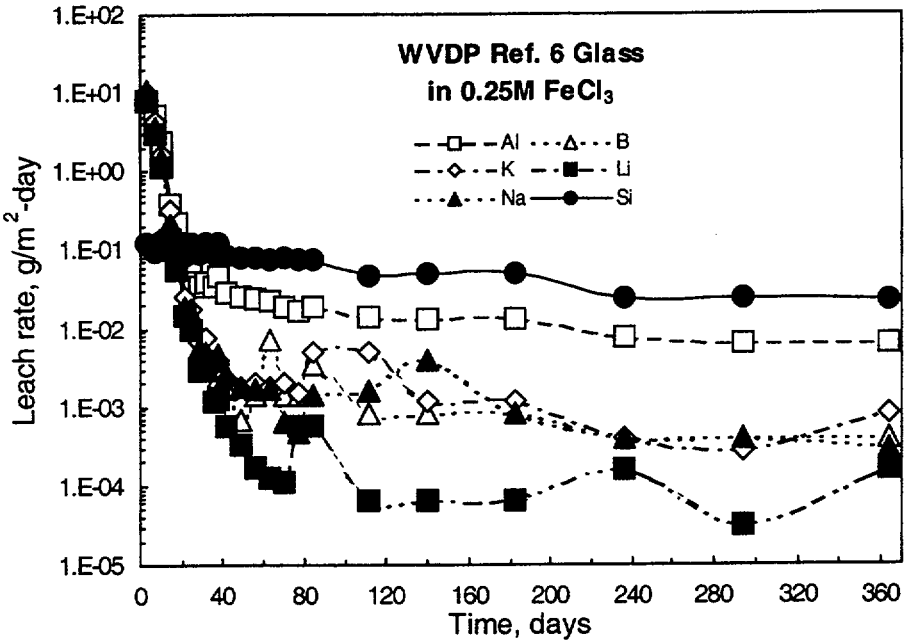


**Figure 2-6. Normalized Leach Rates for Various Elements as a Function of Time for WVDP Ref. 6 Glass in 0.25 M $FeCl_3$ Solution at 90 °C**

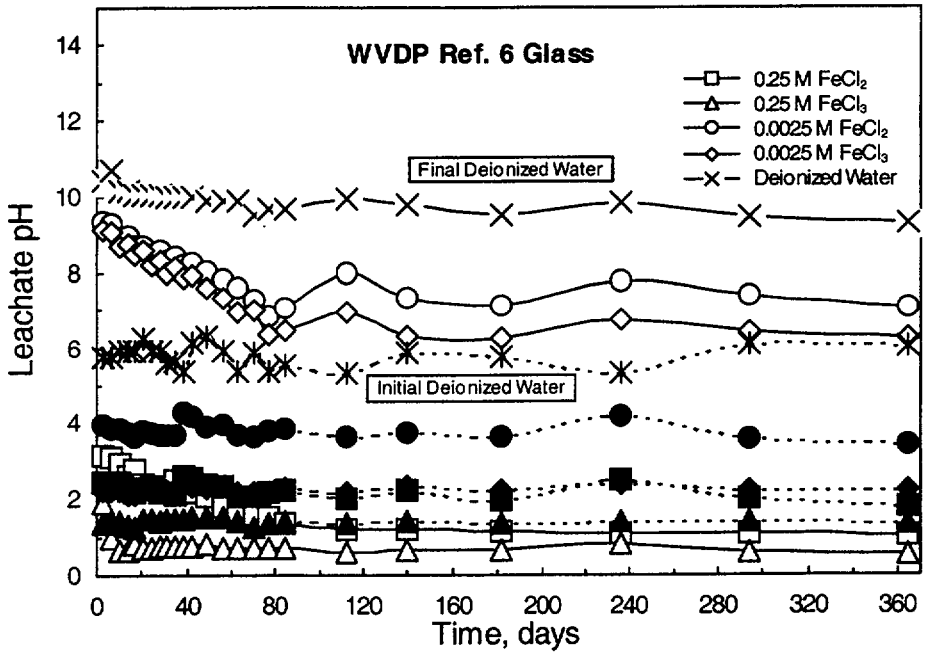


**Figure 2-7. Leachate pH Versus Time for WVDP Ref. 6 Glass in Various Solutions at 90 °C (Closed Symbols for the Initial pH and Open Symbols for the Final pH)**

elemental releases in the SRL EA glass as a result of a higher leachate pH (≈11.6) in comparison with two other glasses (pH≈10.2).

The effects of pH on glass dissolution have been widely investigated (Jantzen, 1992; Knauss, et al., 1990). Jantzen (1992) reported various regression equations for glass durability as a function of solution pH as well as other parameters using a hydration thermodynamics model. To determine the role of pH on glass dissolution in this study, the final leachate pH data for both WVDP Ref. 6 and DWPF Blend 1 glasses are plotted as a function of $NLR_B$ in Figure 2-8. The measurement for WVDP Ref. 6 glass in 0.25 M HCl solution is also included. A linear regression relationship between log $NLR_B$ and leachate pH can be defined for both WVDP Ref. 6 and DWPF Blend 1 glasses, respectively, as

$$\log NLR_B \text{ (WVDP Ref. 6)} = -0.1789\ \text{pH} + 0.9774 \quad (2\text{-}7)$$

$$\log NLR_B \text{ (DWPF Blend 1)} = -0.1780\ \text{pH} + 0.6414 \quad (2\text{-}8)$$

The slopes of Eqs. (2-7) and (2-8) are almost identical for these two test glasses. This correlation indicates that, under the test conditions investigated in this study, the effect of leachate pH on boron release may be independent of the glass. In addition, the value measured for the reference test in 0.25 M HCl solution correlates well with the regression line. These observations strongly suggest the important role of the leachate pH in the leaching behavior of these simulated waste glasses.

WVDP Ref. 6 glasses, both before and after leaching, were analyzed to determine their morphology and chemical composition using scanning electron microscopy. Figure 2-9 shows

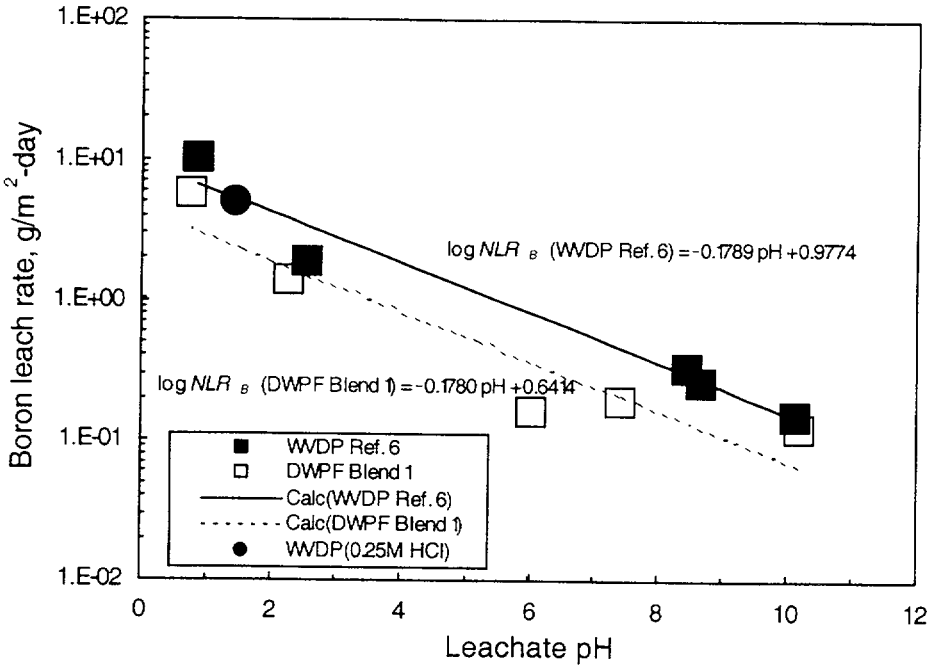


**Figure 2-8. Linear Regression Plot of Normalized Leach Rate for Boron Versus Leachate pH after First Solution Replacement for WVDP Ref. 6 and DWPF Blend 1 Glasses in Various Solutions at 90 °C**

representative micrographs of WVDP Ref. 6 glass particles before leaching and after leaching in deionized water and in 0.25 M $FeCl_3$ solution. As shown in Figure 2-9, while the surface of the starting glass particles was clean, the leaching process formed surface layers and precipitates on the particle facets. It is also noted that after leaching in the 0.25 M $FeCl_3$ solution, the particle size of WVDP Ref. 6 glass was significantly reduced. In contrast, the particle size remained essentially unchanged after leaching in deionized water, but evidence of attack can be seen on the glass surfaces. Fragmentation of WVDP Ref. 6 glass in 0.25 M $FeCl_3$ solution may be attributed to a combined effect of chemical dissolution and mechanical breakdown as a result of thermal stresses induced during periodic solution replacements. The chemical composition using the energy-dispersive x-ray spectroscopy analysis from the near surface regions of these three corresponding glass conditions is presented in Table 2-6. The absence of light elements (i.e., lithium and boron) was due to the detection limits of the instrument. Variations of the glass chemistry in relation to leaching conditions were observed. While sodium was substantially less in the deionized water leached glass, all alkali elements were completely removed from the 0.25 M $FeCl_3$ leached glass. These near surface glass chemistry variations are consistent with the leachate analyses discussed previously.

The reaction of borosilicate glasses with aqueous solutions generally includes two independent processes: initial diffusion-controlled extraction of alkali ions out of the glass matrix, and the dissolution of the glass matrix itself. The initial reaction causing alkali release is commonly known as an ion-exchange process as a result of water diffusion into the glass network. As the release rate decreases with increasing depth of the alkali depletion zone in the outer glass surface, matrix-dissolution becomes the dominant reaction.

The results from this study indicate that leachant pH is a dominant factor in the leaching of simulated waste glasses. At the beginning of the tests, the hydronium ion ($H_3O^+$) in solution tends to exchange with the alkalis in the glass matrix through the ion-exchange reaction. The more acidic the test solution, the faster the alkali release rates. This theory is supported by the inductively coupled plasma atomic emission spectrometry analyses shown in Figure 2-5. It is also expected that the ion-exchange reaction consumes hydronium ions and releases alkalis from the glass matrix. As a result, the leachate pH is anticipated to increase at the end of glass leaching. In the case of glass dissolution in 0.25 M $FeCl_3$ solution, an increase of the leachate pH, accompanied by the highest alkali release, was measured for the initial solution replacements (Figures 2-6 and 2-7). However, as the alkali release substantially reduced, the leachate pH was also observed to decrease for the rest of the solution replacements. The effect is clearly noticeable in the 0.0025 M $FeCl_2$ and 0.0025 M $FeCl_3$ solutions in which a steady decrease of the final pH can be observed during the initial 80-day replacement period.

**Table 2-6. Chemical Compositions from Surface Regions of WVDP Ref. 6 Glass Before and After Leaching (in Weight Percent)**

| Test Solution | Al | Fe | K | Na | P | Si | Ti | Zr | Cl | O |
|---|---|---|---|---|---|---|---|---|---|---|
| Before Leaching | 5.2 | 2.7 | 3.0 | 11.1 | 1.1 | 22.8 | 0.4 | 3.4 | — | 50.2 |
| Deionized Water | 5.0 | 8.6 | 5.7 | 3.5 | 1.3 | 32.2 | 0.9 | 4.6 | — | 37.0 |
| 0.25 M $FeCl_3$ | 1.6 | 5.6 | — | — | — | 45.2 | 0.4 | 6.9 | 1.8 | 38.5 |

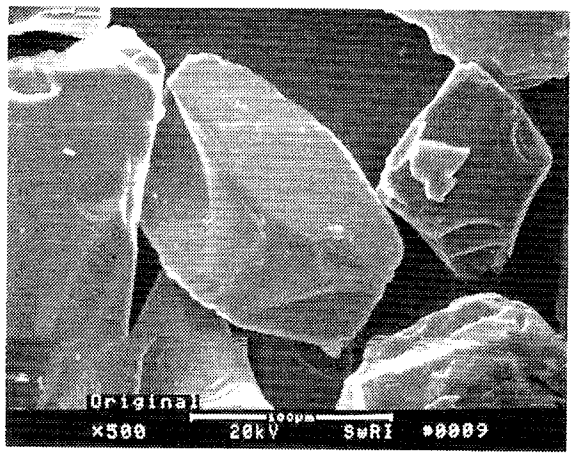


(a)

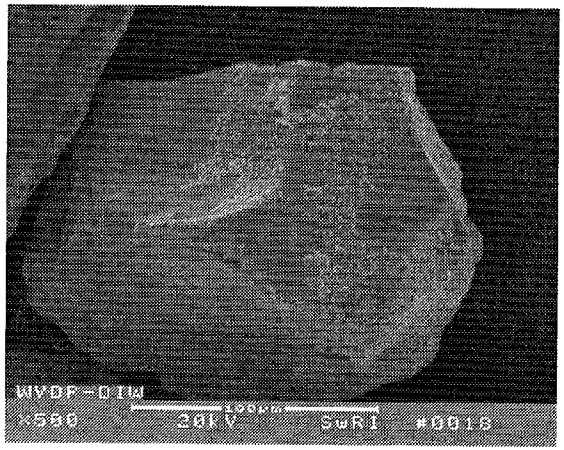


(b)

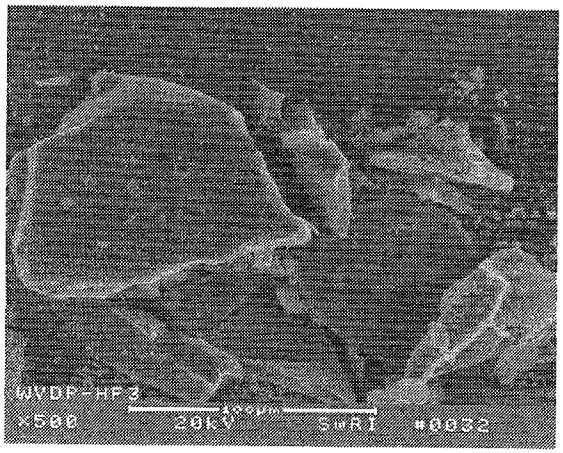


(c)

**Figure 2-9. Scanning Electron Micrographs of WVDP Ref. 6 Glass (a) Before Leaching and After Leaching in (b) Deionized Water and (c) 0.25 M $FeCl_3$ Solution at 90 °C**

From the glass surface analysis results, it is apparent that the high initial leaching resulted in the formation of an alkali-depleted surface layer, and consequently, the leaching rate decreased as a result of the extended diffusion path.

The mechanism by which Fe cations (both $Fe^{3+}$ and $Fe^{2+}$) accelerate the glass leaching process is not clear. The formation of iron silicate precipitates that inhibit saturation effects is generally speculated to enhance glass dissolution in the presence of iron products (McVay and Buckwalter, 1983). The results from this study, however, do not support this speculation. As reported in this study, even though leachate pH has a profound effect on glass dissolution, the leaching rate measured in 0.25 M $FeCl_3$ solution was almost twice that in the 0.25 M HCl solution. These results suggest that both solution pH and the presence of corrosion species such as iron chloride are significant contributing factors to the net glass durability.

## 2.2.2 Dissolution Kinetics and Model Abstraction

Experimental investigations into dissolution kinetics of the two simulated high-level waste glasses were performed. The glasses were subjected to leaching tests in the presence of $FeCl_2$ and $FeCl_3$ at temperatures of 40, 70, and 90 °C. Leach rates calculated after the first solution replacement were used as initial leach rates to provide a conservative account of the effect of glass dissolution and are plotted as a function of final leachate pH in Figure 2-10. The initial leach rates for all major components were pH dependent. While the leach rates for boron and alkali decreased with an increase in pH, the silicon release rate remained relatively constant. The aluminum leach rate showed a minimum for both the 70 and 90 °C tests. The pH value at which the minimum rate occurred varied with both the glass composition and test temperature. For the 40 °C tests, however, the leach rates for all elements decreased continuously with increasing leachate pH. Figure 2-11 shows the log $NLR_B$ as a function of leachate pH at each temperature for both WVDP Ref. 6 and DWPF Blend 1 glasses, based on the initial release of boron. A linear regression between log $NLR_B$ and leachate pH was performed, and the regression equations are also given in Figure 2-11. A good correlation between leach rate and pH is found for all test temperatures as indicated by the reasonable high correlation coefficients ($R^2$).

In contrast to a linear pH dependence with a negative slope observed for boron release in this study, Knauss, et al. (1990) and Abraitis, et al. (1998) conducted experiments in controlled pH environments and reported a V-shaped dissolution rate versus pH curves with minima at near-neutral pH for both boron and silicon releases. McGrail, et al. (1997) also studied glass dissolution kinetics at pH values between 6 and 12 and showed that glass dissolution increases with increasing pH. These observations suggest that the effect of pH on glass dissolution depends on the glass compositions and test conditions. While all the experiments in the cited references were conducted in controlled pH environments in the absence of the influence of the affinity term, solution pH was initially set by hydrolysis of $FeCl_2$ or $FeCl_3$ in this study, and the final pH values were generally higher than the initial ones. In the case of glass leaching in deionized water, the leachate pH drifted from acidic to the basic range. The observed discrepancy in the effect of pH on dissolution rate in the basic range could be the result of variations in leachate pH. It is also noted that the initial leach rates for boron and most alkali elements are much higher in comparison with the silicon release rate in the low pH ranges. High-level waste glass dissolution rates could be significantly underestimated if based on measured silicon release rates. In addition, the influence of the affinity term has not been

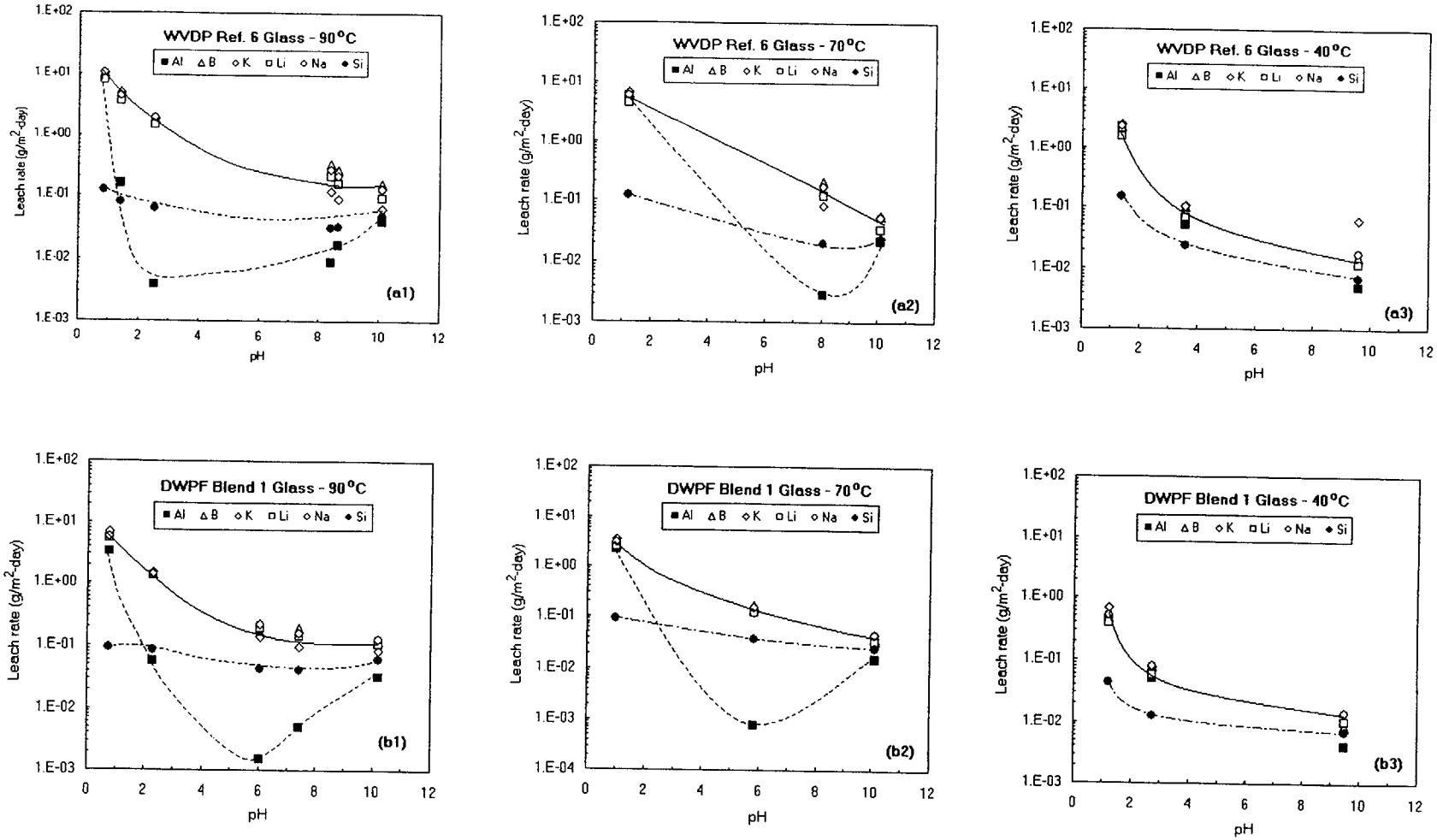


**Figure 2-10. Normalized Leach Rate for Various Elements Versus Leachate pH after First Solution Replacement for (a) WVDP Ref. 6 and (b) DWPF Blend 1 Glasses at Various Temperatures**

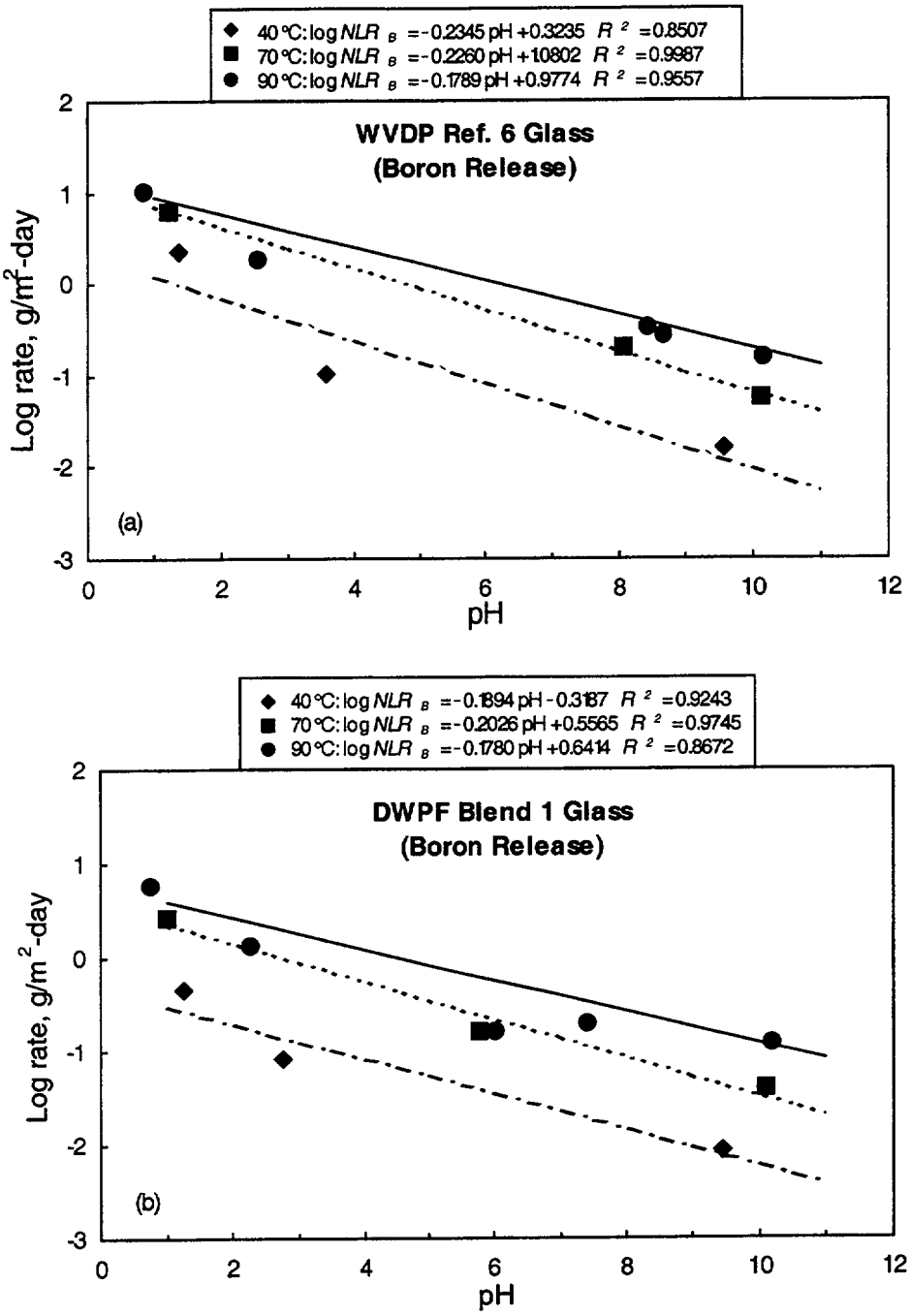


**Figure 2-11. Linear Regression of Normalized Leach Rate for Boron Versus Leachate pH after First Solution Replacement for (a) WVDP Ref. 6 and (b) DWPF Blend 1 Glasses at Various Temperatures**

evaluated under the current test conditions. Nevertheless, the use of boron release rates provides a conservative upper bound to the release rate of radionuclides because boron is released at a rate similar to alkali ions and is not incorporated into secondary phases similar to Tc-99.

The slopes of the linear regression equations plotted in Figure 2-11 provide the pH dependence coefficients (η). It is apparent that η does not significantly change with the test temperature and glass composition. Activation energy ($E_a$) can be regressed from the experimental data by plotting ln $NLR_B$ versus $1/T$ based on the rate equation in Eq. (2-2), and the effective rate constant ($k_{eff}$) can then be determined using the values of η and $E_a$. The model parameters are summarized in Table 2-7. The $E_a$ values for both waste glasses are consistent with the values reported in the literature for borosilicate waste glasses (Knauss, et al., 1990; Advocat, et al., 1991; McGrail, et al., 1997; Abraitis, et al., 1998). The mean and standard deviation values calculated for a combined case are listed in Table 2-8 (Case A) and compared to the bounding parameter values (Case B) adopted by the DOE (CRWMS M&O, 2000c). Note that the rate expression used by the DOE for the basic leg has combined the affinity term with the intrinsic dissolution rate constant. A significantly higher $k_0$ value, $\log_{10} k_0 = 7.91 \pm 0.16$, was measured from the forward rates by conducting MCC–1 tests (CRWMS M&O, 2000c). In addition to the effect of the affinity term, the effective rate constants measured in this study would also include another term that accounts for the effect of corrosion products.

Note that the results listed in Tables 2-7 and 2-8 (Case A) were obtained using the final pH values of the leachates from first solution replacement. Since solution pH changes during the leaching test, the final pH values may not be representative of the pH during the course of the experiment. An average of the initial and final pH values would be more realistic in the absence of pH measurements during exposure. The model parameters calculated using average pH values are also listed in Table 2-8 (Case A′).

The rate expression for dissolution of waste glasses has been evaluated by the DOE (CRWMS M&O, 2000c) primarily based on the experimental results by Knauss, et al. (1990). Because the glass dissolution rates were found to have a V-shaped pH dependence, with minima at near-neutral pH, separate rate expressions were obtained for dissolution under acidic or base conditions, as reflected in Table 2-8 (Case B). In addition, the release of boron occurred faster than that of silicon under some test conditions. The model parameter values based on boron release rates were determined to bound the range of high-level waste glass compositions and environmental conditions. The calculated dissolution rates on the basis of Eq. (2-2) and various model parameters in Table 2-8 are compared in Figure 2-12. It is seen that the model parameters supported by the current experimental data are associated with higher dissolution

**Table 2-7. Glass Dissolution Model Parameters Summary**

| Glass | Temperature (°C) | $\log_{10} k_{eff}$* | η | $E_a$ (kJ/mol) |
|---|---|---|---|---|
| WVDP Ref. 6 | 40 | 8.53 | -0.2345 | 49.2 ± 7.4 |
| WVDP Ref. 6 | 70 | 8.57 | -0.2260 | |
| WVDP Ref. 6 | 90 | 8.22 | -0.1789 | |
| DWPF Blend 1 | 40 | 8.49 | -0.1894 | 52.8 ± 2.5 |
| DWPF Blend 1 | 70 | 8.60 | -0.2026 | |
| DWPF Blend 1 | 90 | 8.37 | -0.1780 | |

*For $k_{eff}$ in g/m² • day.

| Table 2-8. Comparison of Glass Dissolution Model Parameters | | | |
|---|---|---|---|
| **Parameter** | **Case A (CNWRA Rate Expression —Final pH)** | **Case A′ (CNWRA Rate Expression —Average pH)** | **Case B (DOE Rate Expression)** |
| $k_{eff}$ ($g/m^2 \cdot day$) | $10^{8.46 \pm 0.14}$ | $10^{7.49 \pm 0.10}$ | $10^{14.0 \pm 0.5}$ if pH < 7.1 |
| | | | $10^{6.9 \pm 0.5}$ if pH ≥ 7.1 |
| $\eta$ | $-0.20 \pm 0.02$ | $-0.27 \pm 0.02$ | $-0.6 \pm 0.1$ if pH < 7.1 |
| | | | $0.4 \pm 0.1$ if pH ≥ 7.1 |
| $E_a$ (kJ/mol) | $51.0 \pm 5.6$ | $44.4 \pm 2.6$ | $80 \pm 10$ if pH < 7.1 |
| | | | $80 \pm 10$ if pH ≥ 7.1 |

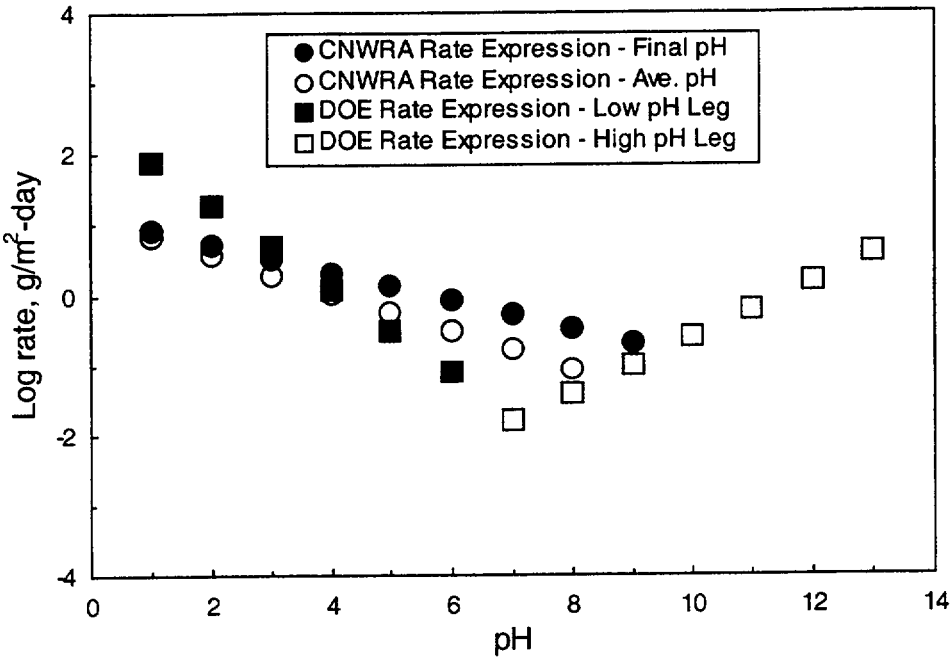


**Figure 2-12. Comparison of Calculated Glass Dissolution Rates Using Different Rate Expressions**

rates in the near-neutral pH range than those reported by the DOE. Considering the dissolution behavior in the alkaline range reported by the DOE (CRWMS M&O, 2000c), the rate expression based on average pH leads to closer agreement with the DOE results in the absence of leaching tests with the initial pH in the alkaline region. Nevertheless, the higher dissolution rates are consistent with the observations of enhanced glass dissolution in the presence of iron-containing corrosion products.

### 2.2.3 CNWRA Approach to Performance Estimation

The NRC and CNWRA have been developing a tool, the Total-system Performance Assessment code (Mohanty and McCartin, 2000), intended to support review activities for a potential license application by the DOE for construction of a high-level waste repository at Yucca Mountain. Based on a Monte Carlo scheme, the Total-system Performance Assessment code is used to compute the expected annual dose (Total Effective Dose Equivalent) to the average member of the critical group in the event of failure of the waste packages to isolate radionuclides. A nominal case (defined as a particular set of models and model parameters describing likely behaviors of the proposed repository system) is generally selected to perform sensitivity and uncertainty analyses and to study the performance of the system as simulated by the code. In the nominal case model or description, it is assumed that 70,040 metric tons of spent nuclear fuel is packaged in 7,176 waste packages and emplaced in the proposed repository. Each waste package contains, on average, 9.8 metric tons of spent nuclear fuel. The nominal case description does not account for the presence of high-level waste in glass form. Equation (2-2) was incorporated into the code to account for glass leaching in the event glass is contacted by water. Computations presented in this section are aimed at evaluating the relative importance of glass dissolution, in units of dose, with respect to spent nuclear fuel dissolution.

In the computer simulations, the model parameters obtained from this work (Case A) and from the DOE (Case B) in Table 2-8 were considered. The current Total-system Performance Assessment Code Version 4.1 does not allow for the simultaneous inclusion of two waste forms in the estimation of the dose. To circumvent that problem, it was assumed that glass was the only kind of waste form in the system and that a total of 4,667 metric tons of high-level waste glass (CRWMS M&O, 2000d) contained in 3,910 waste packages was emplaced in the proposed repository (CRWMS M&O, 2000e). The initial radionuclide inventory was selected from available data (CRWMS M&O, 2000e). To obtain appropriate comparisons of the dose derived from glass dissolution to the nominal case dose, a temperature-versus-time curve for the latter case was employed. The justification is that in the mixed system, spent nuclear fuel and glass waste forms, the temperature of the repository is dictated by the thermal activity of the spent nuclear fuel. The total surface area of the exposed glass waste form per waste package was set equal to 99 $m^2$, as suggested by other studies (CRWMS M&O, 1998b). In the Monte Carlo analysis, the pH was uniformly sampled in the range 4.8 to 10, consistent with predictions of the chemistry inside the waste package (CRWMS M&O, 2000f). Results of the computations are summarized in Figure 2-13.

The mean dose rates for these runs were computed by averaging the total effective dose equivalent for the nominal scenario at an instant of time from 200 Monte Carlo realizations and are plotted in Figure 2-13 for each case. As shown in Figure 2-13, the predicted mean dose rates for Case A are higher than those computed for Case B (Cases A and B refer to the notation in Table 2-8), which are a direct consequence of the higher dissolution rates in the

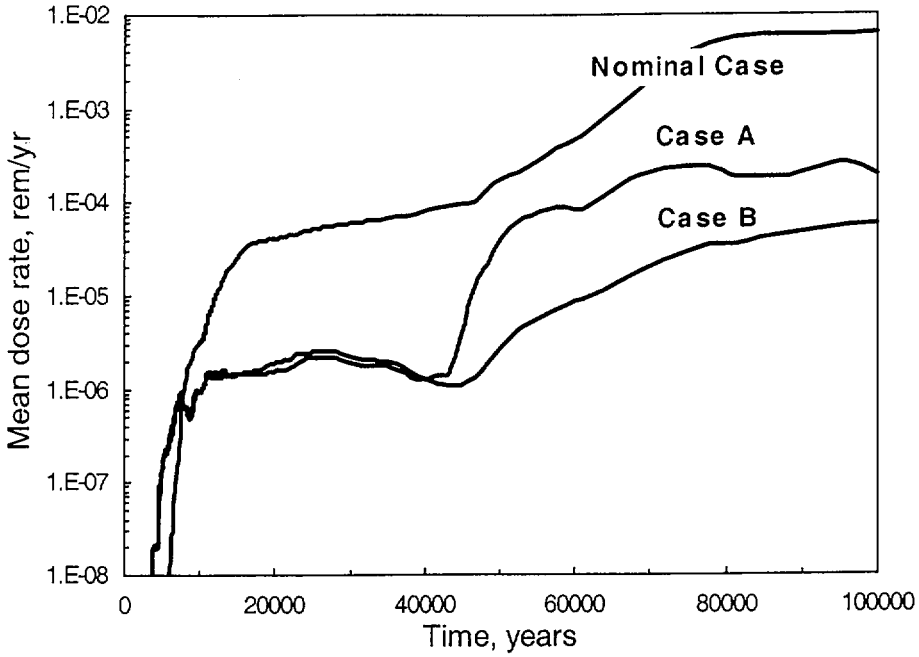


**Figure 2-13. Calculated Mean Dose Rates for Three Cases from 200 Realizations. The Cases A and B That Account for 4,667 Metric Tons of High-Level Waste Glass Refer to the Parameters in Table 2-8. The Nominal Case of the Total System Performance Assessment Code Models 70,040 Metric Tons of Spent Nuclear Fuel in the Repository System.**

near-neutral pH associated to Case A that accounts for the effect of corrosion products (see Figure 2-12). The impact of glass dissolution on the predicted mean dose rate in Case A could be up to 30 percent of the nominal case at times of the order of 52,000 years. Within the first 10,000 years, the dose deriving from glass dissolution is of the same order of magnitude as the nominal case dose. Nevertheless, the magnitude of these predicted mean dose rates is less than $10^{-3}$ rem/yr at times t < 60,000 years in Figure 2-13. The dose at earlier times are a consequence of the assumption that initial defects could be present in waste containers. At times greater than 40,000 years, a significant number of waste packages would fail caused by general corrosion; thus, additional sources of radionuclide release would be available in the system, causing the increase in the dose. Figures 2-14 and 2-15 present the corresponding release rates of various radionuclides for the nominal case and Case A, respectively. As evident in both figures, while Np-237 is the predominant radionuclide contributing to the mean dose rate at all times, Tc-99 and I-129 are significant contributors at early times (< 15,000 years) because of their high solubility in the water contacting the waste form.

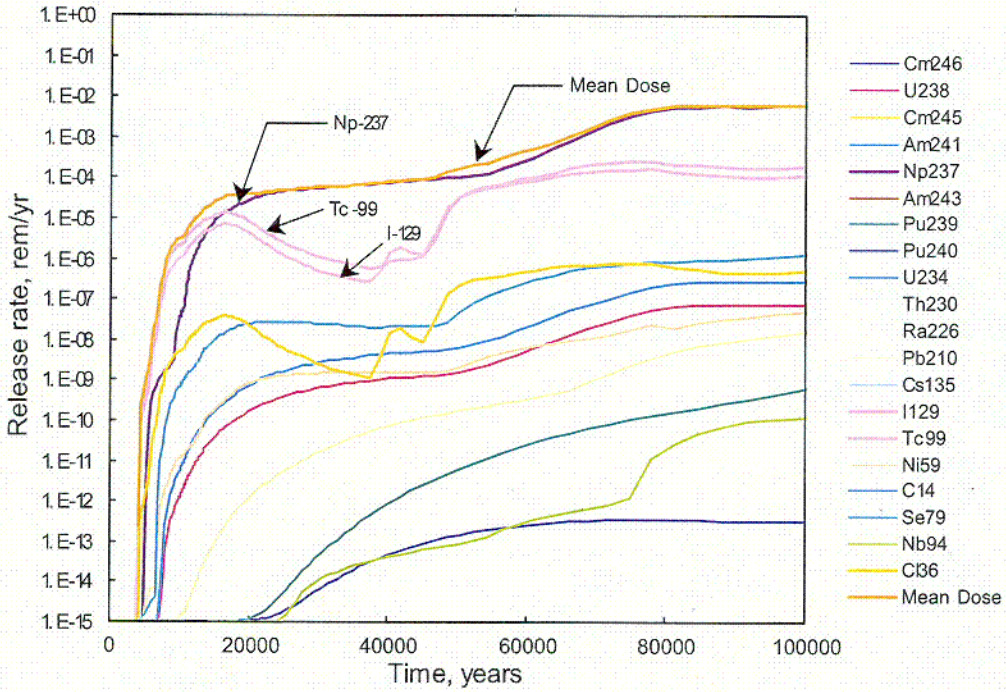


**Figure 2-14. Calculated Release Rates for Various Radionuclides for the Nominal Case from 200 Realizations. The Nominal Case of the Total System Performance Assessment Code Models 70,040 Metric Tons of Spent Nuclear Fuel in the Repository System.**

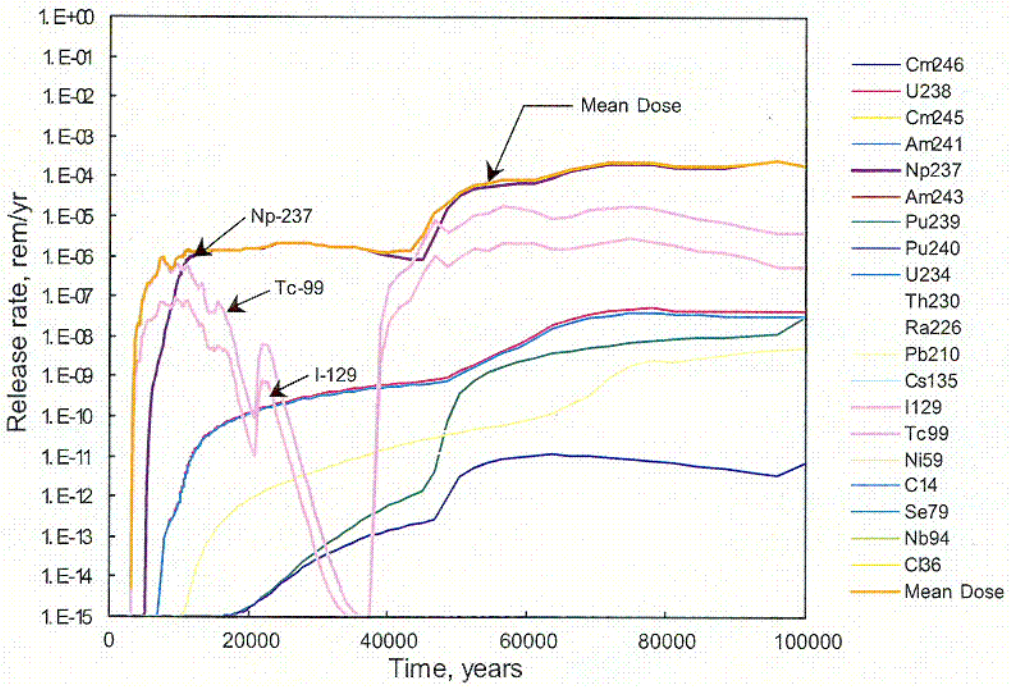


**Figure 2-15. Calculated Release Rates for Various Radionuclides for Case A from 200 Realizations. The Case A that Accounts for 4,667 Metric Tons of High-Level Waste Glass Refers to the Parameters in Table 2-8.**



C02

# 3 DEGRADATION OF COMMERCIAL SPENT NUCLEAR FUEL CLADDING

## 3.1 DOE INVESTIGATIONS

DOE considered the most likely forms of degradation that may affect the integrity of the commercial spent nuclear fuel cladding during disposal conditions in the proposed repository at Yucca Mountain. DOE developed a model to evaluate Zircaloy cladding degradation as part of the waste form degradation model (CRWMS M&O, 2000d) to determine the rate at which the commercial spent nuclear fuel matrix is exposed to the in-package aqueous environment. The degradation of the commercial spent nuclear fuel cladding is assumed to occur in two stages (CRWMS M&O, 2000d,g). The first stage of degradation corresponds to rod failure as a result of perforation of the cladding. The second stage is caused by the progressive exposure of the spent nuclear fuel matrix as a result of splitting (wet unzipping) of the cladding caused by oxidation of the irradiated $UO_2$ pellets by an aqueous environment.

In-package chemistry parameters included in the Total System Performance Assessment–Site Recommendation abstraction are pH, redox potential, ionic strength, total aqueous carbonate concentration, chloride concentration, and fluoride concentration. To calculate the evolution of these parameters, the EQ 3/6 code is used by the DOE. However, direct use of a complex code such as EQ 3/6 within the Total System Performance Assessment–Site Recommendation analysis calculations was not practical. Thus, DOE used abstractions of in-package processes based on a series of multiple linear regression analyses of the output from the EQ 3/6 simulations (CRWMS M&O, 2000c, 2001b,c). The pH is the most important in-package chemistry parameter. Thus, the time discretization used by the DOE for all abstracted parameters was based on changes in pH. Both total carbonate and redox potential are pH dependent and may be calculated directly from the abstracted pH value. The fluoride concentration and ionic strength were given a range of values to be sampled in the Total System Performance Assessment–Site Recommendation analysis. A more detailed discussion is presented in Chapter 4.

It is important to note that the chloride and fluoride concentrations and the $O_2$ and $CO_2$ fugacities were set to constant values (CRWMS M&O, 2000d). The fugacities for both gases were considered equal to the partial pressures under atmospheric conditions at the repository site. The chloride concentration was set to $2.01 \times 10^{-4}$ M (equal to the value in J–13 Well water) whereas the fluoride concentration was assumed to be sufficiently high to promote corrosion of Zircaloy, even though it was noted that the concentration in J–13 Well water is only $1.1 \times 10^{-4}$ M.

Cladding perforation may occur prior to or after waste package emplacement. The initial condition of the cladding and the percentage of rods perforated at the time of disposal are evaluated by the DOE taking into account data obtained from reactor operation, pool storage, dry storage, and transportation, including fuel handling (CRWMS M&O, 2000h). A distribution of initially perforated Zircaloy fuel rods, expressed as a complementary cumulative distribution function, was developed from the available data.

Cladding perforation after waste package emplacement is assumed to be caused by localized corrosion, creep, stress corrosion cracking, and mechanical failure caused by seismic events

(CRWMS M&O, 2000g). To evaluate the possibility of creep and stress corrosion cracking for disposal conditions, the temperature history of the cladding during storage and transportation and the evolution of temperature after waste package emplacement, as well as the distribution of internal pressure and corresponding hoop stresses (CRWMS M&O, 2000g,h) were estimated. However, the analyses of DOE investigations on both creep and mechanical failure as a result of seismic events are out of the scope of this report. Another form of degradation of Zircaloy cladding considered by the DOE analysis is delayed hydride cracking. The DOE approach has been described and evaluated elsewhere (NRC, 2001b), and it is not included in this report. In the following sections, localized corrosion and stress corrosion cracking of Zircaloy cladding in the expected in-package aqueous environments are discussed, and the DOE model abstractions are described and evaluated. No change to the approach and content of the Total System Performance Assessment–Site Recommendation abstraction has been introduced in the Supplemental Science and Performance Analysis for the evaluation of cladding.

### 3.1.1 DOE Model Abstraction

Localized corrosion is considered as a process leading to the perforation of the commercial spent nuclear fuel cladding (CRWMS M&O, 2000g). Fluoride is assumed to be the anionic species promoting accelerated corrosion on a relatively small area of cladding (about 10 mm of rod length). The fraction of fuel cladding surface on different fuel rods inside the same waste package is considered to be proportional to the volume of water entering the waste package in a flow-through scenario. This approach is considered a bounding analysis because it implicitly assumed 100-percent efficiency in the chemical reaction of fluoride with Zircaloy.

Corrosion data, generated outside the Yucca Mountain program by Teledyne Wah Chang (a producer of zirconium alloys) and reported by Yau and Webster (1987), are presented in the analysis and model report (CRWMS M&O, 2000i) to support the localized corrosion failure model for Zircaloy-2 or -4 cladding. Most data provided are for commercial purity zirconium instead of Zircaloy. In the report, it is noted that the behavior of commercial purity zirconium (containing hafnium and lacking the Zircaloy alloying elements) is comparable to that of Zircaloy. Although the previous statement is acceptable in general terms, there are no specific data provided for environments postulated to simulate the in-package water chemistry. Although data on localized corrosion by chloride anions are presented, it is claimed that this process cannot occur because the pH is too high to maintain sufficient concentration of $Fe^{3+}$ ions in solution, implicitly assuming this cation is the single species capable of increasing the corrosion potential above the pitting potential. Instead, corrosion is assumed to be caused only by fluoride anions. Corrosion rate data from 24- to 72-hour tests in aqueous solutions containing fluoride and chloride were used to generate a parametric equation including the concentration of these anionic species (CRWMS M&O, 2000i). However, the equation is not used in the model abstraction. In the analysis and model report (CRWMS M&O, 2000g), corrosion by fluoride to stoichiometrically form $ZrF_4$ is conservatively assumed to be determined by its concentration in the J–13 Well water, the volume of water entering the waste package, and the flow rate; but the attack is considered to be confined to a small 1-cm long cladding ring portion of the fuel rod.

The possibility of stress corrosion cracking was considered by DOE based on the calculated distribution of hoop stresses. The causative species for stress corrosion cracking of commercial spent nuclear fuel cladding is considered to be iodine, found free as a fission product in the pellet-cladding gap (CRWMS M&O, 2000g). Although the iodine concentration is asserted to be

negligible, conservatively it is assumed that in the fuel matrix-cladding gap is higher than the threshold value of $5 \times 10^{-6}$ g/cm$^2$ required to promote iodine-stress corrosion cracking. If the hoop stress is higher than a critical stress level of 180 MPa, this form of internal stress corrosion cracking is assumed to occur. This value is relatively high and can be attained by no more than a few rods. As noted in the analysis and model report (CRWMS M&O, 2000g), the model abstraction for stress corrosion cracking is based on the assumption that iodine as a fission product is the causative species.

### 3.1.2 Assessment of the DOE Approach

Model abstractions for localized corrosion and stress corrosion cracking developed by the DOE are not sufficient because the abstractions do not consider the range of chemical conditions that may prevail in the in-package aqueous environment. DOE agreed to provide additional information on the in-package water chemistry according to agreements CLST 3.01, CLST 3.02, CLST 3.03, CLST 3.04, CLST 3.05, ENFE 3.03, ENFE 3.04, TSPAI 3.08 and TSPAI 3.14.

Localized corrosion in the form of pitting promoted by chloride, although a possible failure process (NRC, 2001b), is excluded by the DOE (CRWMS M&O, 2000j) by assuming that (i) the chloride concentration is lower than the minimum concentration required for pit initiation; (ii) the concentrations of inhibiting anions such as nitrate, sulfate, and bicarbonate are sufficient to overcome the detrimental effect of chloride; and (iii) the concentration of dissolved $Fe^{3+}$ ions, considered to be the single species that may increase the corrosion potential of the cladding above the pitting potential, is assumed to be insufficient for the range of expected pH of the in-package water. Instead, DOE proposed accelerated corrosion by fluoride ions as the most plausible degradation process caused by a chemical reaction controlled by the volume of water entering the waste package in a flow-through scenario, the flow rate, and the concentration of fluoride in the water (CRWMS M&O, 2000g).

In the process model report (CRWMS M&O, 2000d), the role of fluoride as a specie promoting accelerated corrosion in local areas is emphasized, but insufficient technical basis has been offered (CRWMS M&O, 2000i). In addition, the analysis of the flow and volume of water contacting the fuel rods to evaluate the local attack by fluoride is limited and requires additional justification. There are inconsistencies regarding evaluation of the in-package pH because a low pH is assumed for the attack by fluoride, whereas it was not taken into account to estimate the concentration of $Fe^{3+}$ ions in solution that may promote the oxidizing conditions required for pitting corrosion in chloride solutions.

It should be noted that the chloride concentration inside breached waste packages was not properly bounded in the DOE analyses, and the presence of $Fe^{3+}$ ions cannot be considered an absolute requirement because corrosion potentials higher than the pitting potential can be attained in the presence of other oxidizing species, including radiolytic products such as $H_2O_2$. A detailed discussion, based mostly on data on commercial purity zirconium relevant to chemical processes and industry applications, was provided in the analysis and model report devoted to localized corrosion (CRWMS M&O, 2000i) questioning the occurrence of pitting corrosion induced by chloride during repository conditions. It is claimed in the DOE discussion of pitting corrosion in chloride solutions that acidic pHs (pH < 3.5) are not attained in the in-package environment to maintain sufficient concentration of $Fe^{3+}$ ions in solution (CRWMS, 2000i). However, in the screening arguments used in several features, events, and processes (CRWMS M&O, 2000j) the existence of acidic conditions inside waste packages is assumed

claiming that acidic pHs may affect the occurrence of localized corrosion. Regardless of the qualitative character of both statements, the arguments used in the two reports are in contradiction.

Stress corrosion cracking of Zircaloy cladding may occur in the presence of hoop stresses of sufficient magnitude under the same environmental and electrochemical conditions that promote pitting corrosion by chloride (NRC, 2001b). As noted, instead of chloride, the causative species for stress corrosion cracking is considered by the DOE to be iodine (CRWMS M&O, 2000g). However, the possibility of stress corrosion cracking induced by iodine discussed in the process model report (CRWMS M&O, 2000d) does not appear important because it is limited essentially by the availability of iodine. The phenomenon as such was postulated as the cause of pellet cladding interaction failure for reactor operating conditions following steep power ramps, but it does not seem plausible for disposal conditions.

Although the threshold stress value adopted by the DOE seems to be appropriate for evaluating iodine stress corrosion cracking and represents a lower bound, the data that have been obtained for test conditions are not necessarily applicable to disposal conditions where stress corrosion cracking may be initiated on the cladding outer surface by other species present in the modified groundwater. In addition, an adequate technical basis should be provided for the selection of the critical stress relevant to the environment in which external stress corrosion cracking may occur.

There is no adequate verification of the model abstraction for the degradation of cladding. As noted before, no empirical demonstration through experiments has been provided by the DOE using simulated in-package environments to verify that localized corrosion by fluoride anions is a valid process to be modeled and abstracted for incorporation into the Total-system Performance Assessment code or at least bound the rate at which other corrosion processes may perforate the cladding. A similar argument is valid for the model abstraction of stress corrosion cracking in which only iodide is considered the causative agent for stress corrosion cracking. This internal stress corrosion cracking process has not been verified for the conditions expected in the repository. DOE agreed to provide the necessary information on localized corrosion and stress corrosion cracking of cladding in agreements CLST 3.06, CLST 3.07, and CLST 3.09.

In summary, the technical bases provided to support the modeling of cladding degradation as a result of both the corrosion by fluoride and the internal stress corrosion cracking by iodine are limited (NRC, 2001b). Finally, no alternative models have been considered for localized corrosion and external stress corrosion cracking. This model could be acceptable if DOE can demonstrate in the analysis and model report that the environmental conditions are not conducive to localized corrosion or stress corrosion cracking induced by chloride because (i) the chloride concentration is too low, (ii) the corrosion potential is lower than the pitting potential, or (iii) anionic species such as nitrate are present at a sufficiently high concentration ratio with respect to chloride that can act as efficient localized corrosion inhibitors. The hoop stress calculations used to evaluate creep are applicable to the assessment of chloride-induced stress corrosion cracking. DOE agreed to provide additional information according to agreements CLST 3.06, CLST 3.07, and CLST 3.09.

Failure of cladding by hydrogen or hydride embrittlement, delayed hydride cracking, and hydride reorientation were screened out by DOE as possible events in the repository (CRWMS M&O,

2000j). It should be noted that hydrogen entry occurs during reactor operation as a result of high temperature aqueous corrosion followed by hydride precipitation upon cooling, but it is not expected under the oxidizing conditions prevailing in the in-package environment after disposal. DOE considered that stresses and temperatures of the cladding are too low for hydride orientation to occur and that the cladding material would maintain sufficient strength even if hydride reorientation did occur such that cladding failure would be unlikely. However, additional information should be provided by the DOE according to agreement CLST 3.08.

## 3.2 CNWRA INVESTIGATIONS

### 3.2.1 As-Polished Zircaloy-4

The localized corrosion of Zircaloy-4 has been evaluated at the CNWRA using potentiostatic and cyclic potentiodynamic polarization testing with a single heat of Zircaloy-4, whose chemical composition is shown in Table 3-1. Creviced specimens were constructed by pressing a serrated polytetrafluoroethylene crevice former, with a torque of 0.35 N·m, against the flat portion of a 1.9 × 1.9 × 1.3 cm (length × width × thickness) block of specimen. Specimens were machined from an annealed 9.5-mm-thick plate, wet polished to a 600-grit finish, cleaned, and dried prior to assembling the crevice device inside the solution. Initial tests were performed in chloride solutions containing 0.25 mM sulfate ($SO_4^{2-}$), 0.16 mM nitrate ($NO_3^-$), 0.10 mM fluoride ($F^-$), and a total carbonate ($HCO_3^- + CO_3^{2-}$) concentration of 1.4 mM to simulate the chemical composition of the prevalent groundwater chemistry at the proposed repository at Yucca Mountain. The chloride concentrations examined ranged 1mM to 4M. All solutions were prepared using reagent grade sodium salts and 18 MΩ · cm water. To modify the solution pH, 0.01 M HCl was added to lower the pH to 2.1, and $Na_2CO_3$ was used to raise the pH to 10.7. All tests were conducted at 25, 65, and 95 °C. After the bulk solution was prepared, the initial pH was measured at room temperature, and the solution was introduced to the test cell. The solution was purged with high purity $N_2$ and heated to the desired temperature. The specimen was then introduced into the cell, and the test started after measuring the initial rest potential. After the test was completed, the final pH of the solution was measured at room temperature. An additional series of tests was also performed in chloride solutions with different concentrations of other anions (particularly sulfate and nitrate) to examine the possibility that these anions may inhibit localized corrosion. All tests were conducted using a saturated calomel reference electrode maintained at room temperature and connected to the cell through a salt bridge/Luggin probe filled with either 100 mM or 1 M chloride solution depending on the concentration of the testing solution. A platinum foil was used as a counter electrode. Cyclic potentiodynamic polarization tests were initiated at 0.1 V less than the open circuit potential after the specimens had been immersed in solution for a period of time such that a steady-state corrosion potential was reached. A potential scan rate of 0.167 mV/s was used, and the scans were reversed when a current density of 5 mA/cm$^2$ was reached.

**Table 3-1. Composition of Zircaloy-4 Utilized in Current Study (in Weight Percent)**

| Sn | Fe | Cr | Ni | O (ppm*) | Zr |
|---|---|---|---|---|---|
| 1.51 | 0.20 | 0.10 | 0.0035 | 1420 | bal. |

*ppm = parts per million.

Figure 3-1 shows a typical polarization curve for Zircaloy-4 in deaerated, simulated groundwater (pH 8.4) containing 0.1M NaCl at 95 °C. In addition to a wide passive range that extends over almost 1 V above the corrosion potential, which is approximately -0.7 $V_{SCE}$ in the deaerated solution, breakdown potential, $E_b$, of about 0.20 $V_{SCE}$ and a repassivation potential, $E_{rp}$, of about 0.10 $V_{SCE}$ are clearly noticeable in the cyclic polarization curve. Figure 3-2 shows the typical morphology of the localized corrosion of Zircaloy-4 specimens exposed to chloride-containing simulated groundwater at 95 °C. The localized corrosion burrowed beneath the oxide layer cutting a shallow, irregularly shaped network of pits and leaving a thin film of oxide suspended above the pits. In more dilute chloride solutions, the shallow, irregular network of pits exhibited a spider web or tree branch pattern on the exposed surfaces of the specimen. The most important observation, however, is the absence of detectable localized attack beneath the crevice former feet, despite that this occluded geometry represents the most aggressive environmental condition for many passive metals and alloys (Szklarska-Smialowska, 1986). Localized corrosion, in the form of shallow, covered pits, was confined to the boldly exposed specimen surfaces.

The values of the potential for passivity breakdown in deaerated, simulated groundwater (pH 8.4) are plotted as a function of the chloride concentration and shown in Figure 3-3 for the three temperatures studied. It is seen that in the temperature range 25 to 95 °C there was little variation of the breakdown potential for any given chloride concentration. All the data for tests in solutions with chloride concentrations ranging from 0.01 M to 4 M fit a linear logarithmic relationship, independent of temperature as given by Eq. (3-1),

$$E_{crit} = E^0_{crit} - B \log [Cl^-] \qquad (3\text{-}1)$$

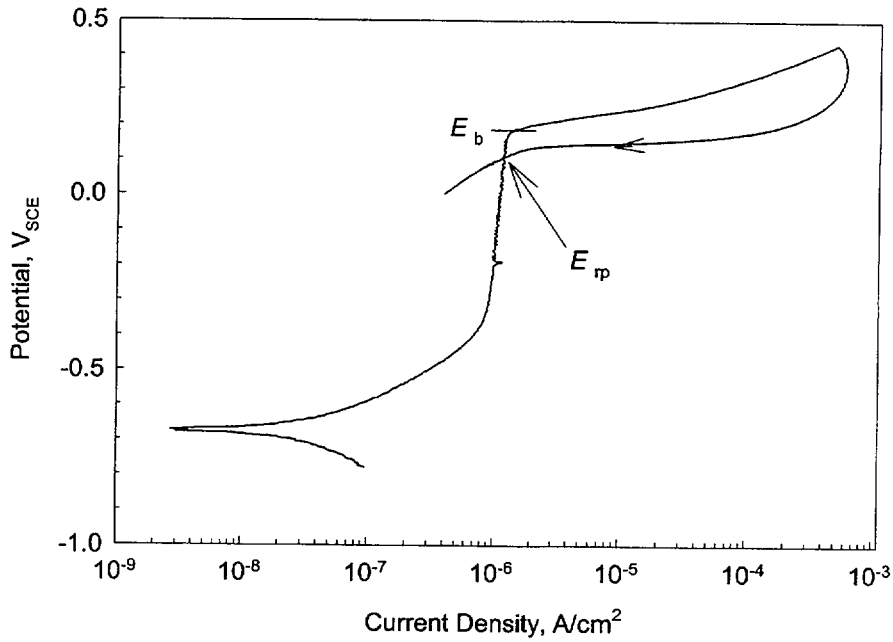


**Figure 3-1. Potentiodynamic Polarization Curve for Zircaloy-4 in Deaerated, Simulated J–13 Well Water (pH 8.4) Containing 0.1 M NaCl at 95 °C. A Scan Rate of 0.167 mV/s was Used**

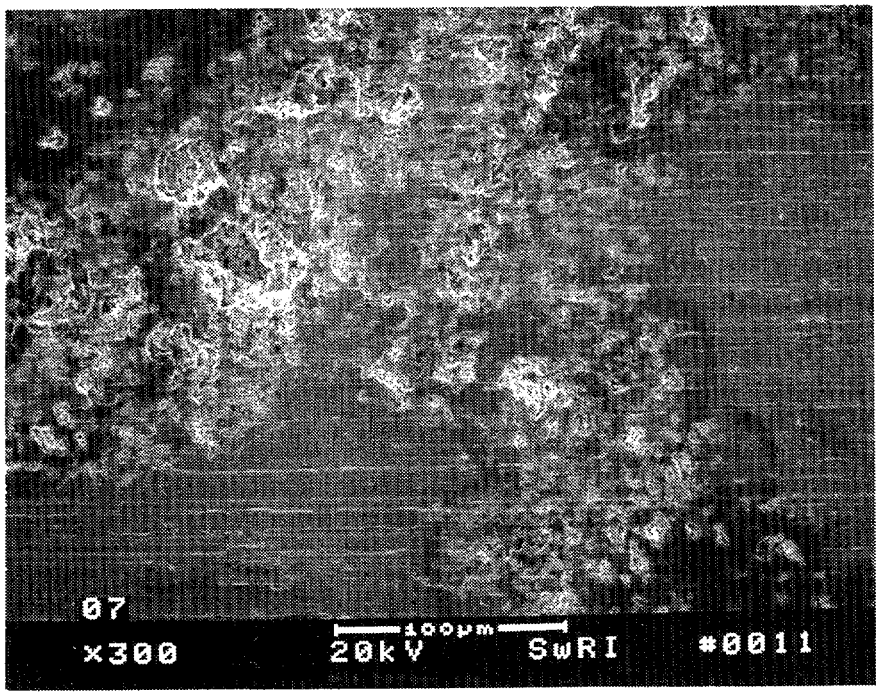


**Figure 3-2. Scanning Electron Microscopy Micrograph Showing Typical Pitting Morphology Observed after Polarization of Zircaloy-4**

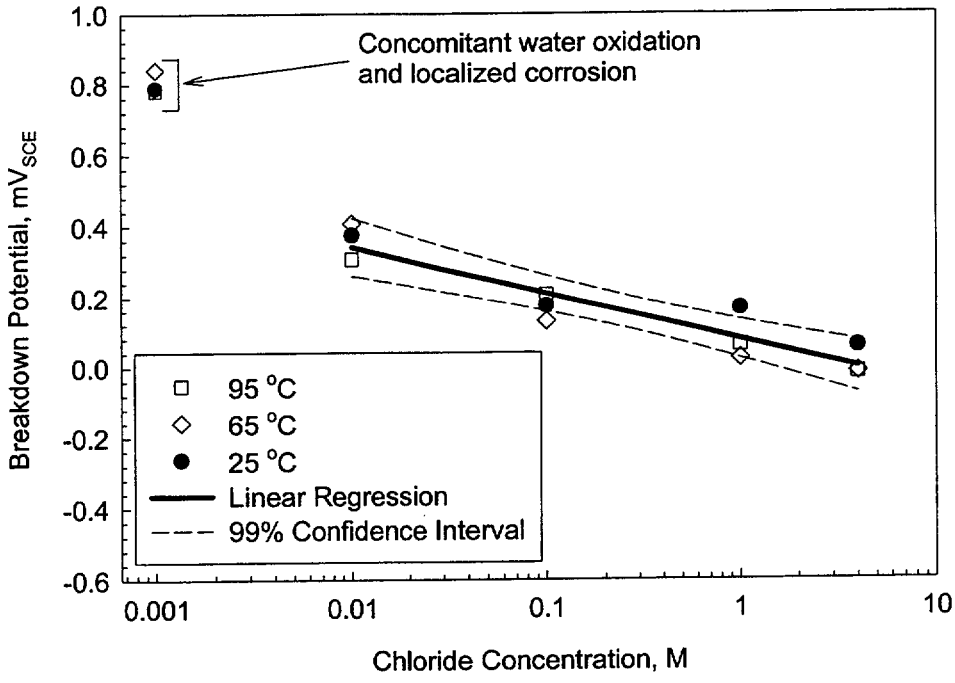


**Figure 3-3. Breakdown Potentials as a Function of Chloride Concentration for Zircaloy-4 in Simulated J–13 Well Water; $E_b(V_{SHE}) = 0.079–0.131 \log [Cl^-]$**

where $B$ is the slope of the dependence of the critical potential ($E_{crit}$, either the breakdown potential or the repassivation potential), and $E^0_{crit}$ is the value of the critical potential at 1 M chloride concentration. For the breakdown potential, $B$ and $E^0_b$ were found to be equal to 131 mV/decade and 0.08 $V_{SCE}$, respectively. At a chloride concentration of 0.001 M, the breakdown potential was high, exhibiting a significant deviation of the linear dependence on the logarithm of the chloride concentration presumably associated with the concomitant oxidation of water and the evolution of oxygen.

As shown in Figure 3-4, a plot of the repassivation potential as a function of chloride concentration for the tests conducted in the simulated groundwater (pH 8.4) exhibits a similar independence of temperature as that observed for the breakdown potential. The repassivation potential displayed a linear logarithmic dependence on chloride concentration, as described by Eq. (3-1). However, the linear dependence extends to the lowest chloride concentrations. The values of $B$ and $E^0_{rp}$ are both lower than those for passivity breakdown and equal to 83 mV/decade and 0.04 $V_{SCE}$ respectively. Figure 3-4 also shows the values of $E_{rp}$ for tests conducted in 0.1 M chloride solution at 95 °C with the addition of 0.0005 and 0.010 M NaF. It is clearly shown in Figure 3-4 that the measured values lie within the 99-percent confidence interval for the linear logarithmic plot of $E_{rp}$ as a function of the chloride concentration for the simulated groundwater in which the NaF concentration is only at 0.0001 M. The slope of the dependence of the repassivation potential on the logarithm of the chloride concentration, $B$ in Eq. (3-1), is similar to that reported by Maguire (1984) and slightly higher than the theoretical value derived by Galvele (1976) in his model of pitting corrosion. From the data shown in Figure 3-4, it can be inferred that both $B$ and $E^0_{rp}$ are independent of temperature practically up to the boiling point of water. This observation confirms and extends previous findings of Maguire (1984) for pure Zircaloy and reveals that Zircaloy-4, contrary to the case of many metals and alloys (Szklarska-Smialowska, 1986; Dunn, et al., 1996), does not exhibit a

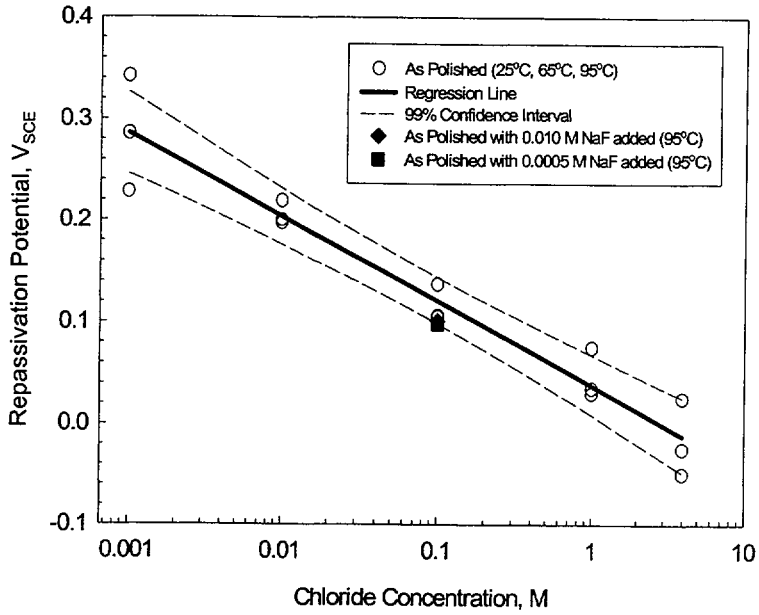


**Figure 3-4. Repassivation Potentials as a Function of Chloride Concentration for Zircaloy-4 in Simulated J–13 Well Water; $E_{rp}(V_{SHE})$ = 0.038–0.083 log [$Cl^-$]**

decrease in the repassivation potential and $E^0_{rp}$ with increasing temperature in the range 25 to 95 °C. For $E^0_{rp}$, the value observed here is about 60 mV lower than that found by other authors in pure chloride solutions at room temperature (Cox, 1973; Cragnolino and Galvele,1978). The difference cannot be related to the anions present in the simulated groundwater because their effect should be just the opposite. The most reasonable explanation for the difference in the literature data appears to be related to the method used to determine the value of the repassivation potential from cyclic potentiodynamic polarization testing. If the repassivation potential is estimated from the intersection of the forward current density with the approximately linear extrapolation of the reverse current density once pitting has been initiated, the value obtained could be 50 to 60 mV greater than that obtained through the intersection of the plotted curves. The bend in the reverse current density plot approaching the intersection with the forward current (Figure 3-1) may be the result of using a relatively fast potential scan rate, which introduces an error in the determination of $E_{rp}$. Nevertheless, the values reported in Figure 3-4 can be considered a lower bound for $E_{rp,}$ and therefore, can be used with confidence in long-term performance assessments.

The plot of the breakdown potential shown in Figure 3-3 also exhibits a linear dependence on the logarithmic of the chloride concentration which is independent of temperature but the values of $E^0_b$ and $B$ are significantly higher than those corresponding to repassivation. The difference between the breakdown and repassivation potentials, and, as a consequence, between $E^0_b$ and $E^0_{rp}$, is related to the stochastic nature of the pit initiation process and the deterministic character of repassivation once pit growth has occurred. Indeed, Mankowski, et al. (1984) demonstrated that the initiation time for pitting of Zircaloy-4 under potentiostatic conditions at potentials above the repassivation potential obeys a log-normal distribution, and the mean initiation time increases with decreasing potentials. Therefore, if sufficient time is allowed for pit initiation to occur, the difference between the breakdown and repassivation potentials tends to become negligible and justifies the use of the repassivation potential as a useful threshold parameter for predicting the occurrence of localized corrosion (Dunn, et al., 1996).

The difference in the value of $B$ between initiation and repassivation, however, deserves additional discussion. The high value of $B$ for the expression of the breakdown potential suggests that the calculation of this important parameter for modeling pitting corrosion using results from cyclic potentiodynamic polarization testing, as many times has been reported (Szklarska-Smialowska, 1986), may not be as useful because it is dominated by the random nature of the pit initiation process and, therefore, extremely dependent on experimental factors, such as surface roughness, potential scan rate, passivation times, and other test procedures. For example, Mankowski, et al. (1984) found that the initiation time increases with the decrease in surface roughness and with increases in the prepolarization time in the passive range. Shibata and Ameer (1992) have shown that the pit initiation potential is extremely dependent on the film formation potential for Zircaloy anodized in sulfuric acid prior to polarization in NaCl solutions.

Figure 3-5 shows the effect of pH on the breakdown and repassivation potentials in deaerated simulated groundwater containing 0.1 M chloride at 95 °C. The pH of the solutions was varied from 2.1 to 10.7. Whereas a significant effect of pH can be noted in the case of the breakdown potential, the effect of pH on repassivation is minor and practically negligible. The dependence of breakdown on pH shown in Figure 3-5 appears to be caused by the experimental procedure (i.e., the potential scan rate used in cyclic potentiodynamic polarization tests), rather than an intrinsic characteristic of the pit initiation process.

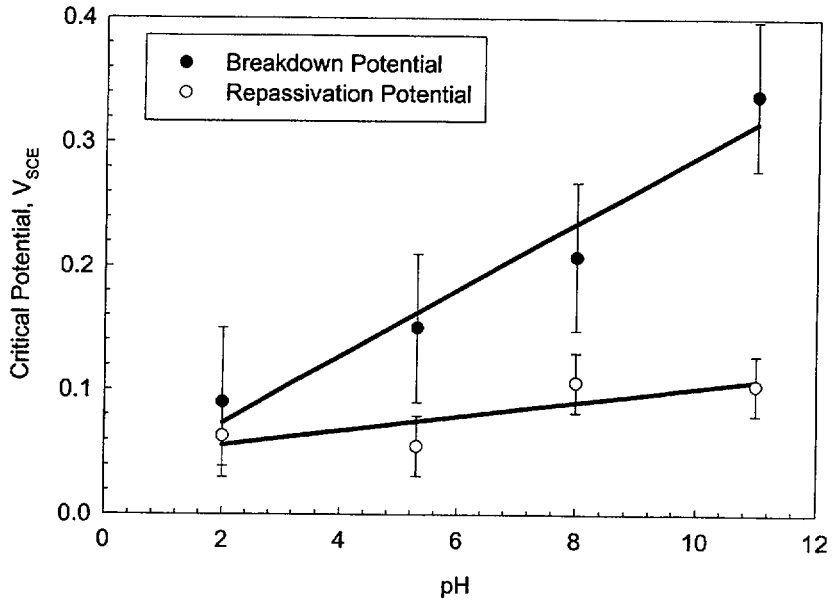


**Figure 3-5. Effect of pH on the Critical Potentials Measured for Zircaloy-4 in Simulated J–13 Well Water Containing 0.1 M NaCl at 95 °C**

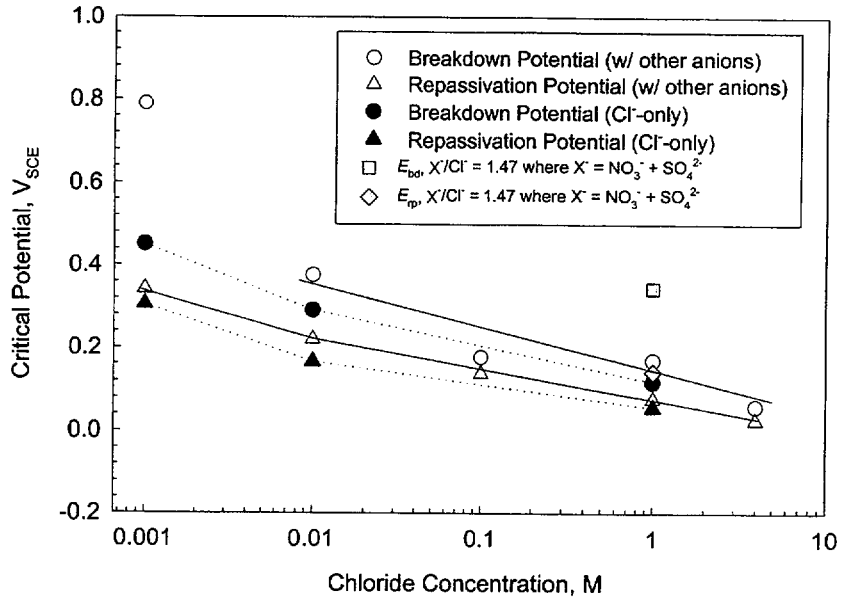


**Figure 3-6. Breakdown and Repassivation Potentials Measured in Solutions with and without J–13 Well Water Anions as Well as Higher Concentrations of Inhibiting Anions**

The conjoint effect of the anions present in the simulated groundwater on the values of breakdown and repassivation is illustrated in Figure 3-6. The data obtained in cyclic potentiodynamic polarization tests conducted in deionized water containing only 0.01 M and 1.0 M NaCl at 25 °C indicate that the anions and their concentration in the simulated groundwater [0.25 mM $SO_4^{-2}$, 0.16 mM $NO_3^-$, 0.10 mM $F^-$, and a total carbonate ($HCO_3^-$ + $CO_3^{2-}$) concentration of 1.4 mM for a total concentration of 1.81 mM excluding $F^-$], have, with the exception of $F^-$, an inhibiting effect at the low chloride concentration because both the breakdown and repassivation potentials increased with respect to the values obtained in the simulated groundwater. Additional testing with higher anion concentrations showed that inhibition of pitting was observed when the ratio of the concentration of inhibitor anions ($X^-$) to the chloride concentration was ~14.7. At lower ratio values (e.g., 0.018 and 0.18 used in simulated groundwater and 1.47 from other tests), localized corrosion was still observed, albeit with higher critical potentials indicating at least partial inhibition of localized corrosion. Maraghini, et al. (1954) found that the strength of the inhibiting effect of these anions decreases in the order $NO_3^- > SO_4^{2-} > HCO_3^-$. It is apparent, however, that the ratio of the sum of the weighted concentration of inhibitor anions to chloride ion concentration is the important parameter to evaluate the inhibiting efficiency as illustrated in Eq. (3-2)

$$\frac{\sum a_i [X^-]_i}{[Cl^-]} > 1 \qquad (3\text{-}2)$$

where $a_i$ is a weighted coefficient. Inhibition only occurs when this ratio is greater than one.

To verify that $E_{rp}$ can be used as a threshold potential for the occurrence of localized corrosion of Zircaloy-4, a potentiostatic test was conducted in simulated groundwater containing 1.0 M NaCl at 95 °C and an applied potential of 0.055 $V_{SCE}$. This potential represents an overpotential of approximately 25 mV with respect to $E_{rp}$ for the same chloride concentration. Upon the application of the potentiostatic step, the current density increased initially to a value of the order of 3 mA/cm$^2$ prior to decaying to a steady state value of 0.75 mA/cm$^2$. The experiment was terminated after only 3 minutes of polarization because extensive attack was observed on the specimen surface. As noted after the cyclic potentiodynamic polarization tests, pitting corrosion was localized outside the area defined by the crevice former and confined to the boldly exposed surfaces of the specimen.

Plots of the evolution of the corrosion potential in air saturated, simulated groundwater containing 1 M NaCl at 95 °C are shown in Figure 3-7. After 60–80 hours exposure to the solution the corrosion potential was found to be approximately -0.30 $V_{SCE}$. Figure 3-7 shows that when 5 mM of hydrogen peroxide was added to the solution, to simulate the formation of hydrogen peroxide as the most stable product from the radiolysis of water, there was a rapid increase in the corrosion potential, followed by a slower decay to the original values. A repeat of the peroxide addition elicited a similar spike with the subsequent decay in the potential. At 160 hours following the addition of 10 mM of ferric chloride ($FeCl_3$), however, the corrosion potential increased rapidly exceeding the repassivation potential and remained just above its value for the duration of the test (approximately 275 hours). Examination of the specimen surface revealed the initiation of localized corrosion, in agreement with the observation that the corrosion potential reached the repassivation potential, which is equal to ~0.03 $V_{SCE}$ in the 1 M NaCl solution.

An additional important effect to consider relates to the role of hydrogen peroxide. It is assumed that reducible species generated by the radiolysis of water may increase the $E_{corr}$ observed in air-saturated solutions above $E_{rp}$. In addition to unstable radicals, hydrogen peroxide is the most stable molecular species generated by water radiolysis. However, hydrogen peroxide seems to decompose rapidly in contact with a Zircaloy-4 surface covered by the thin oxide film (about 4 to 6 nm-thick) formed in aqueous solutions, as shown in Figure 3-7. In line with this, Zircaloy metallic surfaces have been shown to catalyze the decomposition of $H_2O_2$ (International Atomic Energy Agency, 1998). A possible explanation for this effect may be related to the electrochemical decomposition of $H_2O_2$ through its own coupled redox reactions.

As the chloride concentration in the solution increased to values close to the solubility of NaCl, $E_{rp}$ decreased to near 0.0 $V_{SCE}$, as shown in Figure 3-4. This indicates that localized corrosion of Zircaloy-4 is likely to occur if this range of chloride concentration is attained in the presence of oxidizing species such as radiolysis products or reducible cationic species (i.e., $Fe^{3+}$) arising from the corrosion of carbon steel baskets used inside waste packages to maintain the fuel assemblies in position. It is not known if these conditions, in terms of availability of reducible species at a sufficiently high concentration, are likely to occur in the environment in contact with the Zircaloy-4 spent nuclear fuel cladding inside breached waste packages. If this is the case, the possibility of localized corrosion needs to be evaluated further. As noted in Figure 3-7, the addition of $FeCl_3$ also increases $E_{corr}$ above $E_{rp}$ and can lead to the initiation of localized corrosion, as is well documented in the case of Zircaloy (Maguire, 1984; Yau and Webster, 1987). Nevertheless, $Fe^{3+}$ cations may not be available in sufficiently high concentrations if the pH of the waste package internal environment is buffered by the presence of relatively high concentrations of $HCO_3^-$ anions, which may result in precipitation of ferric oxyhydroxides.

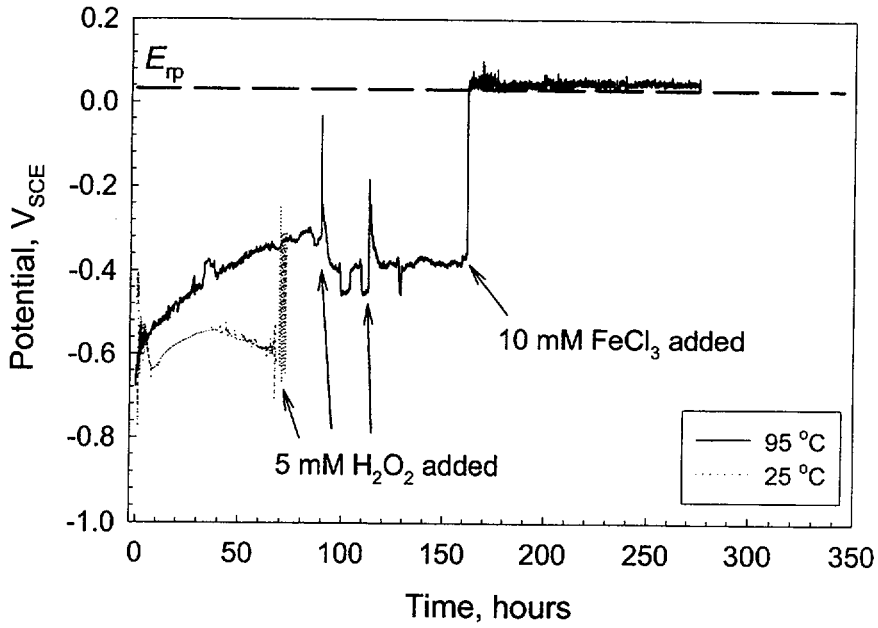


**Figure 3-7. Effect of $H_2O_2$ and $FeCl_3$ Additions on the Open Circuit Potential of a Polished Zircaloy-4 Specimen in Simulated J–13 Well Water Containing 1 M NaCl at 25 and 95 °C**

### 3.2.2 Hydrothermally Oxidized Zircaloy-4

To examine the effects of oxide thickness on the corrosion of Zircaloy-4, a set of Zircaloy-4 specimens were oxidized in a 316L stainless steel autoclave using deionized water at 300 °C for various time periods up to 12 weeks. Using the measured weight gain and the relationship between oxide thickness and weight gain found in Hillner, et al. (1994), the oxide thickness was estimated.

Figure 3-8 shows the same cyclic potentiodynamic polarization curve shown in Figure 3-1 for the as-polished Zircaloy-4 for comparison with the cyclic potentiodynamic polarization curve obtained with a specimen covered with a hydrothermally formed oxide film of about 3.2 $\mu$m in thickness. In the case of the hydrothermally grown oxide, the breakdown potential was 0.75 $V_{SCE}$, which is significantly higher than that measured in the as-polished specimen. The value of the repassivation potential was practically identical for both types of specimens, however. As expected, the corrosion potential was found to be significantly higher (by about 0.5 V) for the specimen covered with the hydrothermally grown oxide. The values for breakdown for the as-polished specimens shown in Figure 3-3 are replotted in Figure 3-9. Also shown in Figure 3-9 are the high breakdown potentials obtained for hydrothermally oxidized specimens (2 and 8 weeks at 300 °C) in 0.1 M chloride solutions at 95 °C. In the case of the repassivation potential, little difference between the as-polished and the hydrothermally grown oxide specimens was observed (within the 99-percent confidence intervals).

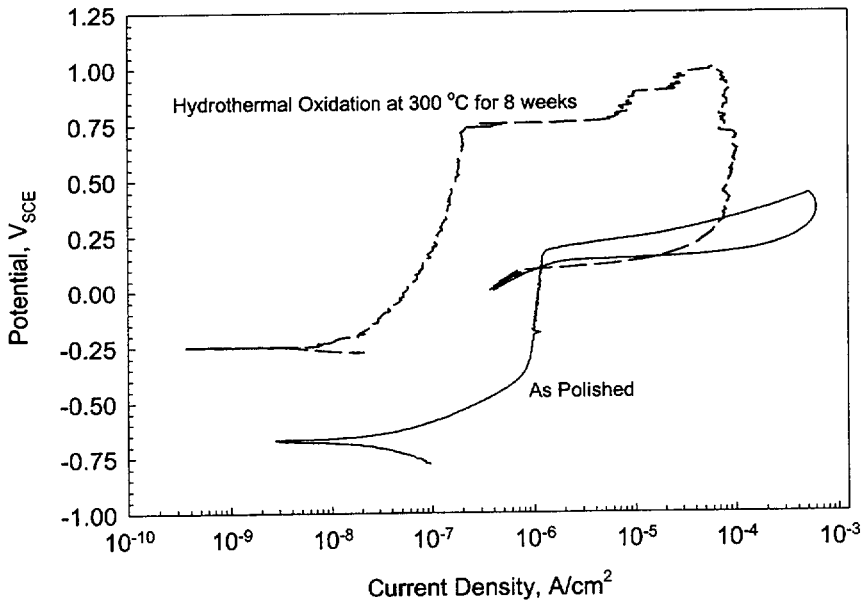


**Figure 3-8. Cyclic Potentiodynamic Polarization Curves for Mechanically Polished and Hydrothermal Oxide Covered Specimens of Zircaloy-4 in Deaerated 0.1 M NaCl Solution at 95 °C Using a Scan Rate of 0.167 mV/s**

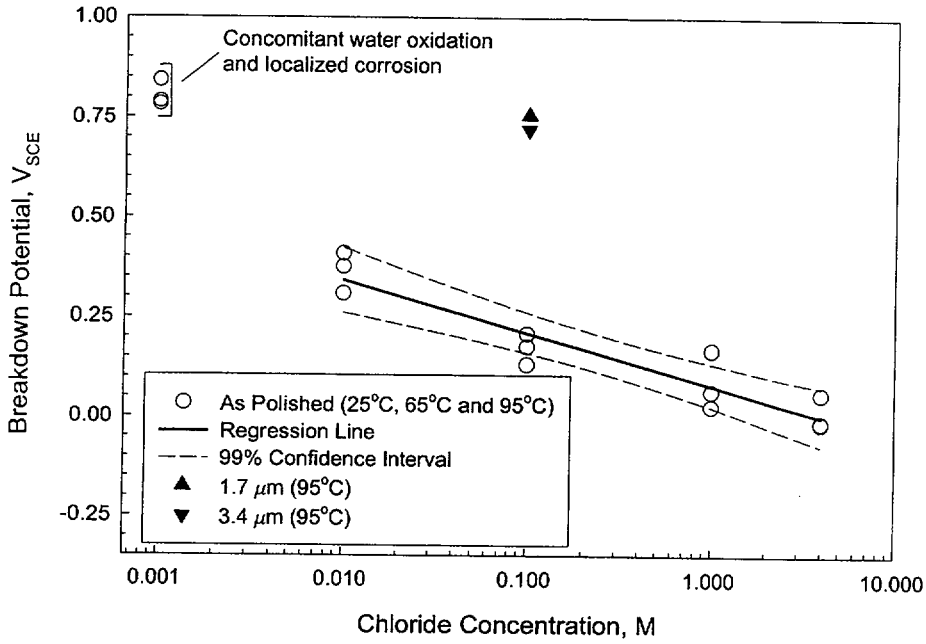


**Figure 3-9. Breakdown Potentials as a Function of Chloride Concentration for Mechanically Polished Specimens of Zircaloy-4 in Simulated J–13 Well Water Compared to Values Obtained for Specimens Covered with a Hydrothermally Grown Oxide**

As shown in Figures 3-8 and 3-9, the breakdown potential was found to be more than 500 mV higher in the case of the specimens covered with the hydrothermally grown oxide layers. No such significant influence of the oxide film was previously observed (Greene, et al., 2000) in the case of specimens covered with an oxide layer formed in air at 200 °C for 8 weeks in which the thickness was estimated to be about 154 nm. It is apparent that a thicker oxide affects significantly the pit initiation process, and this delayed initiation provides an explanation for the high breakdown potentials measured by scanning the potential in a potentiodynamic polarization test. This interpretation is confirmed by the results plotted in Figure 3-10. Figure 3-10 shows plots of the anodic current density as a function of time in 0.1 M NaCl solution at 95 °C and an applied potential of 0.125 $V_{SCE}$ for specimens covered with oxide films grown in water at 300 °C from 2 to 12 weeks (see Table 3-2) as compared to the plot for a polished specimen. Figure 3-10 illustrates that, at a potential only 15 to 25 mV above the repassivation potential, the initiation time for pitting corrosion, as indicated by the abrupt jump in current density from a low current value, increased significantly with oxide layer thickness. It took approximately 42 days to initiate pitting corrosion when the oxide layer was 3.4 $\mu$m thick.

These results suggest that in the presence of thicker oxide films, such as those formed on spent nuclear fuel cladding, extremely long testing times may be required to initiate localized corrosion of Zircaloy. Hence, if sufficient time is allowed for pit initiation to occur, the difference between the breakdown and repassivation potentials tends to become negligible but justifies the use of the repassivation potential as a useful threshold parameter that can be determined in a

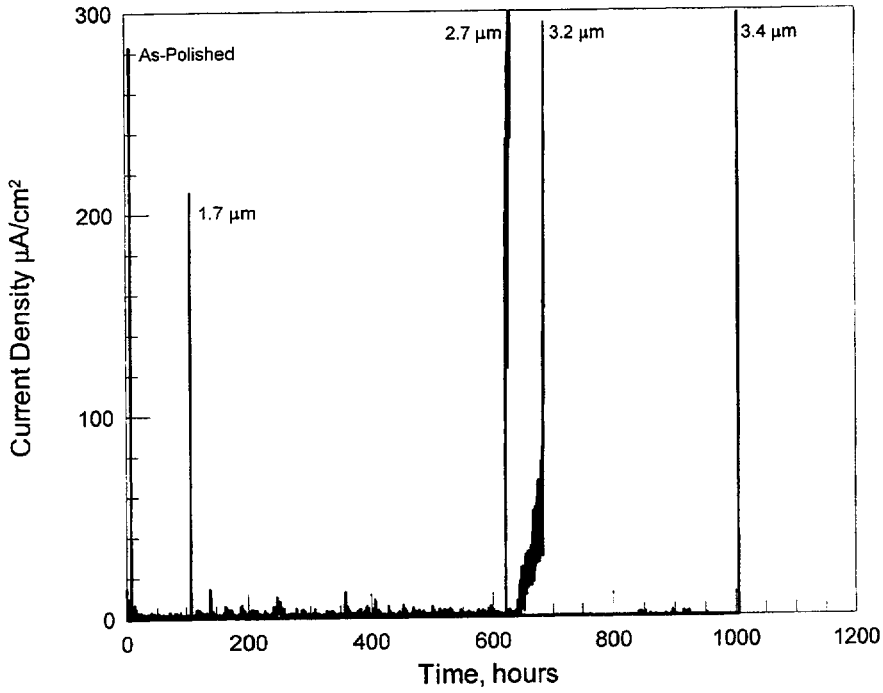


**Figure 3-10. Anodic Current Density as a Function of Time for Mechanically Polished and Oxide Covered Specimens of Zircaloy-4 with Various Film Thicknesses in 0.1 M NaCl Solution at 95 °C under an Applied Potential of 0.125 $V_{SHE}$**

**Table 3-2. Weight Gain and Resulting Oxide Thickness During Hydrothermal Oxidation of Zircaloy-4. Thickness Calculated from Weight Change Using Relationship Provided by Hillner***

| Exposure Time (weeks) | Weight Gain (mg) | Weight Gain/Unit Area ($mg/dm^2$) | Thickness ($\mu m$) |
|---|---|---|---|
| 2 | 2.06 | 25.12 | 1.7 |
| 4 | 3.28 | 40.01 | 2.7 |
| 8 | 3.87 | 47.19 | 3.2 |
| 12 | 4.16 | 50.68 | 3.4 |

*Hillner, E., D.G. Franklin, and J.D. Smee. "The Corrosion of Zircaloy-Clad Fuel Assemblies in a Geologic Repository Environment." WAPD–T–3173. West Miffin, Pennsylvania: Bettis Atomic Power Laboratory. 1994.

short-term electrochemical for predicting the occurrence of localized corrosion (Dunn, et al., 1996).

It should be noted, in relation to the role of the thick, preformed oxide layer, that the morphology of the localized attack changed substantially, as shown by comparing Figures 3-2 with 3-11 through 3-13. For hydrothermally oxidized specimens, the attack was confined to more localized areas and was still partially covered by the oxide, as shown at a lower magnification in Figure 3-11. As revealed in a cross sectional view of the specimen (Figure 3-12), the attack penetrated deep into the metal, apparently along some preferential orientations, leaving behind a highly porous mass of black corrosion products. The spongy appearance of the corrosion products is clearly noticeable in Figure 3-13. X-ray diffraction was used to identify the major components of the black corrosion products easily extracted as a powder from the attacked area. As shown in Figure 3-14, the major components were identified as metallic zirconium and a zirconium hydride ($ZrH_{0.25}$) with only traces of a zirconium oxychloride ($ZrOCl_2 \cdot 6H_2O$), and a minor proportion of zirconium oxide ($ZrO_2$) was present. Thus, it appears that deeper pits can only develop as a result of the better protection offered to the surrounding surface by the thermally grown film, contrary to the case of the thin passive films formed after mechanical polishing in low temperature (< 100 °C) aqueous solutions or air, which are only about 4 to 6 nm thick (Cragnolino, et al., 1999)

Another important observation is the presence of metallic Zircaloy and $ZrH_{0.25}$ as the main corrosion products inside pits. There are two possible alternative explanations for this observation. As observed by Postlethwaite and Onofrei (1979), it appears that anodic disintegration occurred during pitting corrosion forming, in addition to a gel of $Zr(OH)_4$, a metal

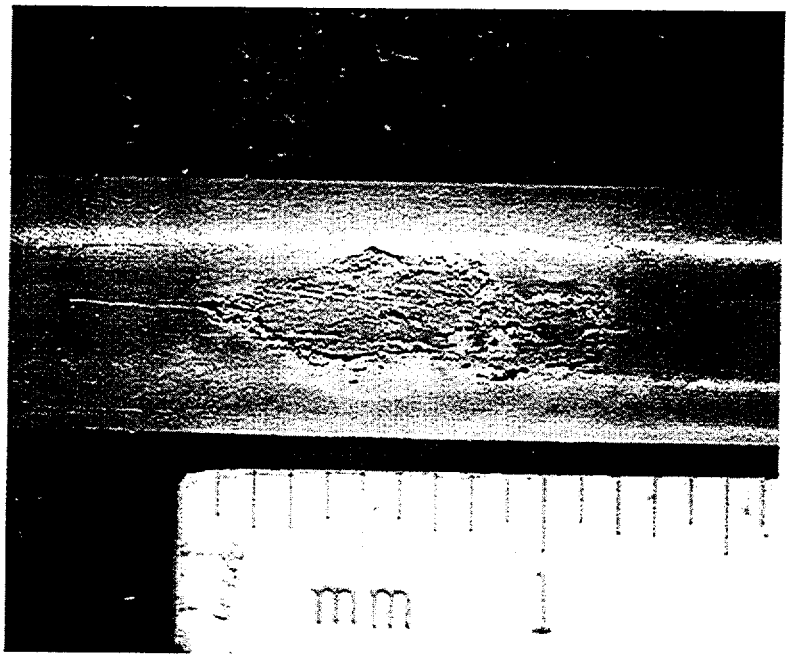


**Figure 3-11. Low Magnification Photograph Showing the Typical Morphology of the Localized Corrosion Observed after Anodic Potentiostatic Polarization of Zircaloy-4 Specimen Covered with a Hydrothermally Grown Oxide Film in Chloride Containing Solutions at Potentials above $E_{rp}$**

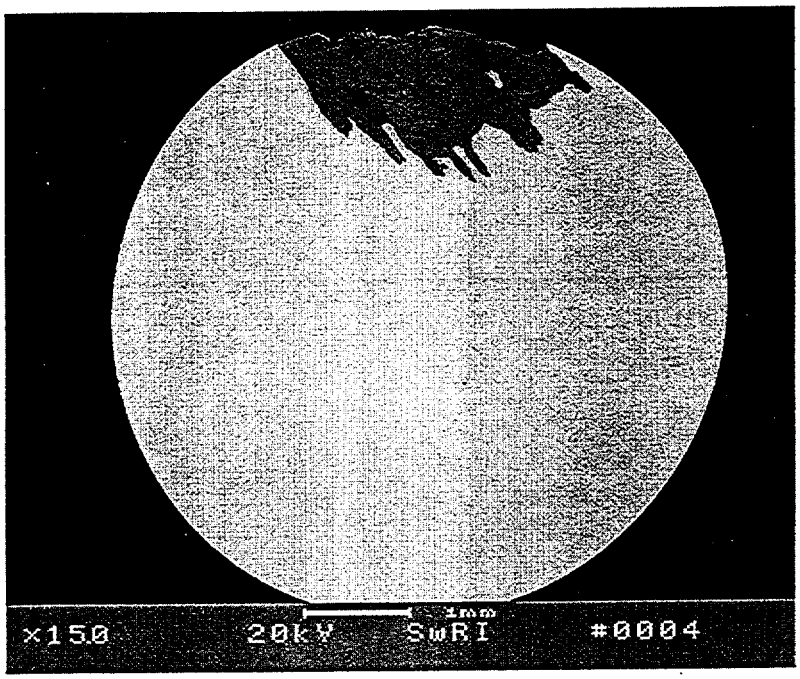


**Figure 3-12. Scanning Electron Microscopy Micrograph Showing a Cross-Sectional View of the Localized Corrosion Observed after Anodic Potentiostatic Polarization of Zircaloy-4 Specimen Covered with a Hydrothermally Grown Oxide Film in Chloride Containing Solutions at Potentials above $E_{rp}$**

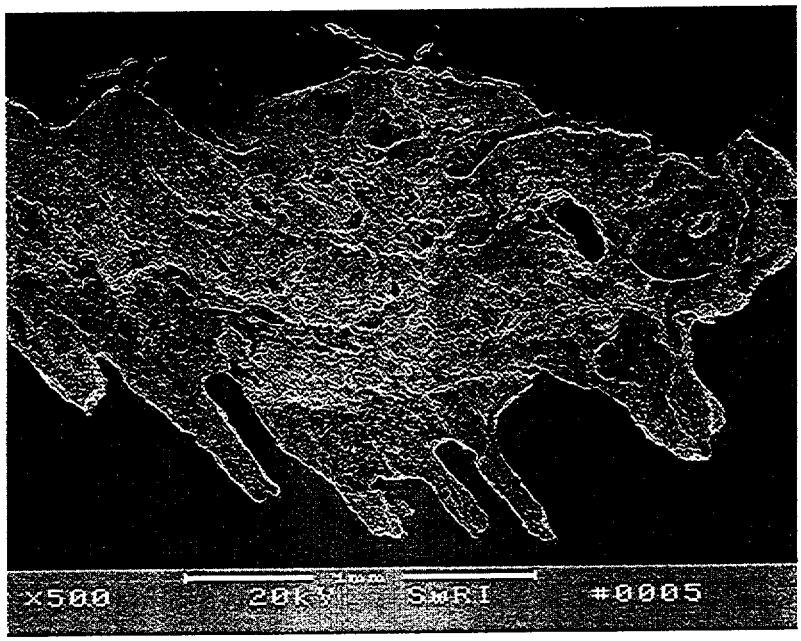


**Figure 3-13. Scanning Electron Microscopy Micrograph Showing a More Detailed View of the Localized Corrosion and the Appearance of the Corrosion Products Observed after Anodic Potentiostatic Polarization of Zircaloy-4 Specimen Covered with a Hydrothermally Grown Oxide Film in Chloride Containing Solutions at Potentials above $E_{rp}$**

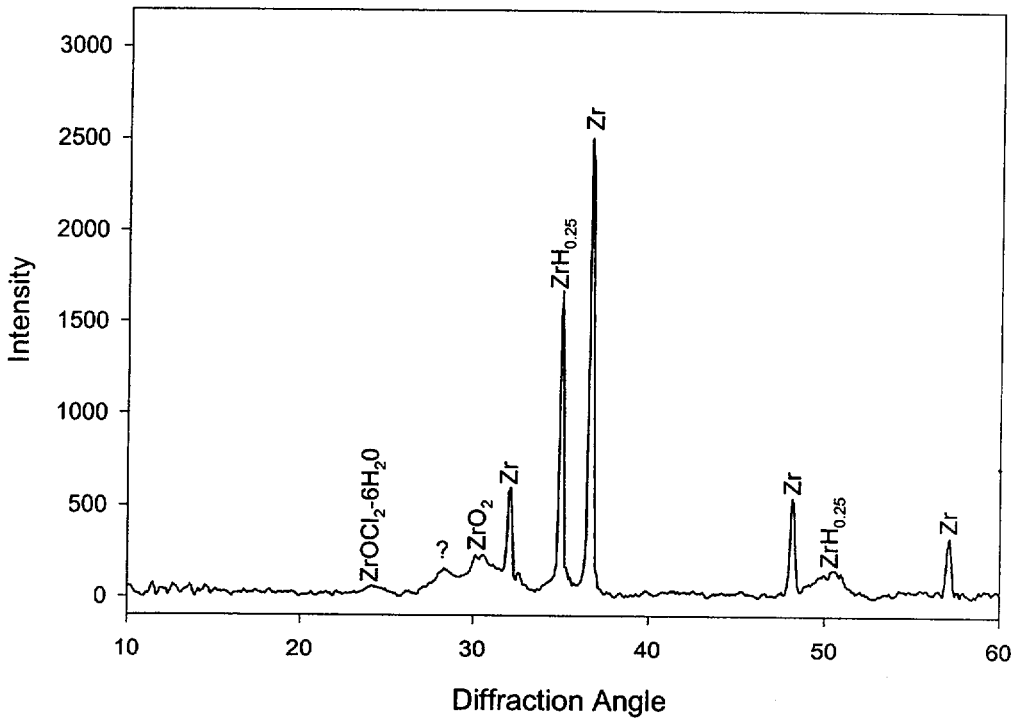


**Figure 3-14. X-Ray Diffraction Pattern of the Corrosion Products Found in a Pit of Zircaloy-4 Showing, in Addition to the Zircaloy Peaks, the Assignment of the High Intensity Peak to $ZrH_{0.25}$**

powder (α-Zircaloy) that can react with water generating $H_2$ gas (and eventually $ZrH_{0.25}$). The other explanation is that $H^+$ ions, generated by hydrolysis of $Zr^{4+}$ ions produced by active dissolution in the pit, are reduced to atomic hydrogen that immediately formed $ZrH_{0.25}$ by reaction with the metal. In this second case, however, the presence of Zircaloy as a metallic powder cannot be easily justified.

Plots of the evolution of the corrosion potential of Zircaloy-4 in air-saturated 0.1 M NaCl at 95 °C, before and after the addition of $H_2O_2$ or $FeCl_3$ (attaining a concentration of 5 mM), are shown in Figure 3-15. Specimens covered with an oxide film hydrothermally grown at 300 °C for 2 and 8 weeks were used in these tests. There are no clear trends in the evolution of corrosion potential during the initial 240 hours of exposure. Specimens with a 2-week oxide film exhibited an initial decay in corrosion potential followed by an increase, with a constant difference of approximately 300 mV between the values of corrosion potential for the two specimens. For the specimens with the thicker oxide film, the difference between the values of corrosion potential was larger, approximately 450 mV, but the potential increased initially, reached a peak, and increased again after a minor decay. As expected, the corrosion potentials were found to be higher in average for the specimens with the thicker oxide film. After the addition of $H_2O_2$, however, the values of the corrosion potential became similar (< 100 mV difference) regardless of the oxide film thickness, reaching, at the end of the test, values approximate to those measured initially in the air saturated solution without $H_2O_2$. On the other hand, corrosion potentials increased with the addition of $FeCl_3$, became higher and remained relatively constant

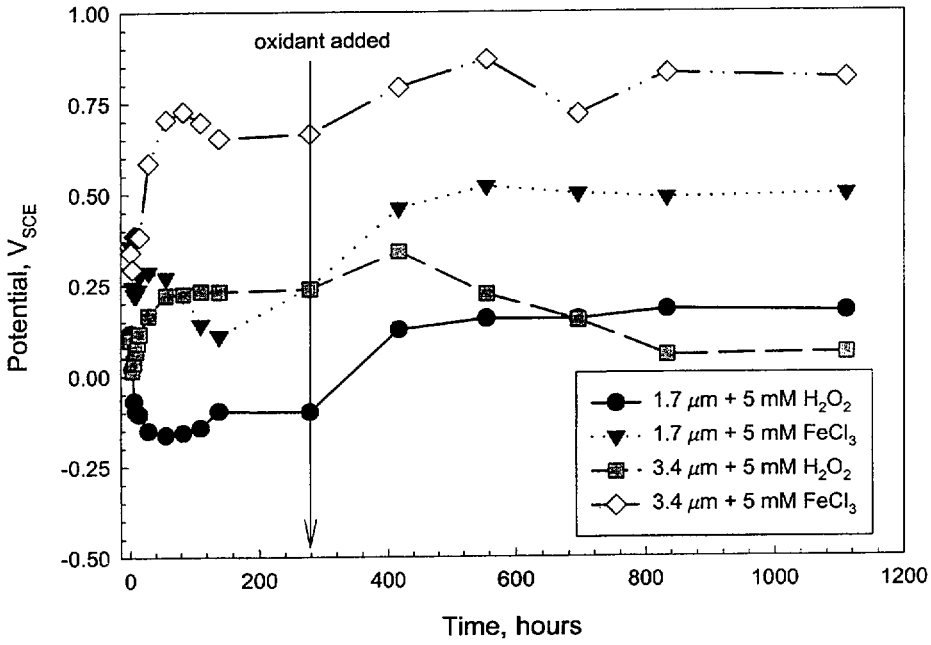


**Figure 3-15. Effect of $H_2O_2$ and $FeCl_3$ Additions on the Open Circuit Potential of Zircaloy-4 Specimens, Covered with Hydrothermally Grown Oxide Films of Different Thickness, in Air Saturated 0.1M NaCl Solution at 95 °C**

for the duration of the test. After approximately 840 hours (~35 days), however, no pitting corrosion initiation was observed on the specimens exposed, under open circuit potential conditions, to the chloride solution after the addition of $FeCl_3$ even though the corrosion potentials (differing in ~300 mV for these two specimens with different oxide thickness) were higher than the repassivation potential. In the chloride solution containing $H_2O_2$, the corrosion potentials were close to the repassivation potential and pitting corrosion was not initiated, suggesting that a certain overpotential is needed to promote pitting under open circuit conditions.

As noted in Figure 3-15, the addition of $FeCl_3$ increases the corrosion potential above the repassivation potential and may lead to the initiation of localized corrosion under open circuit conditions. This represents a situation where a sufficient driving force, as given by the overpotential (difference between the open circuit potential and the repassivation potential), exists to promote pitting corrosion, even though a extremely long time interval may be needed to initiate it. However, it appears, from the results presented in Figure 3-15, that pitting corrosion is not easily initiated under open circuit conditions, at least within the duration of these tests (42 days). One possibility is that the current supplied by the cathodic reduction of $Fe^{3+}$ to $Fe^{2+}$ ions (plus that resulting from the $O_2$ reduction) is not sufficient to promote pit initiation and growth because $ZrO_2$ is a poor electronic conductor. Although the intermetallic particles existing in Zircaloy-4 (Van der Sande and Bement, 1974) constitute a potential electronic conduction path, the path might be interrupted because the particles remained embedded and isolated in an oxide layer of sufficient thickness. In addition, $Fe^{3+}$ cations might not be available in sufficiently high concentrations in the experiment. This may be a possible situation inside containers because, if the pH of the waste package internal environment is buffered by the

presence of relatively high concentrations of $HCO_3^-$ anions, precipitation of ferric oxyhydroxides may occur, decreasing the concentration of free $Fe^{3+}$ cations. Furthermore, hydrogen peroxide, which may also be present, seems to act as a mild oxidant in the presence of a thick oxide layer, as shown in Figure 3-15. This observation is contrary to the effect discussed in Section 3.2.1 in reference to Figure 3-7.

### 3.2.3 CNWRA Model Abstraction and Performance Estimation

In the NRC/CNWRA Total-system Performance Assessment Code Version 4.1, cladding is considered as a potential additional barrier to radionuclide release. There is no explicit or implicit model examining cladding failure, rather it is assumed that cladding will reduce the fraction of spent nuclear fuel surface area exposed to the environment. Modeling of cladding performance is accomplished through the use of a constant that represents the fraction (from 0 to 1) of spent nuclear fuel that is exposed. The base case uses a value of 1, that is all of the spent nuclear fuel is exposed.

To evaluate the possible performance of Zircaloy cladding in the repository, a series of sensitivity studies were conducted. In these simulations, parameters for Zircaloy cladding (e.g., thickness, relationship between the repassivation potential and chloride concentration, and passive corrosion rate) were substituted for waste package outer barrier parameters, and the waste package inner barrier was effectively turned off by setting its thickness to zero. In addition, all disruptive events and the drip shield were also turned off. The simulation results for the various cases examined are shown in Figure 3-16. The basecase simulation resulted in estimated failure times ranging from 661 to 4,710 years depending on the passive corrosion rate

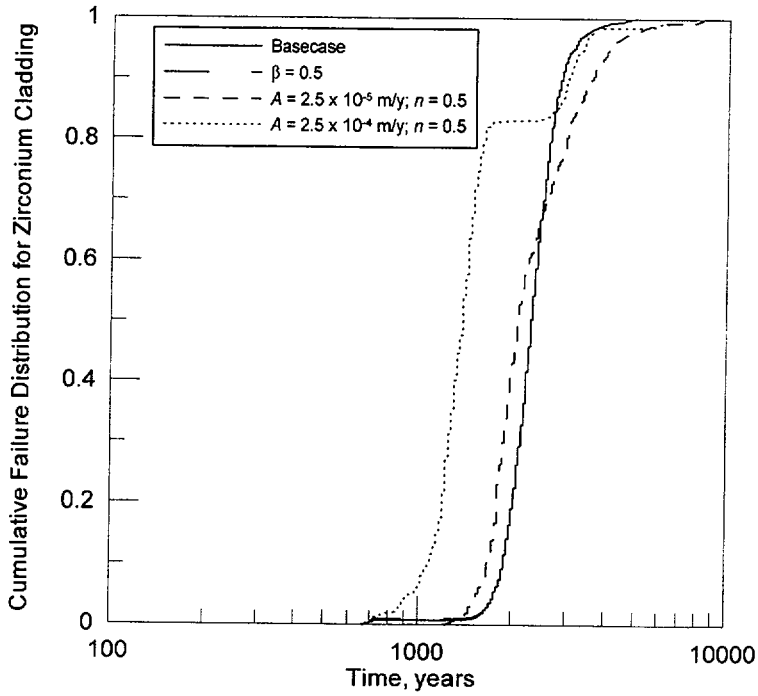


**Figure 3-16. Estimated Failure Times for Zircaloy Cladding Failure Simulated Using the Total-system Performance Assessment Code**

(sampled using a normal distribution between $10^{-4}$ to $10^{-3}$ mm/yr based on short-term potentiostatic tests) and the length of the initial repository dry period. The highest estimated corrosion potential was approximately -0.060 $V_{SCE}$, which was 0.270 V below the estimated repassivation potential. Because this estimated corrosion potential is below that measured for as-polished Zircaloy-4 in air-saturated solutions and well below the corrosion potentials measured for hydrothermally oxidized Zircaloy-4, the β parameter (an indication of the symmetry of the cathodic and anodic reactions; related to the Tafel slope) for the cathodic reduction of oxygen was modified to a value of 0.5 to yield a shallower cathodic Tafel slope (0.12 V/decade) and thereby increase the estimated corrosion potential. The estimated corrosion potential did increase to ~0.020 $V_{SCE}$, which is still well below the estimated repassivation potential, and thus the same failure times were estimated (i.e., failure times were controlled by the distribution of passive corrosion rates).

To increase the predicted corrosion potential further, the passive corrosion rate was decreased to a distribution between $5 \times 10^{-5}$ to $5 \times 10^{-4}$ mm/yr and a constant offset of 0.3 V was introduced. These modifications resulted in increasing the estimated corrosion potential to 0.220 $V_{SCE}$, which is in line with the measured corrosion potentials on the hydrothermally oxidized specimens in air-saturated solutions. Initial simulations using these parameters estimated localized corrosion to occur, and, using the basecase localized corrosion propagation rate of 0.25 mm/yr ($A = 2.5 \times 10^{-4}$ m/yr), cladding failure was estimated to occur within a single timestep (~23 years). To better examine the evolution of the corrosion potential, two modified cases for localized corrosion were examined $A = 2.5 \times 10^{-5}$ m/yr with $n = 0.5$ and $A = 2.5 \times 10^{-4}$ m/yr with $n = 0.5$, using $A$ and $n$ as shown in Eq. (3-3),

$$P = At^n \tag{3-3}$$

where $P$ is the penetration (in m) at any given time, $t$, $A$ is the coefficient for localized corrosion; and $n$ represents the time decay exponent for the corrosion rate. The results for these simulations are shown in Figure 3-16. Assignment of $n$ to a value of 0.5 physically represents the case in which pit propagation is diffusion limited. In the first localized corrosion case ($A = 2.5 \times 10^{-5}$ m/yr with $n = 0.5$), the estimated failure times ranged from 1,220 to 8,160 years as well as estimated corrosion potentials that were above the estimated repassivation potentials. This range of failure times represents a shift to later times compared to the original basecase. This shift, however, is artificial because the value for $A$ is only 25 times larger than the basecase passive current density, and this localized corrosion rate decreases exponentially with time. Utilizing the basecase localized corrosion rate, failure times as short as 136 years were observed. An alternative localized corrosion case ($A = 2.5 \times 10^{-4}$ m/yr with $n = 0.5$) in which the value of $A$ was the same as the basecase, but the localized propagation rate was allowed to decay exponentially, resulted in similar predictions for the corrosion potential and repassivation potential. Failure was estimated to occur earlier compared to the first localized corrosion case, ranging from 680 to 6,100 years.

From these analyses, it is clear that if the estimated values of the corrosion potential are in the range of those observed in the CNWRA experiments, particularly with the hydrothermally oxidized specimens or in the presence of oxidizing species such as $Fe^{3+}$ or $H_2O_2$, localized corrosion can occur and will likely lead to rapid cladding failure. Further simulations attempting to incorporate the effects of inhibiting anions and other possible modifications accounting for variations of in-package water chemistry (as opposed to assuming nominal groundwater chemistry) should be conducted to further evaluate the susceptibility of localized corrosion of Zircaloy under estimated repository conditions.

# 4 IN-PACKAGE CHEMISTRY

## 4.1 DOE INVESTIGATIONS

The composition of the water entering breached waste packages can be influenced and modified by processes, such as evaporation and chemical reactions, with the host rock and components of the engineered barrier subsystem such as drip shield and drift support materials. Ignoring the interactions with the engineered barriers, the groundwater probably would be some combination of the water found in the unsaturated zone and saturated zone J–13 Well water. Variables such as pH, carbonate, and redox potential are influenced by interactions of the groundwater with natural and engineered materials in the repository and can have a substantial effect on waste form corrosion. To study the effect of incoming fluid composition inside the waste package on the outgoing fluid composition, DOE analyzed, using the EQ 3/6 code, the interactions between waste form and several variations of groundwater compositions, such as J–13 Well water, J–13 Well water that has been concentrated to remove 50 percent water, and a synthetic water composition from thermal-hydrochemical modeling (drift-scale test solutions). A review of the evolution of the groundwater chemistry is provided by Brossia, et al. (2001).

### 4.1.1 DOE Model Abstraction

In the Total System Performance Assessment–Site Recommendation (CRWMS M&O, 2000b), the analysis at the process level of the in-package chemical environment is integral to the calculations of waste form degradation, radionuclide solubility, and colloid availability and stability. The DOE evaluation of the evolution of the in-package chemistry (CRWMS M&O, 2001b,c) is based on calculations performed with the numerical code, EQ 3/6, that simulates the reaction of fluids with the waste forms and waste package internal components after the occurrence of the thermal pulse. Therefore, DOE ignored the temperature dependence of these reactions in the calculations. The key input parameters used in the modeling are

- Input fluid composition and groundwater flux
- High-level waste glass and spent nuclear fuel dissolution rates
- Corrosion rate of steel and other alloys
- Identities of the secondary phases
- Amount of cladding failure

In the in-package chemistry analysis, DOE modeled two representative waste packages, a commercial spent nuclear fuel package and a defense spent nuclear fuel/high-level waste glass codisposal package. Commercial spent nuclear fuel waste packages are assumed to be composed of several reactive components, $UO_2$, aluminum alloy, 304L stainless steel, A516 carbon steel, borated and nonborated 316 stainless steel, 316 stainless steel containing $GdPO_4$, and Zircaloy-clad fuel rods. No interaction between the Zircaloy cladding and the internal environment is assumed, although sensitivity analyses included a percentage of fuel area exposed by breached cladding. Codisposal waste packages comprise a defense spent nuclear fuel canister surrounded by five 304L stainless steel canisters of high-level waste glass. The codisposal waste package is assumed to have the properties of a fast flux test facility waste package and have six reactive components, A516 carbon steel, Type 316 stainless steel (with and without $GdPO_4$), 304L stainless steel, high-level waste glass, mixed oxide fuel, and $UO_2$ fuel.

In the in-package chemistry model, water is assumed to fill the void volume, and the waste package internal components are lumped into equivalent masses per unit volume for calculating the reaction products. EQ 3/6 is used to calculate the time evolution of solution composition as a result of these interactions (CRWMS M&O, 2000f). The specific partial pressures of $CO_2$ and $O_2$ of the repository atmosphere are set to $10^{-3.0}$ and $10^{-0.7}$ atmosphere, respectively. A range of degradation rates was used for each component of the waste package.

The DOE analysis using EQ 3/6 showed that the corrosion of inner waste package materials results in relatively large changes in the fluid chemistry. In addition, the analysis showed that relatively low pH values can be expected as a result of corrosion of stainless steel structural components specifically because of chromium oxidation to Cr(VI) species. The pH of the outgoing fluid through the waste package increases through release of uranium from the spent nuclear fuel or the dissolution of alkali cations from the high-level waste glass. The redox conditions in the system are controlled by the free oxygen level in the surrounding atmosphere.

The DOE in-package chemistry abstraction model (CRWMS M&O, 2001b) is based on the process model discussed above. The water chemistry parameters used in the DOE abstraction include pH, redox potential, ionic strength, total aqueous carbonate, fluoride, and chloride concentrations. The abstraction is based on the assumption that the system pH can be used as an indicator for changes in the groundwater chemistry and is used to calculate the total carbonate concentration at a constant carbon dioxide fugacity and the redox potential at a constant oxygen fugacity.

DOE used a series of multiple linear regression analyses of the output from the EQ 3/6 simulations for the abstraction of the in-package processes for commercial spent nuclear fuel waste packages. Three-dimensional response surfaces establishing the pH boundary limits were determined using the extreme (high and low) values of the waste package corrosion rate. The EQ 3/6 simulation results were plotted, as shown in Figure 4-1, in three-dimensional space, and the pH response surfaces were modeled as a planar surface. Discretization of pH was performed based on the pH trends and the principle of realistic conservatism. For each time phase for commercial spent nuclear fuel package, one pH surface was generated for a low waste package corrosion rate scenario, and another pH surface was generated for a high waste package corrosion rate scenario. These surfaces constitute the boundaries of the range of in-package pH values. Figure 4-2 shows the calculated pH evolution of the commercial spent nuclear fuel waste packages. The vertical lines show the time breaks used for the pH abstraction based on the observed pH behavior and are shown in Table 4-1. The waste package corrosion rates used in the Total System Performance Assessment–Site Recommendation analysis are randomly sampled from the range bounded by low and high values.

For the codisposal package, the calculated pH evolution showed very little variation because of changes in water flux. Because of the lack of correlation between water flux and pH, no response surfaces were formulated. However, the pH for the Total System Performance Assessment–Site Recommendation analysis was randomly sampled from a uniform distribution of pH between 3.2 and 10. Figure 4-3 shows the predicted pH evolution of the codisposal waste packages. The vertical lines show the time breaks used for the pH abstraction based on the observed pH behavior and are shown in Table 4-2.

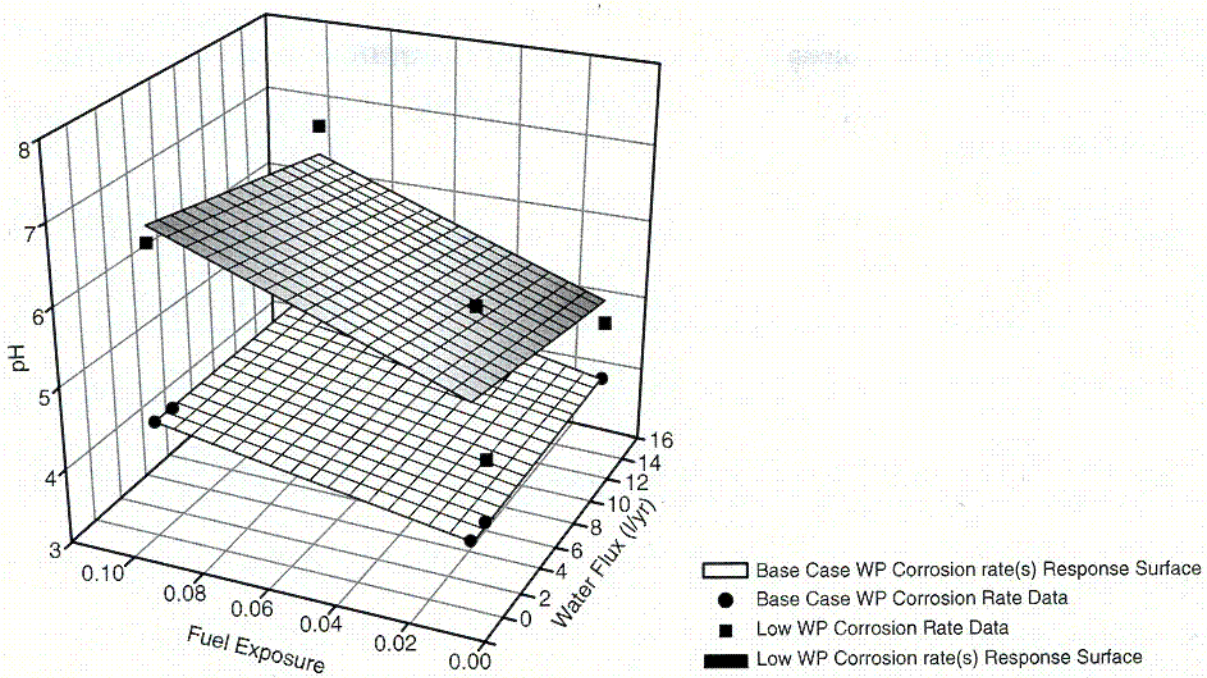


**Figure 4-1. A Typical pH Response Surface for the Commercial Spent Nuclear Fuel Waste Packages for 0–2,000 Years Post Breach (CRWMS M&O, 2001b)**

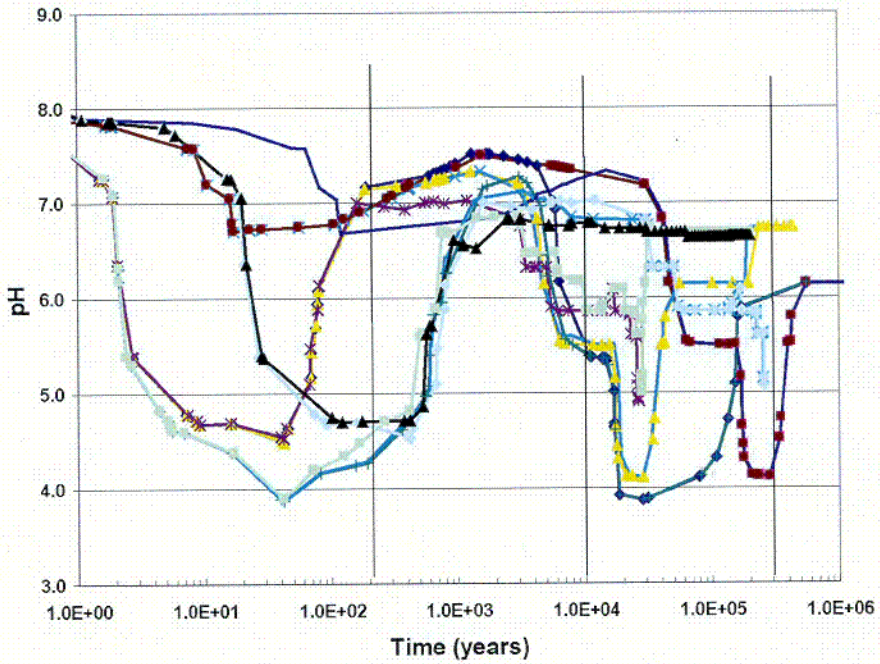


**Figure 4-2. The pH-Time History for the Commercial Spent Nuclear Fuel Waste Packages. Vertical Lines Indicate Time-Breaks in the pH Abstraction Model [Note That Lines Represent Trajectories Predicted over a Range of Water Fluxes (15–0.15 L per Waste Package per Year), Clad Exposures (1–10 Percent), and Steel Degradation Rates] (CRWMS M&O, 2001a).**



C03

| Table 4-1. Criteria Used to Define the pH Ranges for Commercial Spent Nuclear Fuel Package for Each Abstracted Time Period (CRWMS M&O, 2001)* | | |
|---|---|---|
| **Time Period (Years after Post Breach)** | **pH Criteria** | **Expected pH Range** |
| 0–200 | Minimum | 3.9–6.7 |
| 200–10,000 | Average | 6.0–7.3 |
| 10,000–300,000 | Minimum | 3.9–6.6 |
| 300,000–1,000,000 | Stabilized | 6.1–6.7 |

*CRWMS M&O. "Supplemental Science and Performance Analysis–Report Volume 1 of 2." TDR–MGR–MD–000007. Revision 00. Las Vegas, Nevada: CRWMS M&O. 2001.

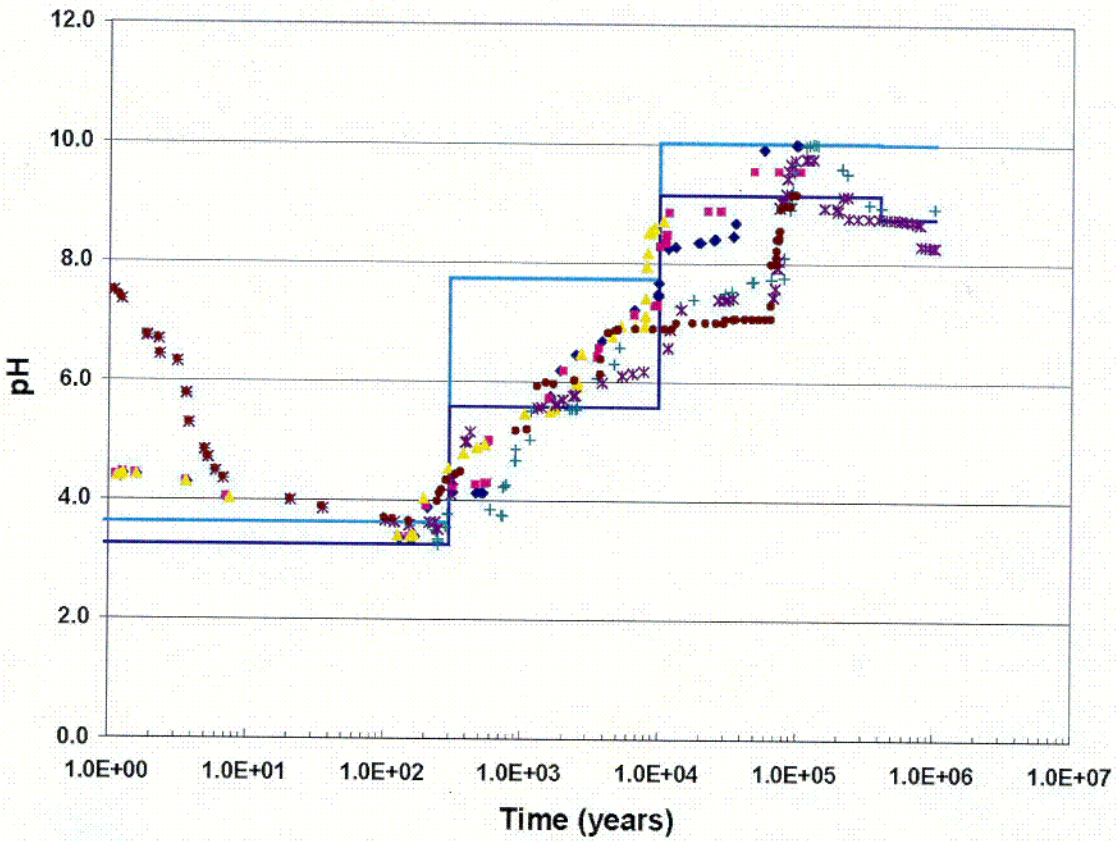


**Figure 4-3. The pH-Time History for the Codisposal Waste Packages. Vertical Lines Indicate Time-Breaks in the pH Abstraction Model [Note That Points Represent Trajectories Predicted over a Range of Water Fluxes (15–0.15 L per Waste Package per Year)]. The Lines Represent Model Abstractions of the Minimum, Maximum, and Average pH Ranges (CRWMS M&O, 2001a).**



C04

| Table 4-2. Criteria Used to Define the pH Ranges for Codisposal Fuel Package for Each Abstracted Time Period (CRWMS M&O, 2001)* | | |
|---|---|---|
| **Time Period (Years after Post Breach)** | **pH Criteria** | **Expected pH Range** |
| 0–300 | Minimum | 3.3–3.6 |
| 300–10,000 | Average | 5.6–7.7 |
| 10,000–400,000 | Maximum | 9.1–10.0 |
| 400,000–1,000,000 | Stabilized | 8.8–10.0 |
| *CRWMS M&O. Supplemental Science and Performance Analysis—Report Volume 1 of 2. TDR–MGR–MD–000007. Revision 00. Las Vegas, Nevada: CRWMS M&O. 2001. | | |

In the Total System Performance Assessment–Site Recommendation, the total carbonate concentration as a function of pH was calculated using Eq. (4-1).

$$\text{Total } C = f_{CO_2}(10^{-1.47} + 10^{(\text{pH}-7.82)} + 10^{(2\text{pH}-18.15)}) \tag{4-1}$$

where $f_{CO_2}$ is fugacity of $CO_2$.

The redox potential of the in-package fluid was calculated using Eq. (4-2).

$$\text{Eh} = 2.303\frac{RT}{F}(20.75 - \text{pH} + 0.25 \log f_{O_2}) \tag{4-2}$$

where $f_{CO_2}$ is fugacity of $O_2$.

In the Supplemental Science and Performance Analysis, two sensitivity cases shown in Figures 4-4 and 4-5 that have the most discernible impact are zero dissolution rate for A516 carbon steel and zero dissolution of glass. In both cases, minimum pH tends to drop between 2 and 3.

### 4.1.2 Assessment of the DOE Approach

A review of the proposed DOE abstraction for the Total System Performance Assessment–Site Recommendation indicates that the abstraction does not address the following aspects of the in-package chemistry.

- The rate equations for corrosion and values used for input parameters for EQ 3/6 modeling requires certain assumptions that may have significant effect on the in-package chemistry. For example, formation of secondary phases predicted by EQ 3/6

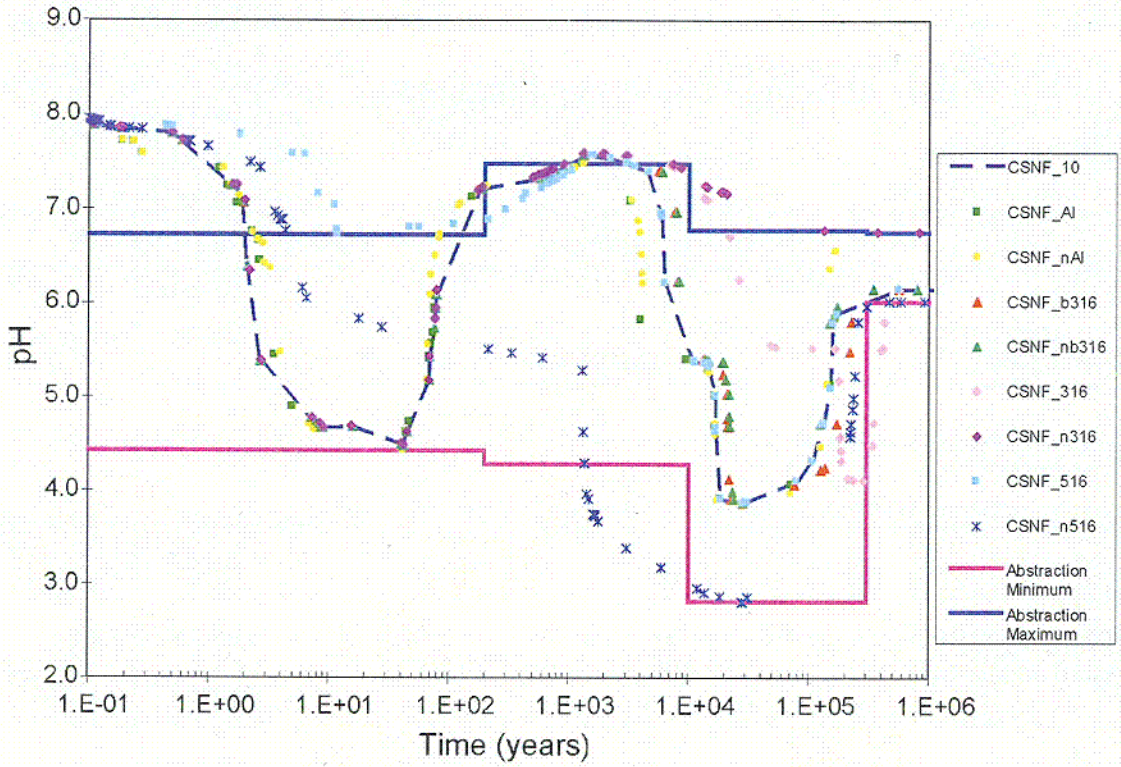


**Figure 4-4. Sensitivity Analysis Showing pH-Time Trajectories for the Commercial Spent Nuclear Fuel Waste Packages Using Zero A516 Steel Dissolution Rate (CRWMS M&O, 2001a)**

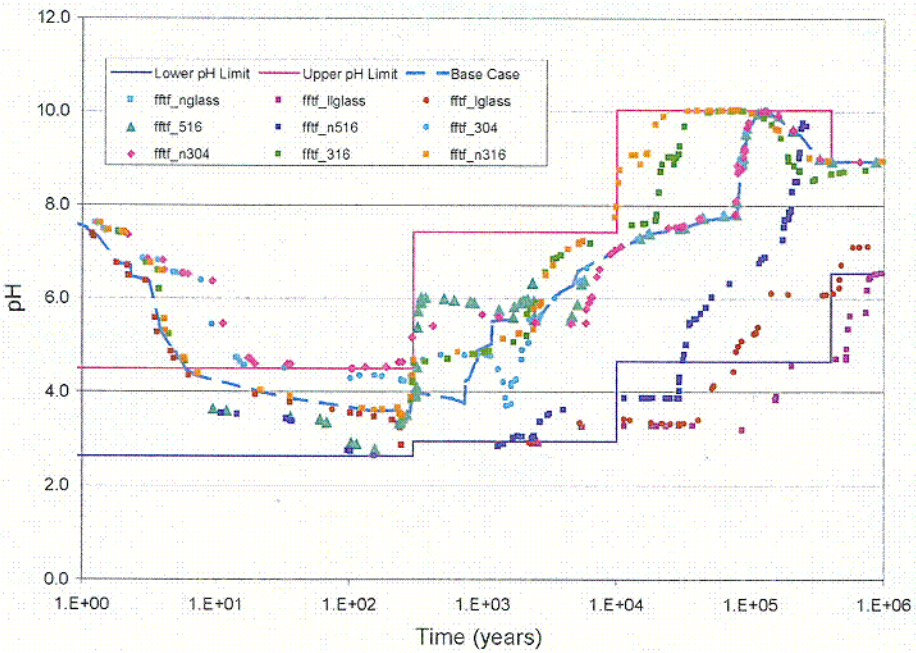


**Figure 4-5. Sensitivity Analysis Showing pH-Time Trajectories for the Codisposal Waste Packages Using Zero Glass Dissolution Rate (CRWMS M&O, 2001a)**



C05

may contradict the experimentally observed phases. DOE agreed to provide additional information in agreements CLST 3.05 and ENFE 3.04.

- The DOE analysis assumes that the aqueous solution fills all the voids in the waste packages and that solutions that drip into the packages have the composition of input water. Dripping water is assumed to enter and exit the waste packages at the same rate and not interact to any significant degree with the waste package walls as it enters the waste packages. This assumption ignores the interaction and equilibration of groundwater with titanium grade 7 drip-shield, Alloy 22 outer waste package, and carbon steel ground support components (i.e., rock bolts, and welded wire fabric), which occurs prior to interaction with 316L stainless steel or waste forms. The DOE analysis considers a simultaneous interaction of waste form and several waste package components, which is questionable. DOE agreed to provide additional information in agreement ENFE 3.03.

- The DOE analysis assumes that glass is released at its maximum rate. This assumption is bounding for the glass release rate. However, the higher the glass dissolution rate, the higher the pH of the fluid in contact. Thus, the real pH may be significantly masked by the bounding rate assumption for glass dissolution. This is further substantiated by the DOE analysis using a glass dissolution rate, which is lower by a factor of 1,000 and indicates that the pH continues to remain between 3 and 4 for 100,000 years. Similar effects are possible for waste package components such as Alloy 22 and 316L stainless steel. DOE agreed to provide additional information in agreement ENFE 3.04.

- The ability of EQ 3/6 to predict the formation of secondary phases resulting from high-level waste glass is not presented or substantiated with experimental results. However, DOE agreed to provide data to support this assumption. Validation of this assumption is important because it will impact the groundwater composition and shift the chemistry of the in-package fluids. The formation of secondary phases may be pH and temperature dependent. Use of software that has limitations in predicting formation of secondary phases imposes significant risk in the analysis. DOE agreed to provide additional information in agreement ENFE 3.04.

- The DOE assumption that the waste package components can be lumped into a single mass for estimating the in-package chemistry may lead to highly nonconservative estimates of pH values. DOE agreed to provide additional information in agreements CLST 3.04 and ENFE 3.03.

- The DOE abstraction has not been validated using experimental results. DOE agreed to provide additional information in agreement ENFE 3.04.

The approach taken by DOE in determining the range of in-package chemistry is appropriate. However, the DOE in-package chemistry model and abstraction couple various corrosion processes together. This approach could mask effects of waste package corrosion on the groundwater chemistry and, hence, underestimate the shifts in the pH and redox potential. In

the Advisory Committee on Nuclear Waste chemistry review report,[6] it also noted that the DOE model abstractions is based on simplified approach assuming a fully saturated environment at ambient temperatures. This model does not address potentially important chemical issues such as radionuclide speciation in the spent nuclear fuel, solubility controlling reactions, or redox reactions at elevated temperatures. Ignorance of these chemical issues imposes uncertainties in the range of in-package chemistry, which control the release and transport of the important radionuclides.

To address the deficiencies identified by NRC staff in its review of the DOE abstraction of radionuclide release and solubility limits, DOE agreed at the DOE and NRC Technical Exchanges on Container Life and Source Term[7] and Evolution of the Near-Field Environment[8] to provide additional documentation according to agreements CLST 3.01, CLST 3.02, CLST 3.03, CLST 3.04, CLST 3.05, ENFE 3.03, and ENFE 3.04. This information will be provided as part of the issue resolution process, and if provided by DOE by the time of any license application, should afford sufficient information for NRC to conduct its licensing review. In an attempt to separate the effects of waste package corrosion and waste form corrosion, CNWRA has conducted a series of experiments to evaluate the chemistry of the fluids entering the inside of the waste packages after corrosion and are discussed in the following sections.

## 4.2 CNWRA INVESTIGATIONS

The chemistry of water contacting the waste forms (e.g., commercial spent nuclear fuel, defense spent nuclear fuel, and high-level waste glass) inside breached waste packages affects the degradation of the waste forms and the subsequent release of radionuclides to the environment. One of the main concerns in evaluating the DOE In-Package Chemistry Model (CRWMS M&O, 2001b,c) is the spatial variation in chemistry that is likely to occur inside waste packages and likely to result in local pH values considerably more acidic than those calculated based on a volume averaged mass. The pH in crevices and other tight spaces differs from bulk pH values because the anodic dissolution reactions become spatially separated from the reduction reactions. Additionally, the range of in-package fluid compositions from the DOE model predictions has not been validated experimentally. To evaluate the effect of some waste package internal structural components on the evolution of the in-package solution chemistry, experimental investigations were conducted using a test cell that simulates some aspects of the internal geometry of the waste package. A perforated stainless steel plate was used for this purpose. An initial water chemistry composition was selected based on the evaporation studies conducted by the DOE (CRWMS M&O, 2001d). The evolution of the solution chemistry, in terms of pH and cation concentration, was determined as a function of applied potential and temperature.

---

[6]Hornberger, G.M. "Review of Chemistry Issues and Related NRC Staff Capability for the Proposed High-Level Waste Repository at Yucca Mountain." Letter (August 13) to R.A. Meserve, NRC. Washington, DC: NRC. 2001.

[7]Schlueter, J.R. "NRC/DOE Technical Exchange and Management Meeting on Container Life and Source Term (September 12–13, 2000)." Letter (October 4) to S. Brocoum, DOE. Washington, DC: NRC. 2000.

[8]Reamer, C.W. "NRC/DOE Technical Exchange and Management Meeting on Evolution of the Near-Field Environment (January 9–12, 2001)." Letter (January 26) to S. Brocoum, DOE. Washington, DC: NRC. 2001.

### 4.2.1 Evolution of Solution Chemistry in Pits and Crevices

Pitting and crevice corrosion are localized forms of attack that result from the breakdown of passive film caused by the evolved aggressive solution chemistry at the pit and crevice areas. The evolved solutions are known to be highly concentrated mixtures of various metal-ion complexes. A few studies have considered the speciation of solution inside pits of stainless steels. Tsuru, et al. (1985) analyzed the solution in a simulated pit of Type 304 stainless steel. They determined the concentration of free chloride by using an Ag/AgCl electrode and the total chloride by extracting the anolyte and titrating with $AgNO_3$. They also analyzed the metal ions in the extracted solution by atomic absorption. They found that the free chloride concentration was lower than the total chloride, indicating the presence of significant metal-chloride complexes. From a measurement of the metal content of the solution and the total charge passed, they estimated that the dissolved Fe was present predominantly as $FeCl^+$ complex and to a lesser extent as $Fe^{2+}$. Brossia, et al. (1998) conducted electrochemical investigations using single pit electrodes to determine the role of alloying elements on solution chemistry changes within the pit. Raman spectroscopy of the pit solution in a Type 308 stainless steel simulated pit showed only the presence of chromium-chloride complexes. At repassivation (about $-0.4V_{SCE}$), the chromium-chloride concentration in the pit solution decreased to a value of about 0.06 M which is about 20 percent of the concentration of chromium-chloride complexes during stable pit growth at 0.9 $V_{SCE}$. In contrast, salt films of $FeCl_2$ and $NiCl_2$ were clearly observed when pure electrodes of iron and nickel were polarized to high potentials. For pure chromium electrode, no salt film was observed because the solubility of $CrCl_3$ is very high. Also, the current transients for the pure chromium electrode did not indicate any signs of salt film precipitation. In addition, the concentration of chromium-chloride complexes for the pure chromium electrode is much smaller than the concentration profile at the stable growth potential for Type 308 stainless steel, despite the lower chromium concentration in the latter. Analyses of cationic concentration of pit solutions from several stainless steels using the atomic absorption spectrochemical technique (Suzuki, et al., 1973) and crevice solutions from 304 stainless steels using capillary electrophoresis (Brossia and Kelly, 1996) revealed that the alloys dissolved stoichiometrically, independent of the extent of the attack.

The pH in pits and crevices differs from bulk pH values because the dissolution reactions become spatially separated from the reduction reactions. Suzuki, et al. (1973) analyzed the solution within artificial pit anodes of some stainless steels in a 0.5 N NaCl solution at 70 °C. They found the pH values of the pit solutions in a range of -0.13 to 0.80, which were lower than the predictions from thermodynamic calculations. The low pH values were attributed to hydrolysis of chromium, molybdenum, or both ions attributed, whereas the differences between the measured and calculated pH were likely due to the presence of hydroxy-chloro complexes of the dissolved metal ions and the high chloride concentrations. Cavanaugh, et al. (1983) studied dissolution behavior of Alloy C–276 on the basis of solution chemistry measurements and hydrolysis of the alloying elements. They reported that the pH values in corroding cavities of Alloy C–276 range from 0.3 to 2.0 as a result of molybdenum and chromium oxidation to high valence states. A fair correlation between pH and molybdenum ion concentration in solution was observed for both the Alloy C–276 data and the data obtained for stainless steels by Suzuki, et al. (1973). It is anticipated that the oxidation of molybdenum to $Mo^{4+}$ can generate a lower pH than that of $Cr^{3+}$. Similar results for pH reduction in crevice corrosion of stainless steels have also been reported in a number of investigations (Alavi and Cottis, 1987).

While *in-situ* monitoring of the solution chemistry evolution within pits is almost impossible because of the size limitations of the pit and the available microelectrodes, a few studies have focus on monitoring changes in solution chemistry inside crevices. Sridhar and Dunn (1994) conducted experiments on Type 304L stainless steel and Alloy 825, where both rectangular and circular crevice samples were instrumented with micro pH, chloride, and reference electrodes. The total current from the crevice was monitored as an indicator of crevice corrosion initiation, while the pH was monitored at three locations in the crevice. They observed a significant lag between the increase in current density indicating the onset of stable crevice corrosion and a decrease in pH, suggesting that the change in pH is not the cause of crevice corrosion, but its result. An alternative model is based in the potential variation in the crevice caused by ohmic drop. Such a potential drop is expected to displace the potential from the passive regime to the active peak. Potential drop alone cannot explain the initiation of crevice corrosion of many high nickel alloys because an active-passive loop is not observed unless the pH becomes quite acidic. Therefore, a combination of acidification and potential drop has been proposed as a mechanism for stable crevice corrosion initiation.

The critical metal-chloride concentration necessary for stabilizing a pit or crevice can be related to a critical dissolution rate coupled to geometric parameters that aid the accumulation of these species. Dunn, et al. (2000) analyzed stabilization of crevice corrosion and pitting in terms of a one-dimensional parameter that combines the dissolution rate and crevice or pit depth. A strong dependence of repassivation potential on pit depth for shallow penetrations was observed for Alloy 825; however, for deep pits the repassivation potential appeared to approach a lower limit. In addition, long-term tests on Alloy 825 under various redox conditions showed that crevice corrosion generally initiates faster than pitting, except at high potentials where both forms of localized corrosion initiate rapidly. While these analyses have advanced our conceptual understanding significantly, they are limited to simple geometries and subject to assumptions that may not be valid for solutions that exist in pits or crevices. Fully coupled reactive-transport models are needed to enable a more detailed and quantitative understanding of the kinetics of processes that lead to repassivation of pits and crevices (Sridhar, et al., 2001a,b).

### 4.2.2 Effect of Waste Package Internal Geometry on Solution Chemistry

The in-package chemistry tests were conducted in an electrochemical cell, shown schematically in Figure 4-6, equipped with a platinum counter electrode and a Luggin probe connected to a saturated calomel electrode. Test specimens were machined from mill-annealed Type 316L stainless steel (Fe-18Cr-12Ni-2.5Mo) plates, having a 33.0-mm diameter well and a 0.4-mm diameter, 6.35-mm deep hole as an artificial pit. The initial solution used for the experiments was 0.028 M $Cl^-$ (as KCl). The chloride concentration of the initial solution is similar to that from the evaporation experiments of synthetic J–13 Well water (CRWMS M&O, 2001d). Initially 4 mL of solution was added to the well, resulting in an exposed surface area of the specimen to the test solution of approximately 11 $cm^2$. The solution is heated using two cartridge heaters inserted into drilled holes in the specimen, and the temperature is monitored by a resistance temperature detector connected to a temperature controller.

In preliminary tests, specimens were held potentiostatically at various potentials for 0.5 hour at temperatures of 20, 60 and 90°C while the current density was recorded. From the current density data a range of potentials were selected for additional experiments in which solution extractions were made to study solution chemistry variations. These tests were performed at

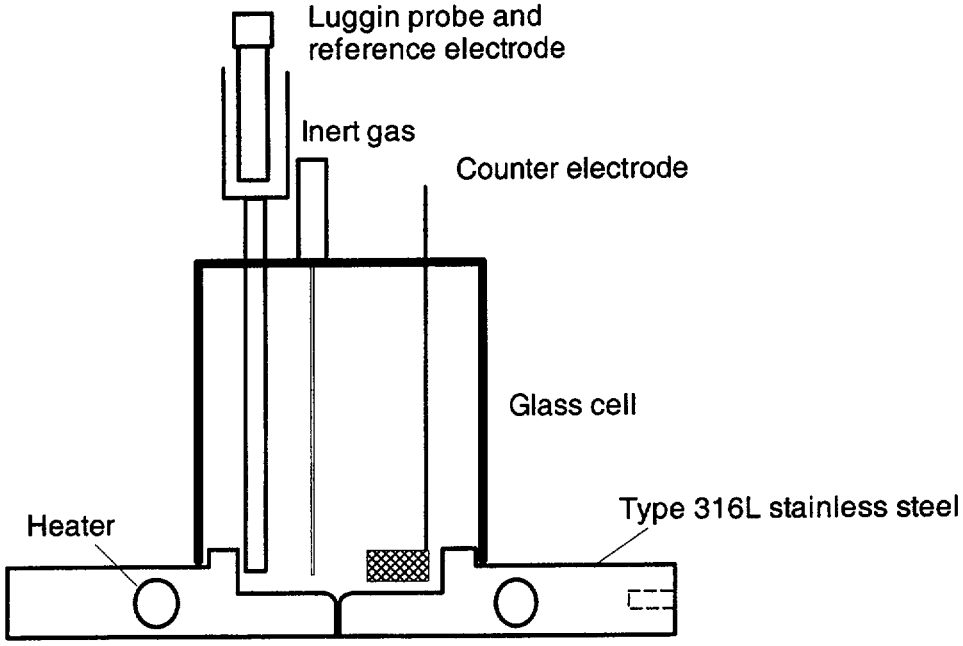


**Figure 4-6. Schematic of the Test Cell That Simulates Internal Waste Package Geometry for In-Package Chemistry Study**

20°C at different potentials for a period of 24 hours. At the end of each test, a micro-syringe was used to extract approximately 5 $\mu$L of solution from inside the pit, followed by a second extraction of 25 $\mu$L of solution from outside the pit. The cation concentration of the solutions was analyzed using capillary electrophoresis, and the pH was measured using a silver-silver chloride microelectrode (Model MI402, Microelectrodes Inc.). Ionic speciation in capillary electrophoresis was achieved based on differences in the ionic migration time of the species present in the solution under an applied electric field, in this case 20 kV. Quantitative analysis is performed by comparison of peak areas to those measured on samples of known concentration. All cations were analyzed using the method described by Krol, et al. (2000). For pH measurements, the microelectrode was connected to a pH/selective ion meter and calibrated using standard buffer solutions before and after the measurements to verify the accuracy of the results. The test matrix for all the experiments conducted is shown in Table 4-3, which also includes the total charge measured in these potentiostatic tests.

Typical plots of potentiostatic current measurements are shown in Figures 4-7, 4-8, and 4-9 for Type 316L stainless steel specimens at temperatures of 20, 60 and 90 °C, respectively. As seen in the plotted current density changes with time, two different types of current evolution behavior were observed. In the first type, the anodic current density decreased with time during the initial potentiostatic step from the open circuit potential and then rapidly reached a steady state of constant current density. This type of current response is characteristic of anodic passivity and is illustrated by the current density-versus-time curves for all three tests at 20 °C in Figure 4-7. The steady-state current density was in the range of $4 \times 10^{-7}$ to $3 \times 10^{-6}$ A/cm$^2$.

| Table 4-3. Total Charge Measured on Type 316L Stainless Steel in 0.028 M $Cl^-$ at Various Applied Potentials and Temperatures for Each In-Package Chemistry Test | | | |
|---|---|---|---|
| **Test ID** | **Temperature (°C)** | **Applied Potential ($mV_{SCE}$)** | **Total Charge (Coulombs)** |
| **0.5-Hour Tests** | | | |
| Intchem 10 | 20 | -150 | 0.0056 |
| Intchem 11 | 20 | -100 | 0.0069 |
| Intchem 12 | 20 | 0 | 0.0070 |
| Intchem 13 | 20 | 100 | 0.0366 |
| Intchem 14 | 20 | 150 | 0.0371 |
| Intchem 15 | 20 | 200 | 0.0563 |
| Intchem 60C10 | 60 | -150 | 0.0119 |
| Intchem 60C11 | 60 | -100 | 0.0126 |
| Intchem 60C12 | 60 | 0 | 0.0129 |
| Intchem 60C13 | 60 | 100 | 0.0147 |
| Intchem 60C14 | 60 | 150 | 0.439 |
| Intchem 60C15 | 60 | 200 | 63.68 |
| Intchem 90C10 | 90 | -150 | 0.0080 |
| Intchem 90C11 | 90 | -100 | 0.0106 |
| Intchem 90C12 | 90 | 0 | 0.440 |
| Intchem 90C13 | 90 | 100 | 41.37 |
| **24-Hour Tests** | | | |
| Intchem 20 | 20 | 0 | 0.057 |
| Intchem 21 | 20 | 50 | 0.076 |
| Intchem 22 | 20 | 100 | 0.17 |
| Intchem 23 | 20 | 150 | 1.96 |
| Intchem 24 | 20 | 200 | 3.38 |

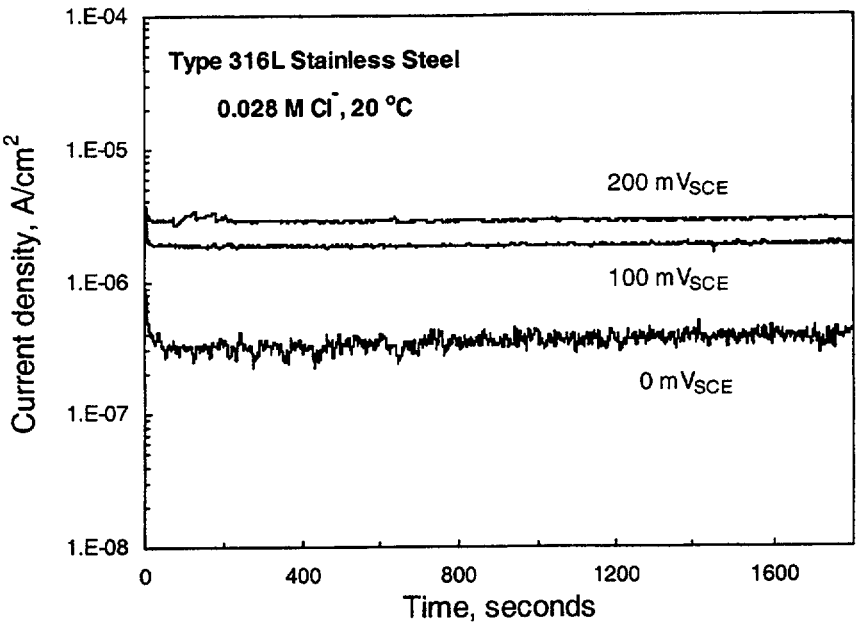


**Figure 4-7. Anodic Current Transients Measured on Type 316L Stainless Steel under Potentiostatic Conditions in 0.028 M $Cl^-$ Solution at 20 °C**

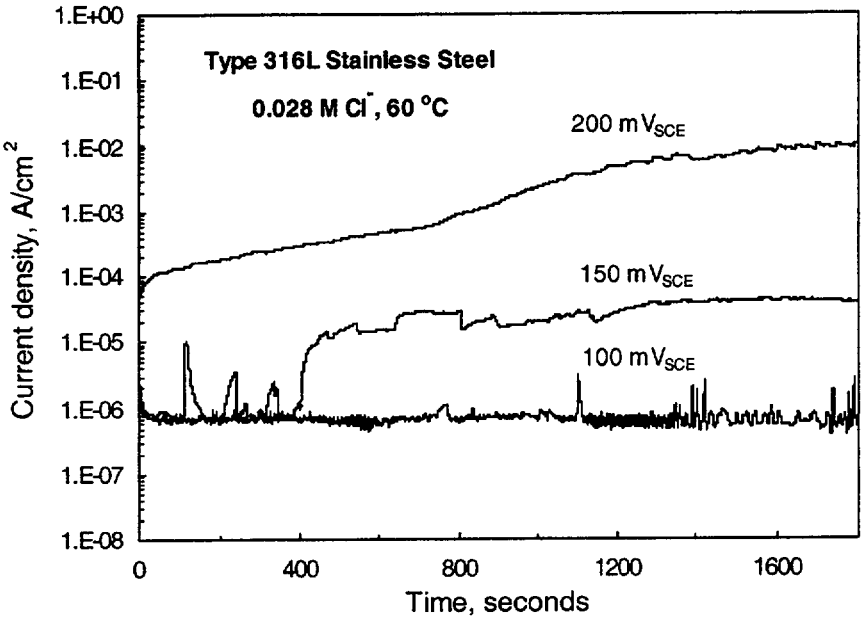


**Figure 4-8. Anodic Current Transients Measured on Type 316L Stainless Steel under Potentiostatic Conditions in 0.028 M $Cl^-$ Solution at 60 °C**

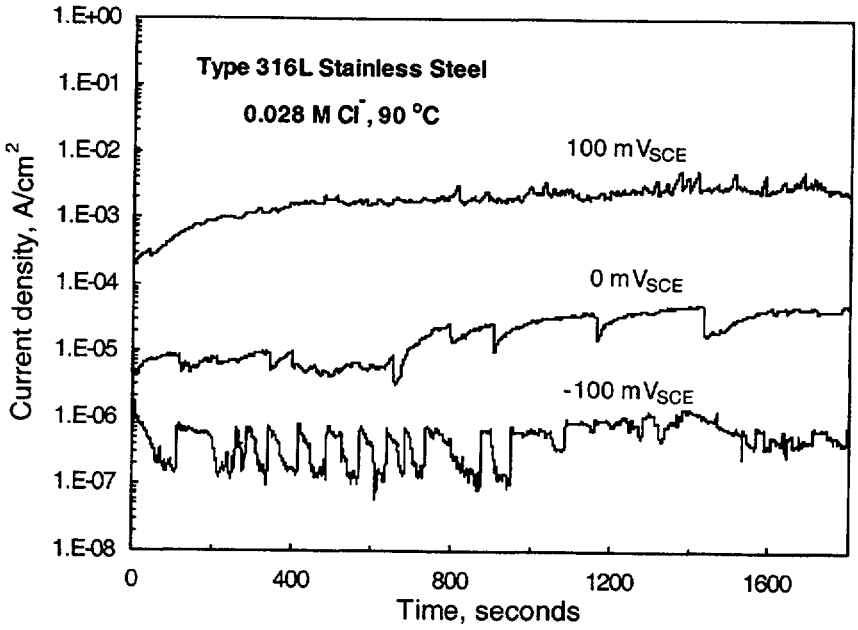


**Figure 4-9. Anodic Current Transients Measured on Type 316L Stainless Steel under Potentiostatic Conditions in 0.028 M $Cl^-$ Solution at 90 °C**

The second type of current response exhibited an increase of current density with time as a result of breakdown of the passive film and enhanced anodic dissolution. This behavior is illustrated by the current curves for the 60 °C tests at potentials of 150 and 200 $mV_{SCE}$ in Figure 4-8 and also for the 90 °C tests at potentials of 0 and 100 $mV_{SCE}$ in Figure 4-9. High anodic dissolution current densities were observed in all these cases at the conclusion of the tests. In the 60 °C test at 200 $mV_{SCE}$, the final current density was as high as $1 \times 10^{-2}$ A/cm$^2$. Tests at 60 °C applying 100 $mV_{SCE}$ and 90 °C applying -100 $mV_{SCE}$ showed the predominantly first type of current response; however, several large current spikes were observed, suggesting periodic events of passivity breakdown and repassivation without an increase in the mean value of the current density.

All the steady-state and final anodic current densities (depending on the type of current response) are shown in Figure 4-10 as a function of potential at the various temperatures for all the tests conducted as listed in Table 4-3. As evident in Figure 4-10, passive corrosion was observed at all temperatures when the applied potential was not greater than a critical value that depends on temperature. Critical potentials at which the current density increases significantly were observed in both 60 and 90 °C tests, indicating the onset of enhanced anodic dissolution. A significant decrease in the critical potential can be seen as the temperature increases from 60 to 90 °C. However, at 20 °C, current density gradually increased with increasing potential, and no critical potential was observed. Integration of the current with time resulted in a total charge, which is a reliable measure of the total dissolution of the specimen. The total charge values for all tests are listed in Table 4-3 and plotted as a function of potential in Figure 4-11 for the various temperatures. The plots of the effects of temperature and potential on total charge shown in Figure 4-11 also exhibit a temperature-dependent critical potential similar to that observed for the current density variations in Figure 4-10.

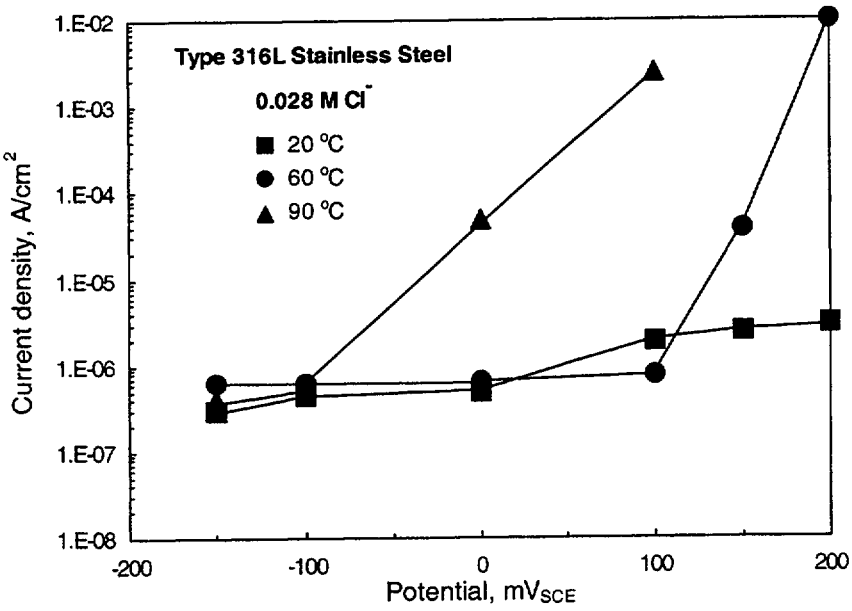


**Figure 4-10. Anodic Current Density Measured on Type 316L Stainless Steel under Potentiostatic Conditions in 0.028 M $Cl^-$ Solution for Various Temperatures**

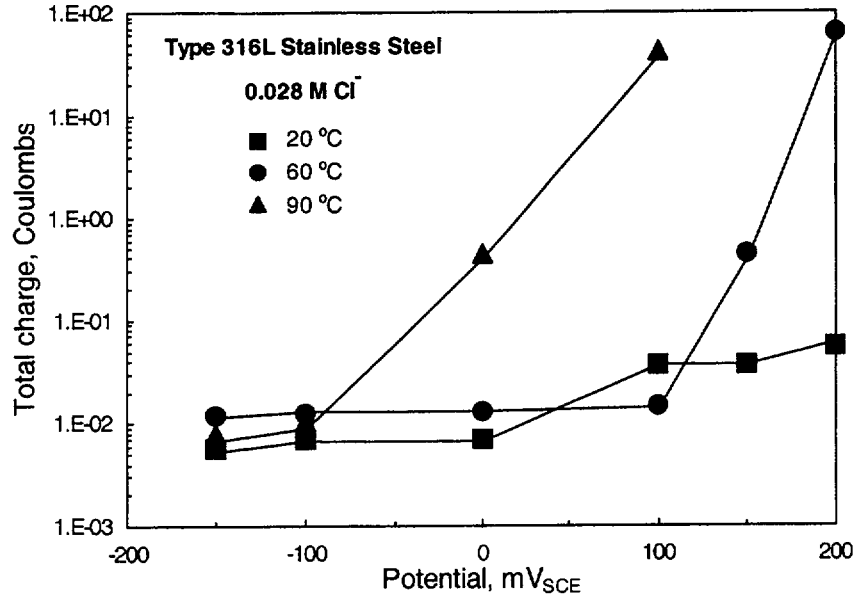


**Figure 4-11. Total Charge Measured on Type 316L Stainless Steel under Potentiostatic Conditions in 0.028 M $Cl^-$ Solution for Various Temperatures**

In-package chemistry tests aimed at evaluating solution chemistry variations were performed at 20 °C by holding the specimen at different potentials for 24 hours. Capillary electrophoresis analyses of the solutions extracted from both inside and outside the pit did not detect the presence of any species released from the test specimen except for the test at 200 $mV_{SCE}$. The measured cation concentrations from the anodic dissolution of Type 316L stainless steel at 200 $mV_{SCE}$ and 20 °C are listed in Table 4-4. It is clearly seen in Table 4-4 that metal concentrations inside the artificial pit are much higher than those outside the pit. Preferential dissolution of Type 316L stainless steel was observed for such conditions. The measured concentrations of chromium and nickel were much lower than the alloying contents in Type 316L stainless steel, particularly the chromium species. Because the characteristic peak of $Cr^{3+}$ is overlapping with that of $Fe^{2+}$ in the capillary electrophoresis spectrum, the chromium concentration could be underestimated, even though a series of solution dilutions was attempted.

The extent of preferential dissolution was evaluated using a selectivity coefficient, Z(M), as discussed by Cavanaugh et al. (1983). In case of Type 316L stainless steel, Z(M) is defined as the ion concentration ratio of component M and iron in solution divided by the weight percent ratio of component M and iron in the alloy. The calculated Z(M) values are also listed in Table 4-4. It is interesting to note that while the solution is more concentrated inside the pit (than outside), the Z values for nickel remain almost constant, suggesting a similar dissolution behavior inside and outside the pit. Preferential dissolution measured in this study is contrary to the results reported by Suzuki, et al. (1973) and Brossia and Kelly (1996), in which no preferential dissolution was observed in either pitting or crevice corrosion of stainless steels. This discrepancy may be attributed to formation of chromium- and nickel-rich corrosion products and surface deposit films.

The current density and total charge as a function of time for the dissolution of Type 316L stainless steel at 20 °C at an applied potential of 200 $mV_{SCE}$ is shown in Figure 4-12. Unlike the steady-state current density observed in the 0.5-hour test, the current density increased initially with time and reached a stable high value of ~$1 \times 10^{-5}$ A/cm$^2$ for a period of 6 hours and decreased afterward. The high anodic current period resulted in a high total charge at the end of the test where a total anodic charge of 3.38 coulombs was recorded. The total charge values were calculated for all the 24-hour tests and are provided in Table 4-3. Assuming congruent dissolution of the major alloying elements as $Fe^{2+}$, $Cr^{3+}$, and $Ni^{2+}$, the

**Table 4-4. Cation Concentrations from Anodic Dissolution and Selectivity Coefficient (Z) for Type 316L Stainless Steel Tested at 200 $mV_{SCE}$ in 0.028 M $Cl^-$ Solution at 20 °C**

| Cation | 5 μL Inside Pit Solution | | 25 μL Outside Pit Solution | |
|---|---|---|---|---|
| | Concentration (ppm) | Z ($M_i$)* | Concentration (ppm) | Z ($M_i$) |
| $Fe^{2+}$ | 12,900 | 1.00 | 550 | 1.00 |
| $Ni^{2+}$ | 270 | 0.12 | 10 | 0.10 |
| $Cr^{3+}$ | 100 | 0.03 | — | — |

*$Z(M_i)$ = [ppm $M_i$ / ppm iron] / [wt % $M_i$ / wt % iron].
†ppm = parts per million.

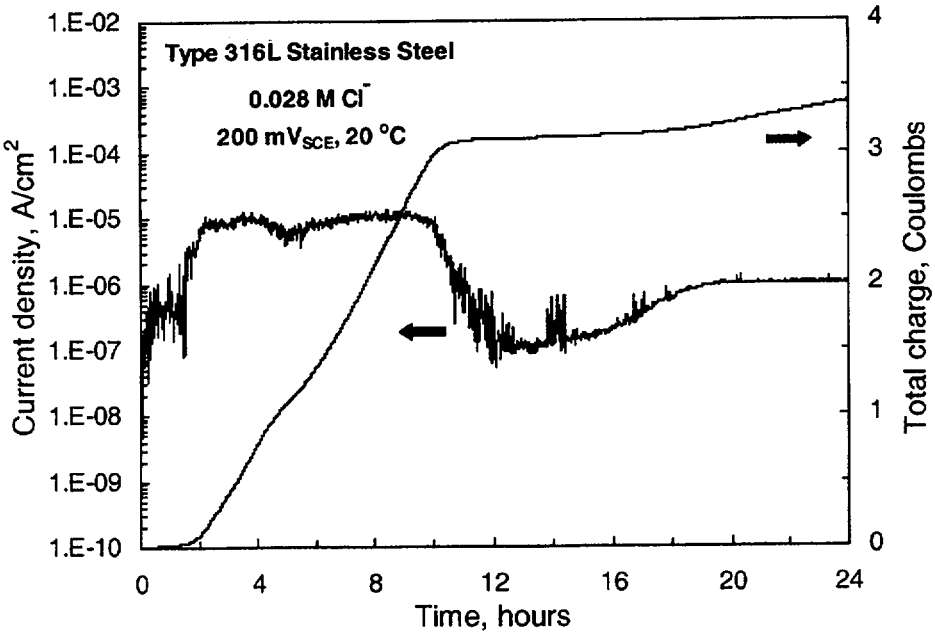


**Figure 4-12. Anodic Current Density and Total Charge as a Function of Time Measured on Type 316L Stainless Steel at 200 mV$_{SHE}$ in 0.028 M Cl$^-$ Solution at 20 °C**

equivalent weight for Type 316L stainless steel is 25.29 g/equivalent (American Society for Testing and Materials, 1999c). The total metal ion concentration from electrochemical reactions can be computed by Faraday's law, which states that one Faraday (or 96,489 coulombs) is the quantity of electrical charge required to produce one equivalent. Thus, the total metal ion concentration for the 4-mL solution of the test at 200 mV$_{SCE}$ as a result of Type 316L stainless steel anodic dissolution should be 221 parts per million, with 155 parts per million iron, 40 parts per million chromium, and 26 parts per million nickel. Comparison with the measured concentrations in Table 4-4 clearly shows that the measured metal cation concentrations within the pit are much higher than the calculated values, with different orders of magnitude for each species. While the high cation concentrations measured inside the pit are attributed to the spatial variation of the anodic dissolution, the $Fe^{2+}$ concentration of 550 parts per million measured outside the pit, which is higher than the calculated bulk value, is probably due to mixing of the pit and bulk solutions during the solution extraction process. Given a detection limit of 100 parts per billion or better for capillary electrophoresis analysis of cations, the absence of metal cations in the solutions extracted from the tests at potentials less than 200 mV$_{SCE}$ is unexpected, in contradiction with the calculations using the total charges measured for each of the tests.

Results of pH measurements of the solutions extracted from inside the pit are given in Table 4-5. At 200 mV$_{SCE}$, the solution pH became considerably acidic reaching a value of 2.61. Solution pH was also calculated by hydrolysis reactions based on the measured ion concentrations from capillary electrophoresis analysis. A minimum value of 2.51 was calculated using the $Cr^{3+}$ concentration and the associated full hydrolysis reaction, in good agreement with the microelectrode measurements. It is apparent that dissolution of the metal in the pit generates the metal cations that then hydrolyze and acidify the pit solution. As reported by

| Table 4-5. Solution pH Measured by Micro-Reference Electrode for Type 316L Stainless Steel Tested at Various Applied Potentials in 0.028 M $Cl^-$ at 20 °C | | |
|---|---|---|
| **Test Number** | **Applied Potential ($mV_{SCE}$)** | **pH for 5 μL Inside Pit Solution** |
| Intchem 20 | 0 | 5.42 |
| Intchem 21 | 50 | 5.70 |
| Intchem 22 | 100 | 5.49 |
| Intchem 23 | 150 | 5.77 |
| Intchem 24 | 200 | 2.61 |

Suzuki, et al. (1973), analyses of pH changes in corroding cavities of stainless steels have shown a significant pH reduction in solution within the cavities mainly due to $Cr^{3+}$ hydrolysis.

Preliminary in-package chemistry studies indicate that because the internal geometry of the waste package will have many tightly packed regions, interactions of waste package internal structural components with the incoming water may have significant influence on the evolution of water chemistry and the subsequent corrosion of waste forms such as spent nuclear fuel. High cation concentrations and a pH of 2.6 were measured in the pit solution using an initial solution of 0.028 M $Cl^-$(as KCl) and holding the potential of the Type 316L stainless steel specimen at 200 $mV_{SCE}$ for 24 hours.

As discussed in Chapter 3, pitting corrosion of Zircaloy occurs in chloride solutions above a critical potential. This potential, equivalent to the repassivation potential, is attained in the presence of reducible species such as $Fe^{3+}$. It is anticipated that $Fe^{2+}$ generated by corrosion of stainless steel components can be oxidized to $Fe^{3+}$ in solution by oxidizing radicals or $H_2O_2$ as the stable product of the γ-radiolysis of water. The combined process of migration of chloride ions and hydrolysis of the dissolved metal ions within a pit will result in a decrease of the pH and an increase of the chloride ion concentration. Pitting of spent nuclear fuel cladding may occur during such environmental conditions. The contribution of cladding as an additional metallic barrier to the release of radionuclides to the near-field environment could be, therefore, substantially diminished.

Premature cladding failure will increase the quantity of commercial spent nuclear fuel exposed to water and available for dissolution. Local decrease of pH may affect the dissolution rate of the irradiated $UO_2$ matrix locally and, hence, the local release rate of highly soluble radionuclides such as Tc-99. Alternative models taking into account electrochemical reactions coupled to transport processes also should be considered in the process level analyses and included, if needed, in the model abstraction. DOE agreed to conduct additional work, both theoretical and experimental, to determine the ranges of solution chemistry that could exist inside waste packages and the consequences of such evolved environmental conditions. This has been addressed in agreements CLST 3.01, CLST 3.02, CLST 3.03, CLST 3.04, CLST 3.05, ENFE 3.03, and ENFE 3.04.

# 5 FUTURE WORK

A significant improvement in the DOE Total System Performance Assessment–Site Recommendation analyses of the waste form degradation model is consideration of the in-package chemistry alteration by reaction with waste package components. However, modeling of the in-package chemistry, assuming the exclusion of spatial variations in chemistry, is still inadequate, which has been addressed in the DOE and NRC agreements. As indicated by the work at the CNWRA, interactions of the waste package with the incoming water in a simulated pit resulted in a significant reduction in pH of the pit solution. Additional experimental efforts and simulations that consider spatial variations, including changes in the incoming water composition, localized corrosion, and corrosion products, are needed to justify the range of environmental conditions expected inside breached waste packages.

The dissolution rate for spent nuclear fuel should be evaluated (or computed) by taking into account the effect of the evolved in-package chemical environments. For high-level waste glass, determination of the intrinsic dissolution rate using the MCC–1 test procedure in the presence of corrosion products is needed to validate the conservative upper bound provided in the glass dissolution model. Several areas regarding Zircaloy-4 corrosion need to be evaluated further. Additional examination of the effects of inhibiting anions such as sulfate and nitrate on localized corrosion susceptibility is needed. The possibility of cathodic limitations to localized corrosion initiation and propagation on hydrothermally oxidized Zircaloy-4 also warrants further examination as a possible explanation for the lack of localized corrosion on these oxidized samples, even though the corrosion potential was greater than the repassivation potential.

# 6 SUMMARY AND CONCLUSIONS

One of the key system attributes for assurance of future repository safety is limited release of radionuclides from the engineering barriers. The chemistry of the aqueous environment inside the breached waste packages and the performance of spent nuclear fuel cladding and waste forms are critical to the release of radionuclides from the waste packages. From the work presented in this report, various deficiencies are identified in the DOE model abstractions of high-level waste form degradation, cladding degradation, and in-package chemistry for use in the Total System Performance Assessment. These deficiencies include the ranges of solution chemistry that could exist inside the waste package and the consequence of the evolved in-package chemistry environments, the effect of waste package corrosion products that could influence corrosion mechanisms and dissolution rates of high-level waste glass, and the effect of environmental variables on localized corrosion and stress corrosion cracking of Zircaloy cladding. Existing agreements between the NRC and the DOE cover the path forward for resolving all of these deficiencies. A summary of the CNWRA results and evaluation of the DOE approach is presented next for each of the subjects.

## 6.1 DEGRADATION OF THE VITRIFIED HIGH-LEVEL WASTE

In spite of a small radionuclide inventory of high-level waste glass, its contribution to performance assessment could be significant if the radionuclide release rate from high-level waste glass is higher than that from spent nuclear fuel. The high-level waste glass degradation process involves transport and contact of reactants (i.e., groundwater or water vapor) to the glass surface, chemical reaction between the reactants and glass surface, and transport of reaction products away from the reaction zone. The dissolution rate is controlled by combination of these processes and depends on factors such as chemical composition of the glass and solubilities of the reaction products, exposed surface area, temperature, pH, relative humidity, and chemical compositions of the aqueous environment. A review of the DOE abstraction of radionuclide release rates from glass waste form in the Total System Performance Assessment–Site Recommendation indicated that DOE has not reasonably accounted for the range of environmental conditions expected inside breached waste packages in its abstraction of high-level waste glass degradation. In addition, the DOE model abstraction ignores the presence of corrosion products from the dissolution of waste package internal components that could influence glass degradation.

The CNWRA has conducted leaching experiments of simulated high-level waste glasses in aqueous solutions of $FeCl_2$ and $FeCl_3$ to simulate the internal waste package environments. The presence of corrosion products such as iron cations, as well as the resultant solution pH, significantly enhances the dissolution of high-level waste glass. Model abstraction and performance assessment analyses using rate expressions, taking into account the effect of corrosion products, showed that the presence of corrosion products enhances glass dissolution and will increase the subsequent release of radionuclides to the environment. DOE should demonstrate that its abstraction of high-level waste glass degradation captures the range of chemical compositions of water, including the effect of nitric acid formation due to radiolysis and the effect of interactions with waste package corrosion products, such as FeOOH, $FeCl_2$, and $FeCl_3$ in the anticipated pH range. DOE agreed to provide additional information on high-level waste glass degradation in agreements CLST 3.02, CLST 3.03, and CLST 4.01.

## 6.2 DEGRADATION OF COMMERCIAL SPENT NUCLEAR FUEL CLADDING

DOE considered the most likely forms of degradation that may affect the integrity of the commercial spent nuclear fuel cladding during disposal conditions in the proposed repository. DOE developed a model to evaluate Zircaloy cladding degradation as part of the waste form degradation model to determine the rate at which the commercial spent nuclear fuel matrix is exposed to the in-package aqueous environment. The degradation of the commercial spent nuclear fuel cladding is assumed to occur in two stages. The first stage of degradation corresponds to rod failure as a result of perforation of the cladding. The second stage is due to the progressive exposure of the spent nuclear fuel matrix as a result of splitting (wet unzipping) of the cladding due to oxidation of the irradiated $UO_2$ pellets by an aqueous environment. The technical bases provided to support the modeling of cladding degradation as a result of both the corrosion by fluoride and the internal stress corrosion cracking by iodine are limited, and no alternative models have been considered for localized corrosion and external stress corrosion cracking. This model could be acceptable if DOE can demonstrate in the analysis and model report that the environmental conditions are not conducive to localized corrosion or stress corrosion cracking induced by chloride because (i) the chloride concentration is too low, (ii) the corrosion potential is lower than the pitting potential, or (iii) anionic species such as nitrate are present at a sufficiently high concentration ratio with respect to chloride that can act as efficient localized corrosion inhibitors. The hoop stress calculations used to evaluate creep are applicable to the assessment of chloride-induced stress corrosion cracking.

CNWRA evaluated the corrosion behavior of Zircaloy-4 for a wide range of conditions. Based on this work, it has been found that Zircaloy-4, either mechanically polished or covered with a hydrothermally grown oxide layer, is susceptible to pitting corrosion in chloride-containing solutions at concentrations above 0.001 M and potentials higher than a repassivation potential. The presence of the hydrothermally grown oxide was not observed to influence the repassivation potential but did increase the breakdown potential as well as the corrosion potential. The corrosion potential can reach and even exceed the repassivation potential in $FeCl_3$-containing solutions and, therefore, pitting corrosion of Zircaloy cladding may occur after a long time interval under natural corroding conditions inside a breached container. However, additional studies on the kinetics of the cathodic reactions on oxide-covered surfaces are needed to predict the long-term performance of cladding as an additional metallic barrier to radionuclide release in the disposal of spent nuclear fuel. DOE agreed to provide adequate information on cladding degradation in agreements CLST 3.06, CLST 3.07, and CLST 3.09. Hydride embrittlement covered under agreement CLST 3.08 is not discussed in this report because hydrogen entry only occurs under reactor operating conditions. No hydrogen entry is expected under disposal conditions in the oxidizing in-package environment.

## 6.3 IN-PACKAGE CHEMISTRY

Composition of the groundwater entering the waste package can be influenced and modified by natural processes such as evaporation, chemical reactions with host rock, and interactions with components of the engineered barriers such as drip shield and waste package materials. Variables such as pH, carbonate, and redox potential are influenced by interactions of groundwater with engineered barriers in the repository and have a substantial effect on waste package and waste form corrosions. To study the sensitivity of incoming fluid composition

inside the waste package on the outgoing fluid composition, DOE analyzed the interactions between the waste form and several variations of groundwater compositions using EQ 3/6. The approach taken by the DOE in determining the range of in-package chemistry may not be appropriate. The DOE in-package chemistry model and abstraction lump various corrosion processes together. This approach could mask the effects of waste package corrosion on the groundwater chemistry and, hence, underestimate shifts in pH and redox potential. Additionally, the possible formation of locally aggressive environments in crevices and tight spaces inside the waste package that could enhance the degradation of waste forms and the solubility of radionuclides has been neglected.

CNWRA performed experimental investigations into changes of the solution chemistry through interactions with the waste package internal structural components using a test cell that simulates certain aspects of the internal geometry of the waste package. Preliminary results indicated that interactions of the waste package internal structural components with the incoming water may have a significant influence on the evolution of water chemistry and the subsequent corrosion of waste forms such as spent nuclear fuel. The range of environmental conditions to be expected inside the breached waste package needs to be experimentally determined by the DOE to validate the predictions from the in-package water chemistry model. DOE agreed to provide additional information on in-package chemistry in agreements CLST 3.01, CLST 3.02, CLST 3.03, CLST 3.04, CLST 3.05, ENFE 3.03, ENFE 3.04, TSPAI 3.08 and TSPAI 3.14.

Finally, additional confirmatory efforts are planned to further evaluate the DOE analyses and the documentation that will be provided according to the DOE and NRC agreements. These efforts include analyzing the effects of incoming water composition, localized corrosion, and corrosion products on the evolution of the in-package solution chemistry; measuring the dissolution rates of waste forms for the evolved chemical environments; and examining the conditions for the occurrence of localized corrosion of Zircaloy cladding in the presence of radiolytic products and chemical species generated by corroding waste packages.

# 7 REFERENCES


Abraitis, P.K., D.J. Vaughan, F.R. Livens, L. Monteith, D.P. Trivedi, and J.S. Small. "Dissolution of a Complex Borosilicate Glass at 60 °C: The Influence of pH and Proton Adsorption on the Congruence of Short-Term Leaching." Proceedings of the Materials Research Society Conference. Symposium Proceedings 506. Pittsburgh, Pennsylvania: Materials Research Society. pp. 47–54. 1998.

Advocat, T., J.L. Crovisier, E. Vernaz, G. Ehret, and H. Charpentier. "Hydrolysis of R717 Nuclear Waste Glass in Dilute Media: Mechanisms and Rate a Function of pH." Scientific Basis for Nuclear Waste Management XIV. T.J. Abrajano and L.H. Johnson, eds. Symposium Proceedings 212. Pittsburgh, Pennsylvania: Materials Research Society. pp. 57–64. 1991.

Alavi, A. and R.A. Cottis. "The Determination of pH, Potential, and Chloride Concentration in Corroding Crevices on 304 Stainless Steel and 7475 Aluminum Alloy." *Corrosion Science.* Vol. 27. pp. 443–451. 1987.

American Society for Testing and Materials. "Standard Test Method for Static Leaching of Monolithic Waste Forms for Disposal of Radioactive Waste: C1220–98." Annual Book of American Society for Testing and Materials Standards. Volume 12.01. West Conshohocken, Pennsylvania: American Society for Testing and Materials. 1999a.

———. "Standard Test Method for Determining Chemical Durability of Nuclear, Hazardous, and Mixed Waste Glasses: The Product Consistency Test (PCT): C1285–97." Annual Book of American Society for Testing and Materials Standards. Volume 12.01. West Conshohocken, Pennsylvania: American Society for Testing and Materials. 1999b.

———. "Standard Practice for Calculation of Corrosion Rates and Related Information from Electrochemical Measurements: G102–89." Annual Book of American Society for Testing and Materials Standards. Volume 03.02: Wear and Erosion—Metal Corrosion. West Conshohocken, Pennsylvania: American Society for Testing and Materials. 1999c.

Bates, J.K. "Secondary Phases in Waste Form Alteration." DOE/NRC Technical Exchange on Total System Performance Assessment–Viability Assessment Meeting, San Antonio, Texas, March 17–19, 1998. San Antonio, Texas: CNWRA. 1998.

Brossia, C.S. and R.G. Kelly. "On the Role of Alloy Sulfur in the Initiation of Crevice Corrosion in Stainless Steel." *Critical Factors in Localized Corrosion II.* P.M. Natishan, et al., eds. Pennington, New Jersey: The Electrochemical Society. pp. 201–217. 1996.

Brossia, C.S., D.S. Dunn, and N. Sridhar. "The Role of Metal Salt Film Formation on Localized Corrosion Stabilization." *Critical Factors in Localized Corrosion III.* R.G. Kelly, ed. Pennington, New Jersey: The Electrochemical Society. pp. 485–499. 1998.

Brossia, S., D. Dunn, L. Yang, and L. Browning. "Effect of Environment on the Corrosion of Waste Package and Drip Shield Materials." CNWRA 2001-003. San Antonio, Texas: CNWRA. 2001.

Budnitz, B., R.C. Ewing, D.W. Moeller, J. Payer, C. Whipple, and P.A. Witherspoon. "Peer Review of the Total System Performance Assessment–Viability Assessment Final Report." Las Vegas, Nevada: Total System Performance Assessment Peer Review Panel. 1999.

Burns, W.G., A.E. Hughes, J.A.C. Marples, R.S. Nelson, and A.M. Stoneham. "Effects of Radiation on the Leach Rates of Vitrified Radioactive Waste." *Journal of Nuclear Materials.* Vol. 107. pp. 245–270. 1982.

Cavanaugh, M.A., J.A. Kargol, J. Nickerson, and N.F. Fiore. "The Anodic Dissolution of a Ni-Base Superalloy." *Advances in Localized Corrosion.* NACE–9. Houston, Texas: NACE International. pp. 144–150. 1983.

Cox, B. "Stress Corrosion Cracking of Zircaloy-2 in Neutral Aqueous Chloride Solutions at 25 °C." *Corrosion.* Vol. 29. pp. 157–166. 1973.

Cragnolino, G.A. and J.R. Galvele. "Anodic Behavior and Pitting of Zirconium and Zircaloy-4 in Aqueous Solutions of Sodium Chloride." *Passivity of Metals.* R.P. Frankenthal and J. Kruger, eds. Princeton, New Jersey: The Electrochemical Society. pp. 1,053–1,057. 1978.

Cragnolino, G.A., D.S. Dunn, C.S. Brossia, V. Jain, and K.S. Chan. "Assessment of Performance Issues Related to Alternate Engineered Barrier System Materials and Design Options." CNWRA 99-003. San Antonio, Texas: CNWRA. 1999.

CRWMS M&O. "Total System Performance Assessment–Viability Assessment (TSPA–VA) Analyses Technical Basis Document. Waste Form Degradation, Radionuclide Mobilization, and Transport through the Engineered Barrier System." B00000000–01717–4301–00006. Revision 00. Las Vegas, Nevada: CRWMS M&O. 1998a.

———. "Total System Performance Assessment–Viability Assessment (TSPA–VA) Analyses Technical Basis Document." B00000000–01717–4301. Revision 01. Las Vegas, Nevada: CRWMS M&O. 1998b.

———. "Repository Safety Strategy: Plan to Prepare the Safety Case to Support Yucca Mountain Site Recommendation and Licensing Considerations." TDR–WIS–RL–000001. Revision 4. ICN 01. Las Vegas, Nevada: CRWMS M&O. 2000a.

———. "Total System Performance Assessment for the Site Recommendation." TDR–WIS–PA–000001. Revision 00. ICN 01. Las Vegas, Nevada: CRWMS M&O. 2000b.

———. "Defense High-Level Waste Glass Degradation." ANL–EBS–MD–0016. Revision 00. ICN 01. Las Vegas, Nevada: CRWMS M&O. 2000c.

———. "Waste Form Degradation Process Model Report." TDR–WIS–MD–000001. Revision 00. ICN 01. Las Vegas, Nevada: CRWMS M&O. 2000d.

———. "Inventory Abstraction Analysis Model Report." ANL–WIS–MD–000006. Revision 00. Las Vegas, Nevada: CRWMS M&O. 2000e.

———. "Summary of In-Package Chemistry for Waste Forms." ANL–EBS–MD–000050. Revision 00. Las Vegas, Nevada: CRWMS M&O. 2000f.

———. "Clad Degradation—Summary and Abstraction." ANL–WIS–MD–000007. Revision 00. Las Vegas, Nevada: CRWMS M&O. 2000g.

———. "Initial Cladding Condition." ANL–EBS–MD–000048. Revision 00. ICN 01. Las Vegas, Nevada: CRWMS M&O. 2000h.

———. "Clad Degradation—Local Corrosion of Zirconium and Its Alloys under Repository Conditions." ANL–EBS–MD–000012. Revision 00. Las Vegas, Nevada: CRWMS M&O. 2000i.

———. "Clad Degradation—FEPs Screening Arguments." ANL–WIS–MD–000008. Revision 00. ICN 01. Las Vegas, Nevada: CRWMS M&O. 2000j.

———. "Supplemental Science and Performance Analysis—Report Volume 1 of 2." TDR–MGR–MD–000007. Revision 00. Las Vegas, Nevada: CRWMS M&O. 2001a.

———. "In-Package Chemistry Abstraction." ANL–EBS–MD–000037. Revision 01. Las Vegas, Nevada: CRWMS M&O. 2001b.

———. "In-Package Chemistry for Waste Forms." ANL–EBS–MD–000056. Revision 00. Las Vegas, Nevada: CRWMS M&O. 2001c.

———. "In-Drift Precipitation/Salts Analysis." ANL–EBS–MD–000045. Revision 00. ICN 02. Las Vegas, Nevada: CRWMS M&O. 2001d.

Dunn, D.S., N. Sridhar, and G.A. Cragnolino. "Long-Term Prediction of Localized Corrosion of Alloy 825 in High-Level Nuclear Waste Repository Environments." *Corrosion.* Vol. 52. pp. 115–124. 1996.

Dunn, D.S., G.A. Cragnolino, and N. Sridhar. "An Electrochemical Approach to Predicting Long-Term Localized Corrosion of Corrosion-Resistant High-Level Waste Container Materials." *Corrosion.* Vol. 56. pp. 90–104. 2000.

Ebert, W.L. and S.W. Tam. "Dissolution Rates of DWPF Glasses from Long-Term PCT." Scientific Basis for Nuclear Waste Management XX. W.J. Gray and I.R. Triay, eds. Symposium Proceedings 465. Pittsburgh, Pennsylvania: Materials Research Society. pp. 149–156. 1997.

Ebert, W.L., J.C. Cunnane, and T.A. Thornton. "An HLW Glass Degradation Model for TSPA-SR." Proceedings of the Ninth International Conference on High-Level Radioactive Waste Management, Las Vegas, Nevada, April 29–May 3, 2001. LaGrange Park, Illinois: American Nuclear Society. No page numbers. Published on CD-ROM. 2001.

Ewing, R.C., W. Lutze, and A. Abdelouas. "Natural Glasses and the 'Verification' of the Long-Term Durability of Nuclear Waste Glasses." Proceedings of the XVIII International Congress on Glass. Westerville, Ohio: American Ceramic Society. 1998.

Fortner, J.A. and J.K. Bates. "Long-Term Results from Unsaturated Durability Testing of Actinide-Doped DWPF and WVDP Waste Glasses." Scientific Basis for Nuclear Waste Management XIX. W.M. Murphy and D.A. Knecht, eds. Symposium Proceedings 412. Pittsburgh, Pennsylvania: Materials Research Society. pp. 205–211. 1996.

Fortner, J.A., S.F. Wolf, E.C. Buck, C.J. Mertz, and J.K. Bates. "Solution-Borne Colloids from Drip Tests Using Actinide-Doped and Fully Radioactive Waste." Scientific Basis for Nuclear Waste Management XX. W.J. Gray and I.R. Triay, eds. Symposium Proceedings 465. Pittsburgh, Pennsylvania: Materials Research Society. pp. 165–172. 1997.

Galvele, J.R. "Transport Processes and the Mechanism of Pitting of Metals." *Journal of the Electrochemical Society.* Vol. 123. pp. 464–474. 1976.

Greene, C.A., C.S. Brossia, D.S. Dunn, and G.A. Cragnolino. "Environmental and Electrochemical Factors on the Localized Corrosion of Zircaloy-4." Proceedings of the Corrosion 2000 Conference. Paper No. 210. Houston, Texas: NACE International. 2000.

Hillner, E., D.G. Franklin, and J.D. Smee. "The Corrosion of Zircaloy-Clad Fuel Assemblies in a Geologic Repository Environment." WAPD–T–3173. West Miffin, Pennsylvania: Bettis Atomic Power Laboratory. 1994.

International Atomic Energy Agency. "Waterside Corrosion of Zirconium Alloys in Nuclear Power Plants." IAEA–TECDOC–996. Vienna, Austria: International Atomic Energy Agency. p. 220. 1998.

Jantzen, C.M. "Nuclear Waste Glass Durability I—Predicting Environmental Response from Thermodynamic (Pourbaix) Diagrams." *Journal of American Ceramic Society.* Vol. 75. pp. 2,433–2,448. 1992.

Knauss, K.G., W.L. Bourcier, K.D. McKeegan, C.I. Merzbacher, S.N. Nguyen, F.J. Ryerson, D.K. Smith, and H.C. Weed. "Dissolution Kinetics of a Simple Analogue Nuclear Waste Glass as a Function of pH, Time, and Temperature." Scientific Basis for Nuclear Waste Management XIII. V.M. Oversby and P.W. Brown, eds. Symposium Proceedings 176. Warrendale, Pennsylvania: Materials Research Society. pp. 371–381. 1990.

Krol, J.M., M. Benvenuti, and J. Romano. *Ion Analysis Methods for IC and CIA® and Practical Aspects of Capillary Ion Analysis Theory.* Milford, Massachusetts: Waters Corporation. 2000.

Luo, J.S., W.L. Ebert, J.J. Mazer, and J.K. Bates. "Dissolution Rates of DWPF Glasses from Long-Term PCT." Scientific Basis for Nuclear Waste Management XX. W.J. Gray and I.R. Triay, eds. Symposium Proceedings 465. Pittsburgh, Pennsylvania: Materials Research Society. pp. 157–163. 1997.

Maguire, M. "The Pitting Susceptibility of Zirconium in Aqueous $Cl^-$, $Br^-$, and $I^-$ Solutions." Proceedings of the Industrial Applications of Titanium and Zirconium: Third Conference. R.T. Webster and C.S. Yong, eds. ASTM STP 830. Philadelphia, Pennsylvania: American Society for Testing and Materials. pp. 175–189. 1984.

Mankowski, G., Y. Roques, G. Chatainier, and F. Dabosi. "Stress Corrosion Cracking of Zircaloy-4 in Neutral Aqueous Chloride Solutions." *British Corrosion Journal.* Vol. 19. pp. 17–22. 1984.

Maraghini, M., G.B. Adams, Jr., and P. Van Rysselberghe. "Studies on the Anodic Polarization of Zirconium and Zirconium Alloys." *Journal of the Electrochemical Society.* Vol. 101. pp. 400–409. 1954.

McGrail, B.P., W.L. Ebert, A.J. Bakel, and D.K. Peeler. "Measurement of Kinetic Rate Law Parameters on a Na-Ca-Al Borosilicate Glass for Low-Activity Waste." *Journal of Nuclear Materials.* Vol. 249. pp. 175–189. 1997.

McKenzie, W.F. "Natural Glass Analogues to Alteration of Nuclear Waste Glass: A Review and Recommendations for Further Study." UCID–21871. Livermore, California: Lawrence Livermore National Laboratory. 1990.

McVay, G.L. and C.Q. Buckwalter. "Effect of Iron on Waste-Glass Leaching." *Journal of American Ceramic Society.* Vol. 66. pp. 170–174. 1983.

Mohanty, S. and T.J. McCartin. "Total-system Performance Assessment (TPA) Version 4.0 Code: Module Description and User's Guide." San Antonio, Texas: CNWRA. 2000.

NRC. "Issue Resolution Status Report, Key Technical Issue: Evolution of the Near-Field Environment." Revision 3. Washington, DC: NRC. 2000.

———. "Integrated Issue Resolution Status Report (Draft)." Revision 0. Washington, DC: NRC. 2001a.

———. "Issue Resolution Status Report, Key Technical Issue: Container Life and Source Term." Revision 3. Washington, DC: NRC. 2001b.

Nuclear Waste Technical Review Board. "Report to the U.S. Congress and the U.S. Secretary of Energy." Arlington, Virginia: Nuclear Waste Technical Review Board. November 1998.

Pan, Y.M., V. Jain, M. Bogart, and P. Deshpande. "Effect of Iron Chlorides on the Dissolution Behavior of Simulated High-Level Waste Glasses." Ceramic Transactions of the Environmental Issues and Waste Management Technologies in the Ceramic and Nuclear Industries. Volume 119. D. Spearing, et al., eds. Westerville, Ohio: American Ceramic Society. 2001.

Postlethwaite, J. and M. Onofrei. "Hydrogen Evolution and Anodic Disintegration During Electrochemical Pitting of Zirconium in Alkaline-Chloride Solutions." *Corrosion.* Vol. 35. pp. 185–189. 1979.

Shibata, T. and M.A. Ameer. "Stochastic Processes of Pit Generation on Zirconium with an Anodic Oxide Film." *Corrosion Science.* Vol. 35. pp. 1,633–1,643. 1992.

Sridhar, N. and D.S. Dunn. "Effect of Applied Potential on Changes in Solution Chemistry inside Crevices on Type 304L Stainless Steel and Alloy 825." *Corrosion.* Vol. 50. pp. 857–872. 1994.

Sridhar, N., D.S. Dunn, C.S. Brossia, and G.A. Cragnolino. "Stabilization and Repassivation of Localized Corrosion." Proceedings of the Corrosion 2001 Research Topical Symposium on Localized Corrosion. G.S. Frankel and J.R. Scully, eds. Houston, Texas: NACE International. pp. 1–29. 2001a.

Sridhar, N., D. Dunn, and M. Seth. "Application of a General Reactive Transport Model to Predict Environment Under Disbonded Coatings." *Corrosion.* Vol. 57, No. 7. pp. 598–613. 2001b.

Suzuki, T., M. Yamabe, and Y. Kitamura. "Composition of Anolyte within Local Anode of Stainless Steel." *Corrosion.* Vol. 29. pp. 18–22. 1973.

Szklarska-Smialowska, Z. *Pitting Corrosion of Metals.* Houston, Texas: NACE International. 1986.

Tsuru, T., K. Hashimoto, and S. Haruyama. "Mass Transport and Solution Chemistry in Localized Corrosion." Proceedings of Critical Issues in Reducing the Corrosion of Steels. H. Leigheiser and S. Haruyama, eds. Houston, Texas: NACE International. pp. 110–120. 1985.

Van der Sande, J.B. and A.L. Bement. "An Investigation of Second Phase Particles in Zircaloy-4 Alloy." *Journal of Nuclear Materials.* Vol. 52. pp. 115–134. 1974.

Wronkiewicz, D.J., C.R. Bradley, J.K. Bates, and L.M. Wang. "Effect of Radiation Exposure on SRL 131 Composition Glass in a Steam Environment." Scientific Basis for Nuclear Waste Management XVII. A. Barkatt and R.A. Van Konynenburg, eds. Symposium Proceedings 333. Pittsburgh, Pennsylvania: Materials Research Society. pp. 259–267. 1994.

Wronkiewicz, D.J., J.K. Bates, E.C. Buck, J.C. Hoh, J.W. Emery, and L.M. Wang. "Radiation Effects in Moist-Air Systems and the Influence of Radiolytic Products Formation on Nuclear Waste Glass Corrosion." ANL–97/15. Argonne, Illinois: Argonne National Laboratory. 1997.

Yau T.-L. and R.T. Webster. "Corrosion of Zirconium and Hafnium." *Metals Handbook.* Vol. 13. Materials Park, Ohio: ASM International. pp. 707–721. 1987.

[redacted]

CNWRA 2002-01

EFFECT OF IN-PACKAGE CHEMISTRY ON THE DEGRADATION OF VITRIFIED HIGH-LEVEL RADIOACTIVE WASTE AND SPENT NUCLEAR FUEL CLADDING